AD-A053 441 AIR FORCE INST OF TECH WRIGHT-PATTERSON AFB OHIO SCH--ETC F/G 1/3
INVESTIGATION OF A DISCRETE C-STAR TRANSIENT RESPONSE CONTROLLE--ETC(U).
DEC 77 P D MONICO

UNCLASSIFIED AFIT/GGC/EE/77-8 NL

1 OF 3
ADA
053441

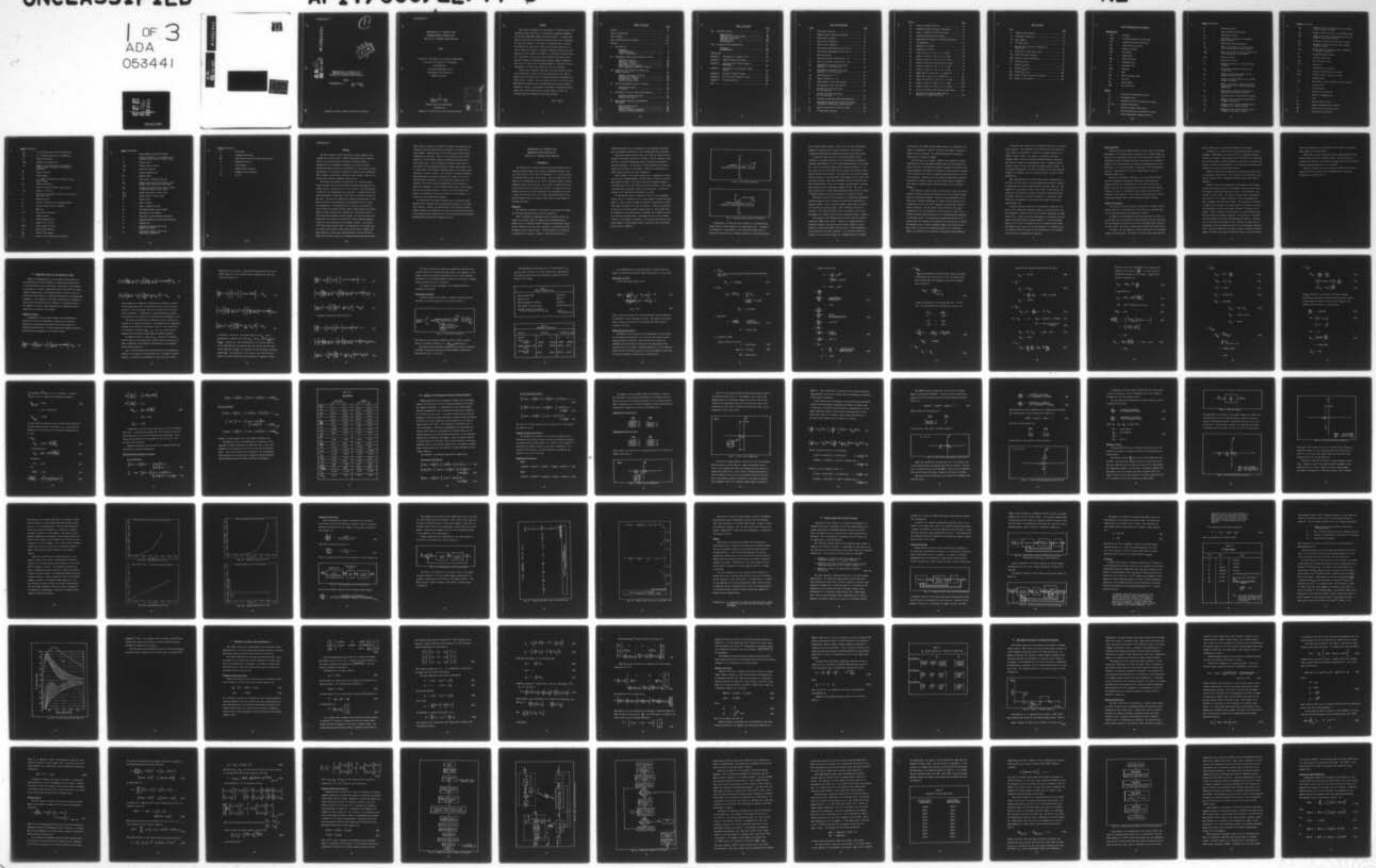

AFIT/GGC/EE/77-8

INVESTIGATION OF A DISCRETE C-STAR TRANSIENT RESPONSE CONTROLLER FOR THE YF-16 AT A SELECTED FLIGHT CONDITION

THESIS

AFIT/GGC/EE/77-8

Paul D. Monico
Capt USAF

AFIT/GGC/EE/77-8

INVESTIGATION OF A DISCRETE C-STAR TRANSIENT RESPONSE CONTROLLER FOR THE YF-16 AT A SELECTED FLIGHT CONDITION

THESIS

Presented to the Faculty of the School of Engineering
of the Air Force Institute of Technology
Air University
in Partial Fulfillment of the
Requirements for the Degree of
Master of Science

by

Paul D. Monico, B.S.
Captain USAF

Graduate Electrical Engineering

December 1977

Approved for public release; distribution unlimited

Preface

This thesis investigates the application of a discrete C-Star (C^*) transient response controller to the unstable longitudinal dynamics of the YF-16 Lightweight Fighter Prototype Aircraft. A reduced state model of the aircraft is developed from wind tunnel data and analyzed for open loop stability. This model is transformed into a discrete time domain state model and a discrete cost function applied to develop a controller capable of tracking a commanded response with zero steady state error within the confines of a defined C^* envelope boundary. The effects of both a Zero Order and First Order Hold on the system C^* response are analyzed using a digital computer simulation. Topics such as sample rates, weighting parameters, saturation effects, and migration of closed loop system roots are also presented.

I would like to thank Mr. Gene James for sponsoring this thesis. I also would like to express my sincere appreciation to Dr. Gary B. Lamont, my thesis advisor, for his guidance and advice throughout this thesis effort. Finally, I wish to express the love I hold for my wife, Mary Ellen and children Chris, Eric, and Jamie who were my strongest supporters. Lastly, I am grateful to my friends, especially by thesis typist, Mrs. Dorothy Grimm, whose constant support, concern, and assistance made the completion of this work possible.

Paul D. Monico

Table of Contents

Table of Contents

List of Illustrations

Figures		Page

List of Tables

List of Abbreviations and Symbols

Abbreviations

A/C	-	Aircraft
AFIT	-	Air Force Institute of Technology
CAL	-	Cornell Aeronautical Laboratory
CDC	-	Control Data Corporation
D/A	-	Digital to Analog
FBW	-	Fly-by-Wire
FL	-	Flight Level
FOH	-	First Order Hold
FS	-	Fuselage Station
HT	-	Horizontal Tail
Imag	-	Imaginary
M	-	Mach
MAC	-	Mean Aerodynamic Chord
SL	-	Sea Level
SM	-	Static Margin
ZOH	-	Zero Order Hold

Symbols

$\bar{A}$	-	Continuous system dynamics matrix
a.c.	-	Aerodynamic center
$\bar{A}_d$	-	Discretized version of continuous A matrix
$A_o - A_m$	-	Variable coefficients
$\bar{B}$	-	Continuous system output matrix
$\bar{B}_d$	-	Discretized version of continuous B matrix
C^*	-	C-Star longitudinal response criteria

Symbols (Continued)

$\bar{C}$	-	Observation matrix
$\bar{c}$	-	Mean aerodynamic chord length
C_D	-	Coefficient of drag
C_D	-	Coefficient of drag due to a change in angle of attack
$\bar{C}_d$	-	Discretized observation matrix
$C_{F_{x_a}}$	-	Effect on the forces in the X direction due to the deflection of the elevator
C_{FZ_a}	-	Effect on the forces in the Z direction due to the deflection of the elevator
c.g.	-	Center of gravity
C_L	-	Coefficient of left
C_L	-	Change in coefficient of lift with angle of attack
C_{m_q}	-	Pitch moment stability derivative due to pitch rate
C_{m_u}	-	Change in the pitching moment due to a change in forward velocity
C_m	-	Change in pitching moment due to a change in angle of attack
C_m	-	Effect of the rate of change of angle of attack caused by $\dot{w}$ on the pitching moment coefficient
C_m	-	Pitch moment stability derivative due to deflection of horizontal stabilizer
C_w	-	Coefficient due to acceleration of gravity
C_{x_q}	-	Change in force in the X direction due to a change in pitch rate
C_{x_u}	-	Change in force in the X direction due to a change in the forward velocity
C_x	-	Change in force in the X direction due to a change in the angle of attack

Symbols (Continued)

$C_{x_{\dot{\alpha}}}$	-	Change in force in X direction due to a change in rate of angle of attack
C_{Z_q}	-	Change in the Z force due to a pitching velocity
C_{Z_u}	-	Change in the force in the Z direction due to a change in the forward velocity
C_{Z_α}	-	Variation of the Z force with angle of attack
$C_{Z_{\dot{\alpha}}}$	-	Variation of the Z force with rate of change in angle of attack
$C_{Z_{\delta_H}}$	-	Z force stability derivative due to deflection of horizontal stabilizer
$\bar{D}$	-	Transformation/work matrix
Del	-	Specified sample rate
E_{θ_c}	-	Error between θ and θ_c
f( )	-	Function of
g	-	Acceleration due to gravity
G(s)	-	Forward transfer function of system
H(s)	-	Feedback transfer function of system
I	-	Identity matrix
Iyy	-	Mass moment of inertia about Y axis of aircraft
i	-	Integer counter
J	-	Cost functional
J_d	-	Discrete cost functional
j	-	Counter or imaginary axis
K	-	Gain
KT	-	Discrete value of time
K_Z	-	Normal acceleration gain constant
$K_{\ddot{\theta}}$	-	Pitch acceleration gain control
$K_{\dot{\theta}}$	-	Pitch rate gain constant

Symbols (Continued)

K_{1_d}	-	(1 x 3) Ricatti gain used to calculate N_d
K_{2_d}	-	(1 x 1) Ricatti gain used to calculate L_d
L_d	-	Scalar control gain
Long	-	Duration of simulation run
ℓ_t	-	Length to tail from quarter chord point of wing to quarter chord point of horizontal stabilizer
m	-	Mass of aircraft
N	-	Finite number
$\bar{N}_d$	-	1 x 3 matrix feedback gain; elements are N_{d_α}, $N_{d_{\dot\theta}}$ and $N_{d_{\delta_H}}$
N_Z	-	Normal acceleration
P	-	Discrete algebraic Ricatti solution matrix
p.h.	-	phugoid oscillation
q	-	Pitch rate, the angular velocity of the aircraft about the Y axis
$\bar{q}$	-	Dynamic pressure
Q_d	-	Discrete trajectory error weighting penalty
R_d	-	Discrete control penalty weighting
S	-	Wing area
s.p.	-	Short period oscillation
s	-	Laplace operator
$S_{1,2}$	-	S-plane conjugate roots
T	-	Sample rate or thrust
TDEL	-	Actual sample rate used
t_p	-	Time to peak overshoot
T_{ph}	-	Period of the phugoid
T_{sp}	-	Period of the short period oscillation

Symbols (Continued)

	-	Total forward velocity of aircraft
u	-	Velocity component of the aircraft in the X axis direction also the Z-plane X axis
$\bar{u}$	-	Control vector
$u(0)$	-	Initial value of control
V_{co}	-	Cross over velocity
v	-	Z-plane imaginary axis
WT	-	Nominal weight
$\bar{x}$	-	State vector, elements $\bar{x}_1$, $\bar{x}_2$, $\bar{x}_3$
$\bar{x}_{ac}$	-	Distance from fixed control point to aerodynamic center divided by chord length
$\bar{x}_{cg}$	-	Distance from fixed control point to center of gravity divided by chord length
$\bar{x}_{s.s.}$	-	Steady state value of state vector
$\bar{x}(o)$	-	Initial values of state vector
$\bar{y}$	-	Output vector
α	-	Angle of attack
α_T	-	Angle of attack from trim
Δ	-	Incremented change in the variable
δ_e	-	Deflection of the elevator
δ_h	-	Deflection of the horizontal stabilizer
δ_{h_c}	-	Commanded defection of horizontal stabilizer
ζ	-	Damping ratio
ζ_{PH}	-	Longitudinal damping ratio of the phugoid oscillation
ζ_{SP}	-	Longitudinal damping ratio of the short period oscillation

Symbols (Continued)

θ	-	Pitch angle
θ_c	-	Commanded pitch angle
Θ	-	Angle between horizontal and X stability axis
ρ	-	Atmospheric density
τ	-	Time variable
ω_d	-	Damped natural frequency
ω_n	-	Undamped natural frequency
$\forall$	-	For all

Abstract

The YF-16 fighter aircraft represents a radical departure from conventional aircraft design. Reduced longitudinal static stability results in an aircraft which is unstable in subsonic flight; a characteristic of considerable challenge in its control aspects. The present analog, fly-by-wire configuration of the aircraft's control system makes it an attractive candidate for digital control adaptation. Such a scheme, if successful, could mean a more compact, lighter, less failure prone, and more adaptable control system.

This thesis investigates the feasibility of a discrete digital flight controller for the YF-16 through the design and analysis of an optimal discrete controller at M = .8 at sea level. The investigation is limited to the longitudinal pitch axis only. A reduced state, short period approximation mathematical YF-16 model is developed from available data. The open loop stability and response characteristics of the model are shown to be unacceptable, necessitating the use of closed loop compensation. The minimization of a discrete cost function is used to develop a recursive discrete control formula which uses present values of output and past error information to successfully control this intentionally unstable aircraft system. The thesis discusses and incorporates the concept of a proposed C^* (C-Star) handling qualities criterion in the determination of acceptable response. The concept of C^*, which blends system states, is incorporated as an integral part of a closed loop, discrete control model for the YF-16. Digital computer simulation, using a Zero Order Hold (ZOH) or First Order Hold (FOH) control scheme, results in a stabilized system model whose output

falls within the bounds of a defined C^* envelope, and capable of performing the limited tracking task of following a 1-G climb, pilot, input command. Typical results in the form of plotted time history information are discussed. Results of the simulation show the ZOH superior to the FOH control scheme in reducing the elapsed time to reach steady state. The time required to achieve steady state is also shown to be appreciably uneffected at sample rates greater than T = 1/50 second. More frequent sampling, however, does result in the production of smaller controls. The variation in optimal feedforward and feedback gain for various combinations of sample rate and cost function penalty parameters is also presented in tabular form. An increase in the control penalty weighting (R), while holding the sample rate constant, is seen as having the same effect on the elapsed time for the transient response to reach a zero error steady state value, as decreasing the sample rate, while R is held constant. In either case, the elapsed time increases.

The possibility of actuator saturation due to excessive control movement rates is pointed out and discussed in relation to the simulation conducted. Finally, an investigation of the closed loop system complex conjugate root migrations show R as being inversely proportional to the system natural frequency (ω_N), with the trajectory error penalty weighting (Q) determining the damping ratio (ζ).

INVESTIGATION OF A DISCRETE C-STAR

TRANSIENT RESPONSE CONTROLLER FOR

THE YF-16 AT A SELECTED FLIGHT CONDITION

I. Introduction

The introduction of flight control systems totally based upon an electrical primary flight control system, emphasizing feedback, such that vehicle motion is the controlled parameter, is a recent occurrence in aircraft flight control system design. This is in part due to the infancy of its technology and the sense of security attached to proven mechanical flight control systems. In an effort to dispel this resistance, and add to the literature, but moreover, to analyze some of the problems encountered in such an approach, this investigation develops a linear time-invariant model of the YF-16 Lightweight Fighter Prototype and combines with it a digital flight control system capable of tracking step inputs.

Background

The important credentials of any would be air-superiority fighter are its speed, maneuverability and loiter capability.

Speed is enhanced by lightweight aircraft components which contribute to favorable thrust to weight ratios; maneuverability is enhanced by the aerodynamic design including the displacement control surface technique used; and loiter capability is enhanced by low fuel consumption and low failure rates. In many instances, one attribute is enhanced at the expense of another. More often than not, the

resulting design reflects a compromise of these important attributes and a corresponding compromise in the resulting aircraft performance.

With these considerations in mind, the design of fighter aircraft becomes a challenging task and is a subject of intense interest in the Air Force. The YF-16 Lightweight Fighter Prototype was designed to meet this challenge. It represents a radical departure from conventional aircraft design in an attempt to achieve an optimal blend of speed, maneuverability, and loiter capability.

With a length of just over forty-six feet, a wing-span of thirty-one feet, and a maximum weight of 27,000 pounds, the YF-16 is considerably lighter and quite a bit smaller than most present-day fighters. Less discernable to the eye, however, the YF-16 exhibits a novel center of gravity (cg), aerodynamic center (ac) relationship. A short discussion of this important relationship is in order.

If the aircraft center of gravity is located at the aerodynamic center, there is a condition of zero static margin or neutral stability (Fig. 1). This situation, though not unstable, could present a difficult dynamic situation for a pilot to control. If the cg is moved aft of the ac, the aircraft becomes unstable (Fig. 2). The aircraft will not maintain a trim condition and if disturbed, will continue to pitch up or down at the induced rate. The amount the cg is aft or forward of the ac is the margin of stability. If the cg is aft of the ac, the static margin is termed negative while a cg ahead of the ac describes positive static stability.

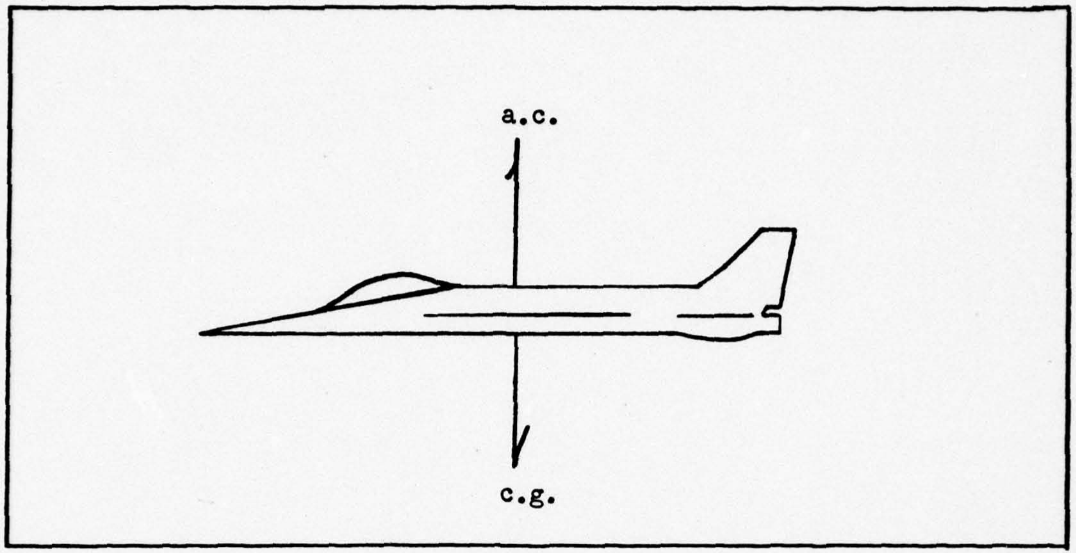

Fig. 1. Zero Static Stability.

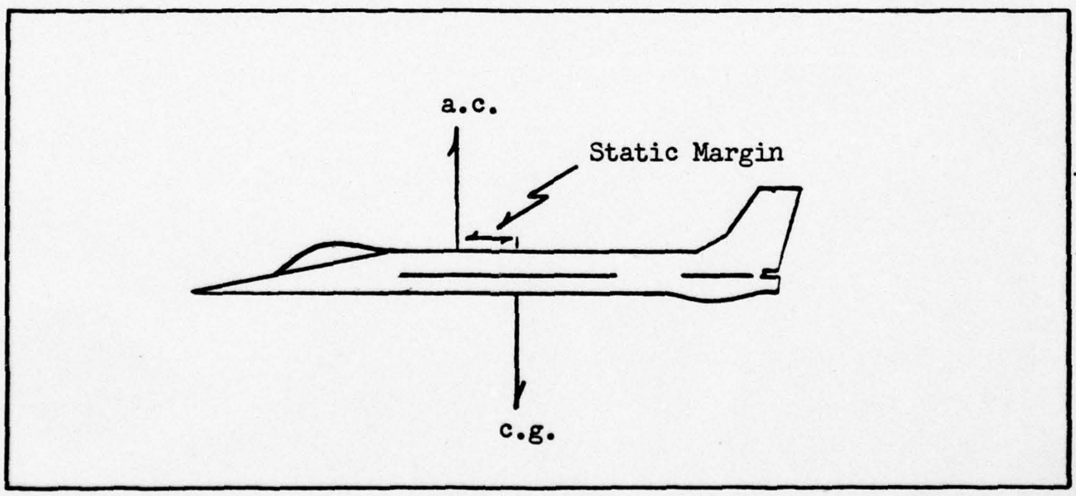

Fig. 2. Negative Static Stability (Unstable).

Traditionally, aircraft have been designed to be aerodynamically stable (positive static margin) in the longitudinal mode. In addition to allowing for a trim condition, this traditional design tends to bring the aircraft back to a straight and level attitude when disturbed

from a trimmed flight condition. Were it not for this intentionally designed-in characteristic of static stability, a pilot would be continuously adjusting and compensating to keep the aircraft flying.

In subsonic flight this type of stability (positive static stability) is desirable; however, as the aircraft passes through the transonic region (Mach $.8^{+} \rightarrow 1.2^{-}$) and becomes supersonic, the ac moves aft. Here, its statically stable nature becomes detrimental. In effect, since the ac is now further aft of the cg, the statically stable aircraft becomes "super stable." This means that the aircraft displays greater resistance to any disturbance which might cause it to move from its stable attitude. When such disturbances result from control commands transmitted by a pilot, the aircraft, not being able to discriminate between a gust or legitimate command, resists. This is an obvious handicap for a modern high-performance fighter which is expected to display exceptional agility in maneuvers at supersonic speeds.

The obvious solution to this problem is to reduce the longitudinal stability margin in order to make the aircraft more maneuverable at supersonic speeds. Such a solution, however, would cause an aircraft to be unstable in subsonic flight. Such a situation could not be tolerated. This obvious dilemma existed for sometime, until recent developments in automatic control system technology offered a solution.

The solution to this dilemma takes the form of what is called a fly-by-wire (FBW) control system. Instead of a complex network of mechanical linkages, this system uses electronic signals to relay requested response requirements from the pilot to electro-hydraulic servos which move the control surfaces. In a constant-G climb, for instance, as the aircraft response to a command begins, the response

is fed back to the flight control computer where it is compared to the pilot's G requirements. When the two match, the signal is nulled; no further control is applied. The aircraft maintains the constant G climb until the command is changed.

The YF-16 uses such a system. However, the relaxation of static stability and all its performance benefits have not been without cost. Since the YF-16 is intentionally designed to maintain from seven to ten percent negative static margin, the stability of the aircraft is reduced to the extent that the YF-16 is unstable in pitching motion at all subsonic airspeeds. Therefore, with an airframe intentionally designed to be unstable in subsonic flight, the YF-16 relies upon the flight control system to maintain tight closed-loop control over its unstable dynamics.

The fly-by-wire control system is used to keep a tight rein on the aircraft, especially during the subsonic portion of the flight envelope where it is inherently unstable. Because of the implementation of relaxed static stability technology, the flight control systems acts as a compensator to fill in for the inadequacy of the aircraft design in terms of stability. The end result is that the YF-16 is not only stabilized but has the advantages of reduced drag as a result of the unstable airframe design and greater ease of maneuverability especially at supersonic speeds. As the gains and compensation networks in the control system are changed, the stability of the aircraft can be varied. The advantage, then, is that in subsonic flight, the aircraft can be made stable, to fly in the conventional manner, and in supersonic flight, the stability can be relaxed to allow greater maneuverability.

At present, the controller for the unstable pitch axis is a complex analog computer. Gain adjustments are controlled by this on-board device. Gains are "scheduled" as a function of flight condition in an adaptive control scheme. For example, one particular airspeed, altitude, angle of attack and pitch rate might identify a particular gain from the schedule of possible gains, while a slightly different airspeed, angle of attack, and pitch rate might identify another. In its analog configuration, the present controller is not only bulky and difficult to mechanize, but also presents problems in terms of future modification.

With some appreciation for the present control configuration of the YF-16 just described, it has been suggested that digital computers be substituted for present analog computer controllers (Ref. 5). This suggestion is reasonable in light of the advent of small digital computers and recent advances in digital integrated circuits which make the digital computer an attractive candidate as a controller. Much effort has been expended in researching this proposed substitution approach (Ref. 18).

A digital controller would have the advantage of being more compact, of less mechanical complexity, lighter, less failure prone, and more adaptable to changes in the form of software adjustments to modify control laws. However, with these advantages, are associated new problems not encountered with the analog controller. Two such problems, among a list of others including the areas of sufficient word length and adequate memory size, are the identification of an adequate recursive digital control algorithm and the determination of the sampling rate with which to implement this algorithm.

Problem Statement

Along this vein, the problem addressed in this study is the design and analysis of an optimal discrete controller at a selected flight condition for the longitudinal pitch axis of the YF-16 using a specific C^* (pronounced C-Star) performance criteria. The scope of the analysis is limited to the consideration of the unstable longitudinal mode of the YF-16 only. It is this mode which is applicable to the C^* performance criteria. Additionally, it is pitch response which is the most divergent dynamic mode.

The cases of both Mach .8 and Mach 1.2 at sea level and 30,000 feet for trim angles of attack are considered. These particular flight conditions were selected based on the availability of data (Ref. 13 and 14), and in consideration of the fact that high subsonic flight at sea level is considered the most critical area for pitch response for this aircraft. Here, control surface deflections produce the greatest dynamic effect on the statically unstable airframe.

Order of Presentation

In an effort to develop, simulate, and discuss a suitable discrete control concept for a pitching model of the YF-16, the remaining chapters of this investigation are organized as follows.

In Chapter II, non-dimensional stability derivatives for Mach .8 at sea level for a three degree of freedom aircraft model are developed. The corresponding derivatives for the three remaining flight conditions are also listed. The model is derived from available wind tunnel data.

In Chapter III, the equations of motion developed in the preceeding chapter are investigated. The nature of the open loop system stability

and the character of its response performance are discussed.

In Chapter IV, a discrete model of the proposed control system is presented. Additionally, the concept of C^* as a plausible stability criteria is presented. This approach, which has gained some popularity, uses a linear blend of normal acceleration, pitch rate, and pitch acceleration to define proper performance. The C^* concept is included as an integral part of the proposed control system.

Chapter V details the development of a discrete system model from its continuous representation. Also included is the development of the observer matrix needed to transform the system states into usable C^* parameters.

Chapter VI presents the mathematical development of the optimal discrete controller using this C^* performance criterion and the recursive digital control algorithm which results. Also discussed is the concept of a hold device. The chapter concludes with a discussion of the structure of the software developed for this investigation and used to implement the controller concept. This program, as a function of sample rate, determines the optimal gains to be applied in the control algorithm to achieve satisfactory transient C^* response of the system. Various assumptions and limitations are also discussed along with the simulation technique conducted. The controller is simulated at various sample rates using a CDC 6600 Digital Computer. The migration of the closed loop system roots as a function of sample rate is investigated along with saturation effects on the horizontal stabilizer servo. Using the simulation, an attempt is made to identify a minimum sample rate which, based upon the saturation limit of the pitch control

servo and characteristic root locations, still results in a response within defined C^* envelope bounds.

Chapter VII discusses observations on the controllability of the system resulting from the simulation effort. Typical results are presented and explained. The effects of sample rates and cost function penalty weighting variations are also included.

Finally, in Chapter VIII, the conclusions drawn from this investigative effort are presented and recommendations are discussed pertaining to further research.

II. Mathematical Model and the Reducation of Data

Before the implementation of any controller and an analysis of its effectiveness can be undertaken, an adequate mathematical model of the aircraft must first be developed. The purpose of this chapter is, therefore, to develop a mathematical model of the YF-16 for longitudinal pitching motion. Generalized equations of motion are first presented and then reduced in complexity through the use of simplifying assumptions. The remainder of the chapter presents the development of rigid stability derivatives which constitute the individual terms of the equations of motion. These derivatives are summarized in table format at the conclusion of the chapter.

Equations of Motion

As explained in the preceding chapter, this investigation is concerned only with the longitudinal pitching mode of the YF-16. Therefore, disregarding the negligible cross-coupling effects of lateral-directional motion, the small perturbation equations of motion which describe the dynamics of the aircraft follow:

$$\left(\frac{mu}{S_q}\acute{u} - C_{x_u}\acute{u}\right) + \left(-\frac{\bar{c}}{2u}C_{x_{\dot{\alpha}}}\acute{\dot{\alpha}} - C_{x_\alpha}\acute{\alpha}\right) + \left(-\frac{\bar{c}}{2u}C_{x_q}\dot{\theta} - C_w(\cos\Theta)\theta\right) = C_{F_{x_a}} \quad (1)$$

$$\left(-C_{z_u} u'\right) + \left[\left(\frac{mu}{Sq} - \frac{\bar{c}}{2u} C_{z_{\dot{\alpha}}}\right)\dot{\alpha}' - C_{z_\alpha}\alpha'\right] + \left[\left(-\frac{mu}{Sq} - \frac{\bar{c}}{2u} C_{z_q}\right)\dot{\theta} - C_w(\sin\Theta)\theta\right] = C_{F_{z_a}} \quad (2)$$

$$\left(C_{m_u} u'\right) + \left(-\frac{\bar{c}}{2u} C_{m_{\dot{\alpha}}}\dot{\alpha}' - C_{m_\alpha}\alpha'\right) + \left(\frac{I_{yy}}{Sq\bar{c}}\ddot{\theta} - \frac{\bar{c}}{2u} C_{m_q}\dot{\theta}\right) = C_{m_a} \quad (3)$$

These equations are Blakelock's non-dimensional equations of motion for the longitudinal axis of an aircraft and will be used to model the YF-16. Their development will not be presented here but can be found in Reference 1. Definitions of individual equation elements are included in the previous List of Abbreviations and Symbols, p.viii.

The various non-dimensional coefficients in these equations are referred to as stability derivatives. The equations can be simplified somewhat by the judicious elimination of three of these derivatives. It is possible to eliminate $C_{x_{\dot{\alpha}}}$, C_{x_q}, and C_{m_u} terms from the equations thus considerably simplifying the modeling equations.

As Blakelock points out, $C_{x_{\dot{\alpha}}}$ and C_{x_q}, the effect of downwash from the wing on the horizontal tail and the effect of pitch rate on drag, respectively, have negligible contributions to the equations and are usually neglected.

C_{m_u}, a term resulting from slipstream, thrust, and flexibility effects, is the change in pitching moment due to a change in forward velocity. As pointed out in Reference 1, this term can be safely

neglected for jet aircraft. Using these simplifications for all the flight conditions in this study results in equations (1), (2), and (3) being expressed as:

$$\left[\frac{mu}{Sq}\,u' - C_{x_u}\,u'\right] + \left[-C_{x_\alpha}\,\alpha'\right] + \left[-C_w(\cos\Theta)\,\theta\right] = C_{F_{x_a}} \tag{4}$$

$$\left[-C_{z_u}\,u'\right] + \left[\left(\frac{mu}{Sq} - \frac{\bar{c}}{2u}C_{z_{\dot\alpha}}\right)\alpha' - C_{z_\alpha}\,\alpha'\right] + \left[\left(-\frac{mu}{Sq} - \frac{\bar{c}}{2u}C_{z_q}\right)\dot\theta - C_w(\sin\Theta)\,\theta\right] = C_{F_{z_a}} \tag{5}$$

$$\left[-\frac{\bar{c}}{2u}C_{m_{\dot\alpha}}\,\alpha' - C_{m_\alpha}\,\alpha'\right] + \left[\frac{I_{yy}}{Sq\bar{c}}\,\ddot\theta - \frac{\bar{c}}{2u}\,C_{m_q}\,\dot\theta\right] = C_{m_a} \tag{6}$$

As Reference 1 points out, the forcing function of $C_{F_{x_a}}$ can be approximated as equaling zero, while $C_{F_{Z_a}}$ and C_{m_a} equal $C_{z_{\delta_e}}\delta_e$ and $C_{m_{\delta_e}}\delta_e$, respectively. Now, substituting for the forcing functions on the right-hand side of equations (4), (5), and (6), with the notational difference that δ_h, the deflection of the horizontal stabilizer, replaces δ_e, the deflection of the elevator, since the YF-16 has a movable horizontal stabilizer and no elevator, the equations become:

$$\left[\frac{mu}{S_q}\dot{u}' - C_{x_u}u'\right] + \left[-C_{x_\alpha}\alpha'\right] + \left[-C_w(\cos\Theta)\,\theta\right] = 0 \tag{7}$$

$$\left[-C_{z_u}u'\right] + \left[\left(\frac{mu}{S_q} - \frac{\bar{c}}{2u}C_{z_{\dot\alpha}}\right)\dot{\alpha}' - C_{z_\alpha}\alpha'\right] + \left[\left(-\frac{mu}{S_q} - \frac{\bar{c}}{2u}C_{z_q}\right)\dot{\theta} - C_w(\sin\Theta)\,\theta\right] = C_{z_{\delta_h}}\delta_h \tag{8}$$

$$\left[-\frac{\bar{c}}{2u}C_{m_{\dot\alpha}}\dot{\alpha}' - C_{m_\alpha}\alpha'\right] + \left[\frac{I_{yy}}{S_q\bar{c}}\ddot{\theta} - \frac{\bar{c}}{2u}C_{m_q}\dot{\theta}\right] = C_{m_{\delta_h}}\delta_h \tag{9}$$

In Laplace notation the equations become:

$$\left[\frac{mu}{S_q}s - C_{x_u}\right]u'(s) - \left[C_{x_\alpha}\right]\alpha'(s) - \left[C_w(\cos\Theta)\right]\theta(s) = 0 \tag{10}$$

$$\left[-C_{z_u}\right]u'(s) + \left[\left(\frac{mu}{S_q} - \frac{\bar{c}}{2u}C_{z_{\dot\alpha}}\right)s - C_{z_\alpha}\right]\alpha'(s) + \left[\left(-\frac{mu}{S_q} - \frac{\bar{c}}{2u}C_{z_q}\right)s - C_w\sin\Theta\right]\theta(s) = C_{z_{\delta_h}}\delta_h(s) \tag{11}$$

$$\left[-\frac{\bar{c}}{2u}C_{m_{\dot\alpha}}s - C_{m_\alpha}\right]\alpha'(s) + \left[\frac{I_{yy}}{S_q\bar{c}}s^2 - \frac{\bar{c}}{2u}C_{m_q}s\right]\theta(s) = C_{m_{\delta_h}}\delta_h(s) \tag{12}$$

In order to evaluate and apply these equations to the YF-16, the various terms must be replaced by actual values. The remainder of this chapter presents the detailed development of each of these stability derivatives for the flight conditions at Mach .8 at sea level. Flexible aircraft effects will not be considered.

As a prelude to this development, the following directional convention is presented.

Directional Convention

A positive control force produces a negative surface deflection and causes a positive moment about the pitch axis (Fig. 3).

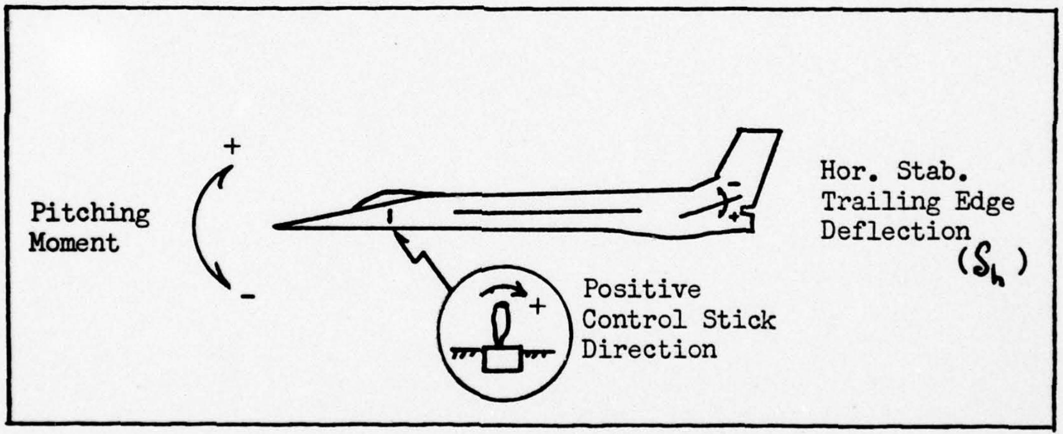

Fig. 3. Directional Convention.

Note that for the horizontal stabilizer control surface, trailing edge up is defined as negative, i.e., $\delta_{h_{0 \text{ to } -N}} \rightarrow$ pitch up.

The rigid stability derivative calculations are based on stability and flight control data furnished by General Dynamics Convair Aerospace Division (Ref. 13 and 14).

The configuration chosen was that of a clean aircraft (i.e., gear up, flaps retracted, etc.) with external fuel tanks removed. The physical specifications and atmospheric conditions listed in Tables I and II apply.

Table I
Physical Specifications

Nominal Weight (WT)	16,519 lbs
Wing Area (S)	280 ft^2
Mean Aerodynamics chord ($\bar{c}$)	10.937 ft
Mass Moment of Inertia (I_{yy})	39,199 ft-lbs-sec^2
Distance from $\bar{c}/4$ of wing MAC to $\bar{c}/4$ of Horizontal Tail MAC (ℓ_t)	15.66 ft (See Appendix A)

Table II
Atmospheric Conditions

Altitude	Sea Level		30,000' (FL 300)	
Mach No.	.8	1.2	.8	1.2
Density (ρ) slug/ft^3	.002378	.002378	.00890	.000890
Dynamic Pressure (q) lb/ft^2	949.44	2136.24	282.02	634.51
Velocity (u) ft/sec	893.6	1340.4	796.08	1194.1

As a preliminary step, it was necessary to determine the trim angle of attack for the selected flight condition (M = .8, sea level).

Trim Angle of Attack

At the trim condition #g's = 1.0.

$$\#g's = \frac{\bar{q}S}{WT}\left[C_{L_{\alpha=0^\circ}} + C_{L_\alpha}\alpha_{TRIM}\right] = 1.0 \tag{13}$$

$$= \frac{949.44\,(280)}{16{,}519}\left[.005 + .078\,\alpha_T\right] = 1.0$$

$$\therefore\ \alpha_T = .73^\circ \tag{14}$$

Here, it has been assumed that the pitching moment and drag equations are satisfied at this trim angle of attack. This angle of attack was used to extract data from the various graphs and tables found in References 13 and 14.

Rigid Stability Derivatives

The purpose of this section is the determination of exact values of the stability derivatives at M = .8 at sea level needed to mathematically model the aircraft. These derivatives are based on a stability axis system with its centroid at the wing quarter chord and waterline of 91.0 inches. Detailed definitions of each derivative beyond the short definitions found in the List of Symbols on page viii, are found in Reference 1 and will not be included here.

a. $C_{m_{\dot{\alpha}}}$:

This derivative was extracted directly from the data tables (Ref. 14).

$$C_{m_{\dot{\alpha}}} = -1.520/\text{Rad} \tag{15}$$

b. $C_{z_{\dot{\alpha}}}$:

$$C_{z_{\dot{\alpha}}} = f(C_{m_{\dot{\alpha}}}) = \frac{\bar{c}}{l_t} C_{m_{\dot{\alpha}}} \tag{16}$$

$$= \frac{10,937'}{15.666'} (-1.520)$$

$$C_{z_{\dot{\alpha}}} = -1.0611/\text{Rad}$$

c. Mass (M):

$$M = \frac{\text{weight}}{\text{gravity}} = \frac{16,519 \text{ lbs}}{32.1725 \text{ ft/sec}^2} \tag{17}$$

$$M = 513.45 \text{ slugs}$$

d. Forward Vel (u):

Speed of sound at sea level

$$c = 1117 \text{ ft/sec} \tag{18}$$

$$\text{Mach } .8 = .8\,(1117) \tag{19}$$

$$u = 893.6 \text{ ft/sec}$$

e. Dynamic Pressure (q):

$$q = \frac{\rho}{2} u^2 \qquad (20)$$

$$= \frac{.002378}{2} (893.6)^2$$

$$q = 949.44 \quad lb/ft^2$$

f. $\frac{mu}{S_f}$:

$$\frac{mu}{S_f} = \frac{(513.45)(893.6)}{(280)(949.44)} \qquad (21)$$

$$= 1.726$$

g. $\frac{I_{yy}}{S_f \bar{c}}$:

$$\frac{I_{yy}}{S_f \bar{c}} = \frac{39{,}199}{280\ (849.44)(10.937)} \qquad (22)$$

$$\frac{I_{yy}}{S_f \bar{c}} = .0135 \text{ sec}^2$$

h. $\frac{\bar{c}}{2u}$:

$$\frac{\bar{c}}{2u} = \frac{10.937}{2\ (893.6)} \qquad (23)$$

$$\frac{\bar{c}}{2u} = .0061 \text{ sec}$$

i. C_W :

$$C_W = \frac{-Mg}{Sq} = \frac{-513.45\ (32.1725)}{(280)\ (949.44)} \qquad (24)$$

$$C_W = -.0621$$

j. $C_{m_{\delta_h}}$:

$C_{m_{\delta_h}}$ was determined for pitch up only. Data was available for horizontal tail deflections of 0° → -10° which, based upon the previously set convention, causes the aircraft's nose to pitch up.

$$C_{m_{\delta_h}} = \frac{\Delta C_m}{\Delta \delta_h}\Big|_{0° \to -10°} \tag{25}$$

A linear interpolation of the data between α = 0° and α = 2.5° was performed to determine C_m for α_T = .73

α		ΔC_m
0°	=	.1120
.73°	=	.1126
2.50°	=	.1140

$$\frac{\Delta C_m}{\Delta \delta_h} = \frac{.1126}{-10\text{ deg}} \quad \frac{(57.3\text{ deg})}{\text{Rad}} \tag{26}$$

$$C_{m_{\delta_h}} = -.6452/\text{Rad}$$

k. C_{m_q} :

$$C_{m_q} = C_{m_{\dot{\theta}}} \tag{27}$$

This value was extracted directly from the tables.

$$C_{m_q} = -4.3900 \tag{28}$$

l. C_{Z_q} :

$$C_{Z_q} = f(C_{m_q}) \tag{29}$$

$$= \frac{\bar{c}}{\ell_t} C_{m_q} = .6981 \cdot (-4.3900)$$

$$C_{Z_q} = -3.0647$$

m. C_{x_α} :

$$C_{x_\alpha} = C_L - \frac{\partial C_D}{\partial \alpha} = C_L - C_{D_\alpha} \tag{30}$$

for $\alpha_T = .73$ $\quad C_{D_\alpha} = .0011/\text{deg} = .0630/\text{Rad}$ (31)

$C_L = .0625$ (interpolation result) (32)

$$C_{x_\alpha} = C_L - C_{D_\alpha} = .0625 - .0630 \tag{30}$$

$$C_{x_\alpha} = -.0005$$

n. C_{x_u} :

$$C_{x_u} = \frac{u}{S_f} \frac{\partial T}{\partial u} - 2C_D - u \frac{\partial C_D}{\partial u} \tag{33}$$

The first term on the right-hand side of equation (33) reduces to zero, that is $\frac{\partial T}{\partial u} = 0$, since thrust is essentially constant for jet aircraft. Equation (33) can now be expressed as:

$$C_{x_u} = -2C_D - u\frac{\partial C_D}{\partial u} \tag{34}$$

or equivalently as:

$$C_{x_u} = -2C_D - \text{Mach}\left[\frac{\Delta C_D}{\Delta \text{Mach}}\right] \tag{35}$$

$$C_D = .0248 \quad \text{(interpolation result)} \tag{36}$$

$$-2C_D = .0496 \tag{37}$$

$$M\left[\frac{\Delta C_D}{\Delta M}\right] = .8\left[\frac{C_{D_{M=.8}} - C_{D_{M=.9}}}{.8 - .9}\right] \tag{38}$$

$$= .8\left[\frac{.0248 - .0268}{.8 - .9}\right]$$

$$= .0160$$

$$\therefore C_{x_u} = -2C_D - M\left[\frac{\Delta C_D}{\Delta M}\right] = -.0496 - .0160 \tag{35}$$

$$= -.0656$$

o. C_{z_α}:

$$C_{z_\alpha} = -C_D - \frac{\partial C_L}{\partial \alpha} \tag{39}$$

$$C_{z_\alpha} = -C_D - C_{L_\alpha} \tag{40}$$

$$-C_D = -0.0248 \tag{41}$$

$$C_{L_\alpha} = (57.3)(.078) \tag{42}$$

$$C_{L_\alpha} = 4.4694/\text{Rad}$$

$$C_{z_\alpha} = -C_D - C_{L_\alpha} \tag{40}$$

$$C_{z_\alpha} = -.0248 - 4.4694$$

$$C_{z_\alpha} = -4.4942$$

p. $C_{z_{\delta_h}}$:

$$C_{z_{\delta_h}} = f(C_{m_{\delta_h}}) \tag{43}$$

$$= \frac{\bar{c}}{l_e} C_{m_{\delta_h}} \; 0^\circ \rightarrow -10^\circ$$

$$= (.6981)(-.6452)$$

$$= -.4504$$

q. C_{m_α}:

$$C_{m_\alpha} = \frac{\partial C_m}{\partial C_L} \cdot \frac{\partial C_L}{\partial \alpha} \tag{44}$$

$$= \left[\text{static margin (S.M.)}\right] \cdot \frac{\partial C_L}{\partial \alpha} \tag{45}$$

$$= \left[\bar{x}_{c.g.} - \bar{x}_{a.c.}\right] \frac{\partial C_L}{\partial \alpha} \tag{46}$$

If C_{m_α} is positive, the aircraft is statically unstable. Recalling the discussion of stability in the previous chapter, we would expect the YF-16 to have a positive C_{m_α} for this subsonic flight condition. As shown earlier:

$$\frac{\partial C_L}{\partial \alpha} = 4.4694/\text{Rad} \tag{42}$$

$$\text{S.M.} = \left[\bar{x}_{cg} - \bar{x}_{a.c.}\right] \tag{47}$$

$$= \left[.35 - .31\right]$$

$$\text{S.M.} = .04$$

$$C_{m_\alpha} = (\text{S.M.}) \frac{\partial C_L}{\partial \alpha} \tag{45}$$

$$= (.04)(4.4694)$$

$$C_{m_\alpha} = .1788$$

As anticipated, C_{m_α}, M = .8, S.L. is positive. A check of C_{m_α}, M = 1.2, S.L. shows this coefficient as negative.

$$C_{m_{\alpha}\,M=1.2,\,S.L.} = (S.M.) \tag{48}$$

$$= (.35 - .56)(5.2143)$$

$$C_{m_{\alpha}\,M=1.2\,S.L.} = -1.0950$$

For this stability derivative then, the model truly reflects the variable stability aspect of the YF-16, i.e., a shift from instability to a stable nature as the aircraft accelerates past M = 1.0.

r. C_{z_u}:

$$C_{z_u} = -2C_L - u\left[\frac{\partial C_L}{\partial u}\right] \tag{49}$$

or equivalently as:

$$C_{z_u} = -2C_L - \text{Mach}\left[\frac{\Delta C_L}{\Delta \text{Mach}}\right] \tag{50}$$

As earlier,

$$C_L = .0625 \tag{32}$$

and

$$-2C_L = -.1250 \tag{51}$$

$$M\left[\frac{\Delta C_L}{\Delta M}\right] = .8\left[\frac{C_{L_{M=.8}} - C_{L_{M=.9}}}{.8 - .9}\right] \tag{52}$$

$$M\left[\frac{\Delta C_L}{\Delta M}\right] = .8\left[\frac{.0625 - .0704}{-.1}\right]$$

$$M\left[\frac{\Delta C_L}{\Delta M}\right] = .0632$$

$$\therefore C_{z_u} = -2C_L - M\left[\frac{\Delta C_L}{\Delta M}\right] \tag{50}$$

$$= -.1250 - .0632$$

$$C_{z_u} = -.1882$$

A tabulation of the values just calculated to be used in equations (10), (11), and (12) follows in Table III. Also involved are the stability derivatives for the three remaining flight conditions. These values were calculated in the same manner as the case of M = .8 at sea level, just presented.

Using the appropriate data from Table III, equations (10), (11), and (12) can be expressed numerically.

<u>YF-16 Longitudinal Equations of Motion</u>

<u>M = .8, Sea Level</u>

$$\left[1.726s + .0656\right] u'(s) + \left[.0005\right] \alpha'(s) + \left[.0621\right] \theta(s) = 0 \tag{53}$$

$$\left[\quad .1882 \quad\right] u'(s) + \left[1.7325s + 4.4942\right] \alpha'(s) - \left[1.7073s\right] \theta(s) = .4504\,\delta_h(s) \tag{54}$$

$$\left[.0093s - .1788\right]\alpha'(s) + \left[.0135s^2 + .0268s\right]\theta(s) = -.6452\delta_h(s) \tag{55}$$

<u>M = 1.2, Sea Level</u>

$$\left[1.1506s + .1033\right]u'(s) + \left[.0813\right]\alpha'(s) + \left[.0276\right]\theta(s) = 0 \tag{56}$$

$$\left[.1200\right]u'(s) + \left[1.1465s + 4.8132\right]\alpha'(s) - \left[1.11862s\right]\theta(s) = -.361\delta_h(s) \tag{57}$$

$$\left[-.00164s + .7392\right]\alpha'(s) + \left[.006s^2 + .01855s\right]\theta(s) = -.5157\delta_h(s) \tag{58}$$

Analysis of these equation sets is the subject of Chapter III.

Investigation of the corresponding sets of equations for the remaining two flight conditions at 30,000 feet shows a close correspondence in root locations to the roots of the sets of equations above. Due to this situation, the remainder of the investigation will concentrate on the above sets of equations leaving the higher altitude flight cases for reference and future investigation.

Table III

Data Summary

	Sea Level		30,000'	
Mach	.8	1.2	.8	1.2
α_T	.73°	1.30°	2.66°	2.05°
mass	513.45	513.45	513.45	513.45
u	893.6	1340.4	796.08	1194.1
q	949.44	2136.24	282.02	634.51
$\frac{mu}{Sq}$	1.726	1.1506	5.176	3.4510
C_{x_u}	-.0656	-.1033	-.0789	-.1057
C_{x_α}	-.0005	-.0813	-.1061	-.1215
C_w	-.0621	-.0276	-.2092	-.0930
Θ	0	0	0	0
C_{Z_u}	-.1882	-.1200	-.5404	-.2014
$\bar{c}/2u$	.0061	.0041	.0069	.0046
$C_{z_{\dot\alpha}}$	-1.0611	1.000	-1.0960	1.000
C_{z_α}	-4.4942	-4.8132	-4.5554	-4.9278
C_{Z_q}	-3.0647	-7.8000	-3.8000	-8.1000
$C_{z_{\delta_h}}$	-.4504	-.3610	-.5157	-.4412
$C_{m_{\dot\alpha}}$	-1.520	.400	-1.500	.100
C_{m_α}	.1788	-.7392	.0917	-.9283
$I_{yy}/Sq\bar{c}$	.0135	.0060	.0454	.0202
C_{m_q}	-4.3900	-4.5252	-4.490	-4.7182
$C_{m_{\delta_h}}$	-.6452	-.5157	-.6017	-.6303

III. Analysis of the Equations of Motion and System Stability

Having derived two sets of equations of motion in the preceding chapter, the YF-16 model can now be analyzed regarding its stability and response performance. To accomplish this, this chapter begins with the determination of the characteristic equations for flight at M = .8, and 1.2 at sea level. For a given system, there is only one polynomial, termed the system characteristic equation, which determines the form of the system transient response regardless of the type of signal chosen as the input. This polynomial is determined and its roots investigated. Short period approximations of both flight conditions, which assume zero perturbation in forward velocity as the aircraft maneuvers, are then developed and the roots of the associated characteristic polynomials investigated. Open loop system responses to various inputs are discussed. After a brief discussion on the high frequency nature of the aircraft actuator servo, the chapter concludes with a variable gain root locus analysis of system stability for both flight conditions.

For reference, the modeling equations are repeated here.

M = .8, Sea Level (Set A)

$$\left[1.726s + .0656\right] u'(s) + \left[.0005\right] \alpha'(s) + \left[.0621\right] \theta(s) = 0 \quad (53)$$

$$\left[.1882\right] u'(s) + \left[1.7325s + 4.4942\right] \alpha'(s) - \left[1.7073s\right] \theta(s) = -.4504\, \delta_h(s) \quad (54)$$

$$\left[.0093s - .1788\right] \alpha'(s) + \left[.0135s^2 + .0268s\right] \theta(s) = -.6452\, \delta_h(s) \quad (55)$$

M = 1.2, Sea Level (Set B)

$$\left[1.1506s + .1033\right] u'(s) + \left[.0813\right] \alpha'(s) + \left[.0276\right] \theta(s) = 0 \tag{56}$$

$$\left[.12\right] u'(s) + \left[1.1465s + 4.8132\right] \alpha'(s) - \left[1.11862s\right] \theta(s) = -.361\,\delta_h(s) \tag{57}$$

$$\left[-.00164s + .7392\right] \alpha'(s) + \left[.006s^2 + .01855s\right] \theta(s) = -.5157\,\delta_h(s) \tag{58}$$

The first set of three equations will be referred to as Set A while the latter as Set B.

Analysis of Equations of Motion

The characteristic equations for both sets of equations were determined using a digital computer subroutine specifically designed for control systems analysis (Ref. 16). Details of the formatted instructions and computer results are presented in Appendix B. The results of this analysis, the model characteristic equations and respective roots, are as follows:

Characteristic Equations

Set A:

$$.040369s^4 + .213799s^3 - .310934s^2 - .012018s - .002090 = 0 \tag{59}$$

Set B:

$$.007915s^4 + .056299s^3 - 1.059076s^2 + .094454s + .002448 = 0 \tag{60}$$

The negative terms in equation (59) are indicative of roots in the right half of the S-plane corresponding to an unstable situation. This is not the case in equation (60) where all roots appear positive. This is confirmed, as the results of Appendix B show, by factoring the characteristic equations into their corresponding roots.

<u>Characteristic Roots of Set A</u>

Real	Imag
.1223932E + 01	0.
-.2093674E - 01	.7804015E - 01
-.2093674E - 01	-.7804015E - 01
-.6478175E + 01	.6967083E - 30

<u>Characteristic Roots of Set B</u>

Real	Imag
-.4474255E - 01	.1790868E - 01
-.4474255E - 01	-.1790868E - 01
-.3511721E + 01	.1099289E + 02
-.3511721E + 01	-.1099289E + 02

These system root locations can be shown pictorially in the S-plane of Figure 4 and Figure 5.

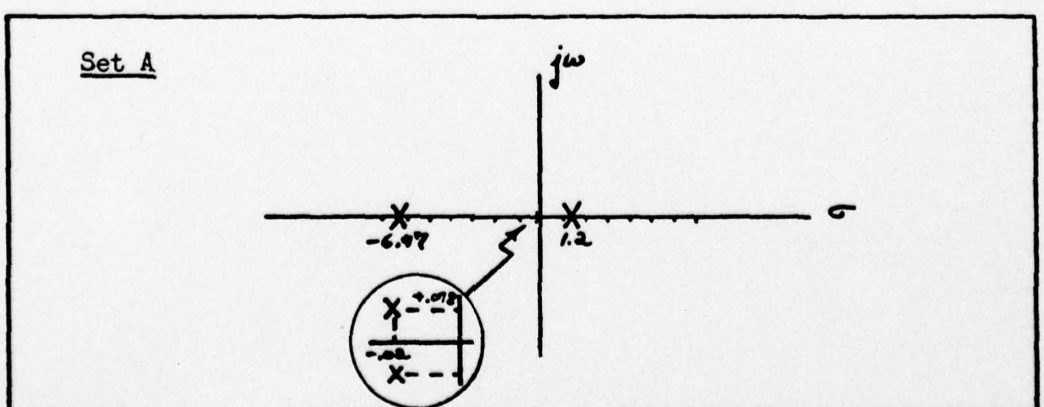

Fig. 4. Roots of Set A Equations.

The root in the right half plane confirms the unstable nature of the system described by Set A. The conjugate roots, close to the imaginary axis, are conventional phugoid roots due to the low frequency and correspondingly long period associated with their oscillatory motion, while the two remaining aperiodic roots (Ref. 4) are considered as short period roots.

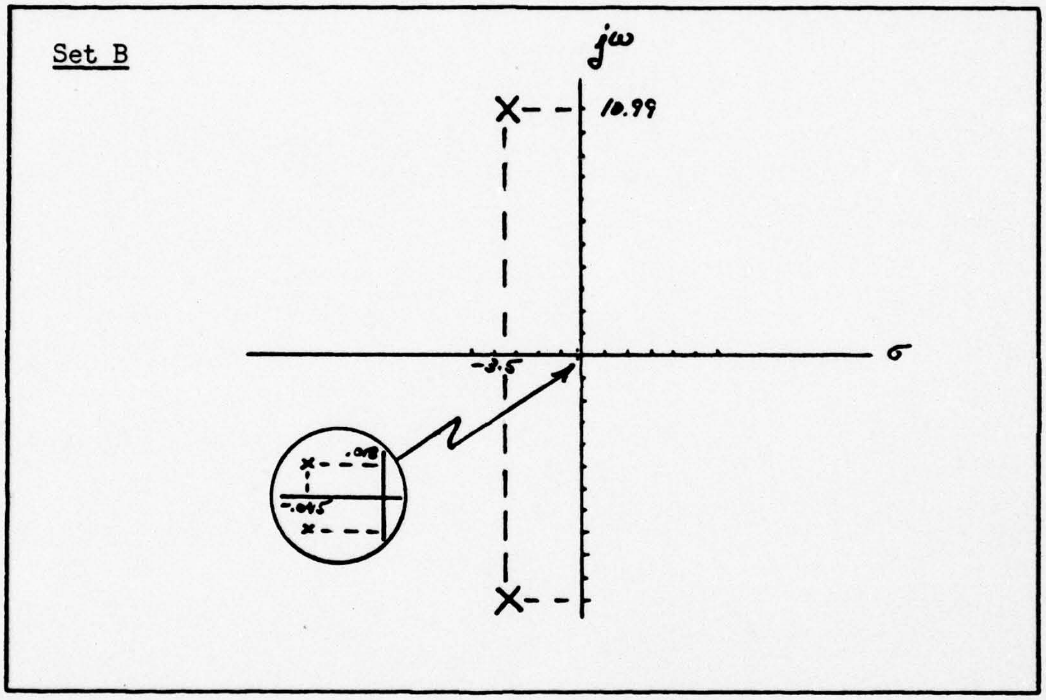

Fig. 5. Roots of Set B Equations.

For the Set B flight condition, unlike Set A, the roots indicate that the system is stable (Fig. 5). Again, the phugoid roots lie close to the imaginary axis while the remaining two roots appear as normal short period roots. Such a shift in system characteristics, from the unstable case of Set A to the stable situation of Set B, is due to the variable location relationship of the center of gravity and aerodynamic center, as a function of Mach number, discussed in

Chapter I. This relationship is expressed in the stability derivative C_{m_α} discussed earlier and is the key term in determining the stability of this system of equations.

Since in both cases, the phugoid roots are well behaved and stable, a short period approximation disgarding the phugoid oscillatory mode is sufficient to adequately model the system. Additionally, it is the rapid, transient response of the aircraft, represented by the short period mode, which is of interest. Again, based upon Reference 1, the short period equations can be expressed as follows:

$$\left[\frac{mU}{Sq} s - C_{z_\alpha}\right] \alpha(s) + \left[-\frac{mU}{Sq} s\right] \theta(s) = C_{z_{\delta_h}} \delta_h(s) \qquad (61)$$

$$\left[-\frac{\bar{c}}{2U} C_{m_{\dot{\alpha}}} s - C_{m_\alpha}\right] \alpha(s) + \left[\frac{I_{yy}}{Sq\bar{c}} s^2 - \frac{\bar{c}}{2U} C_{m_q} s\right] \theta(s) = C_{m_{\delta_h}} \delta_h(s) \qquad (62)$$

The Set A equations reduce to the following:

$$(1.726s + 4.4942)\ \alpha(s) + (-1.726s)\ \theta(s) = -.4504\,\delta_h(s) \qquad (63)$$

$$(.009272s - .1788)\ \alpha(s) + (.0135s^2 + .026779s)\ \theta(s) = -.6452\,\delta_h(s) \qquad (64)$$

Likewise, the Set B equations reduce to:

$$(1.1506s + 4.8132)\ \alpha(s) + (-1.1506s)\ \theta(s) = -.361\,\delta_h(s) \qquad (65)$$

$$(-.00164s + .7392)\ \alpha(s) + (.006s^2 + .018553s)\ \theta(s) = -.5157\,\delta_h(s) \qquad (66)$$

The TRANFUN analysis program (Ref. 16) is used in a similar manner as presented in Appendix B. Results show the characteristic equation of the short period system described by equations (63) and (64) to be:

$$.023301s^3 + .122895s^2 - .1882536s = 0 \qquad (67)$$

which produces the following roots:

Real	Imag
0.	0.
.1240223E + 01	0.
-.6514491E + 01	0.

In the S-plane, these appear as shown in Figure 6.

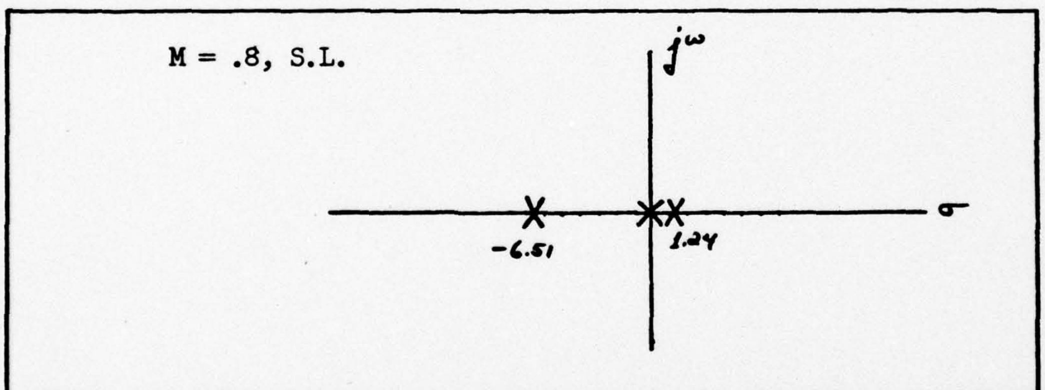

Fig. 6. Short Period Approximation Roots (Set A)

Again, the instability is present while the root locations, due to the simplification, have migrated less than one percent. The pole at S = 0 results from the fact that Θ was taken as zero in equations (61) and (62) which effectively eliminates the effects of gravity.

The system transfer functions of the reduced Set A equations (63) and (64) become:

$$\frac{\alpha(s)}{\delta_h(s)} = \frac{-.26095\ (s + 185.132)}{(s - 1.240223)(s + 6.514491)} \tag{68}$$

$$\frac{\theta(s)}{\delta_h(s)} = \frac{-47.61337\ (s + 2.686213)}{s\ (s - 1.240223)(s + 6.514491)} \tag{69}$$

The same process can be performed on Set B equations (65) and (66). The resulting short period characteristic equation is:

$$.0069s^3 + .04834s^2 + .93982s = 0 \tag{70}$$

The roots of this equation are:

Real	Imag
0.	0.
-3.501	-11.130
-3.501	+11.130

In the S-plane, these appear as shown in Figure 7.

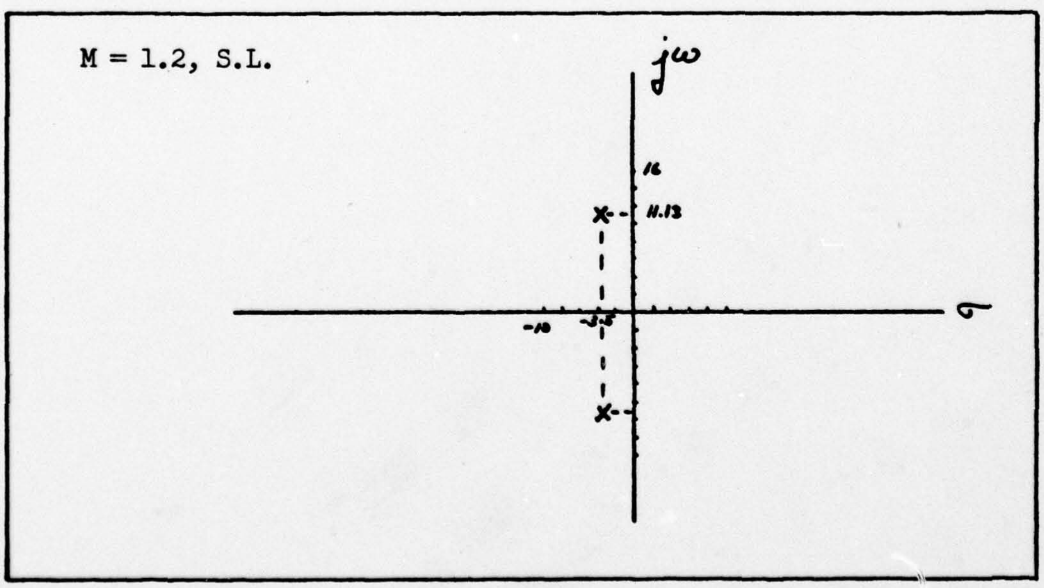

Fig. 7. Short Period Approximation Roots (Set B)

As expected, the system remains stable with only a minor shift in the root locations. Also, an additional root at the origin is introduced for the reason given earlier.

The two short period approximation transfer functions of Set B equations (65) and (66):

$$\frac{\alpha(s)}{\delta_h(s)} = \frac{-.31375\ (s + 277.037)}{(s + 3.501021 \pm 11.13j)} \tag{71}$$

$$\frac{\theta(s)}{\delta_h(s)} = \frac{-86.03576\ (s + 3.729762)}{s\ (s + 3.501021 \pm 11.13j)} \tag{72}$$

where ω_n , ω_d , ζ_{sp} , and τ_{sp} become:

$$\begin{aligned} \omega_n &= 11.667 \text{ Rad/sec} \\ \omega_d &= 11.130 \text{ Rad/sec} \\ \zeta_{sp} &= .3 \\ \tau_{sp} &= .539 \text{ sec} \end{aligned} \tag{73}$$

Response to Inputs

A further appreciation for the dynamic characteristics of the system can be gained by looking at the open-loop system response to various inputs.

The transfer function $\frac{\theta}{\delta_h}$ (Fig. 8) is used to demonstrate this response. This particular transfer function is chosen since pitch (θ), and ultimately pitch rate ($\dot{\theta}$), are of interest in investigating the longitudinal dynamics of an aircraft. The digital computer program PARTL is used to calculate the various responses (Ref. 10). Figure 9 shows the pole-zero locations of the basic airframe for the M = .8 condition at sea level reflected in equation (69).

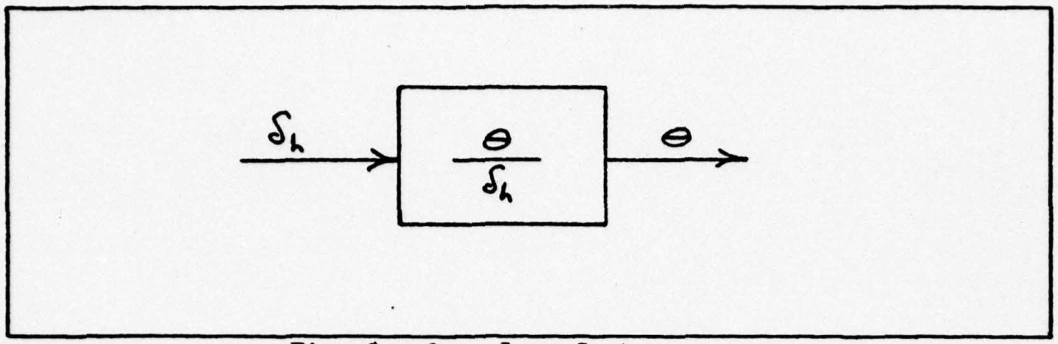

Fig. 8. Open Loop System.

The instability of the model in this flight condition is evident from the pole which lies in the right half plane. Figure 10 shows the pole-zero configuration based on equation (72) for the M = 1.2 case at sea level. In this flight condition, the stability of the model is reflected by the fact that all roots lie in the left half plane.

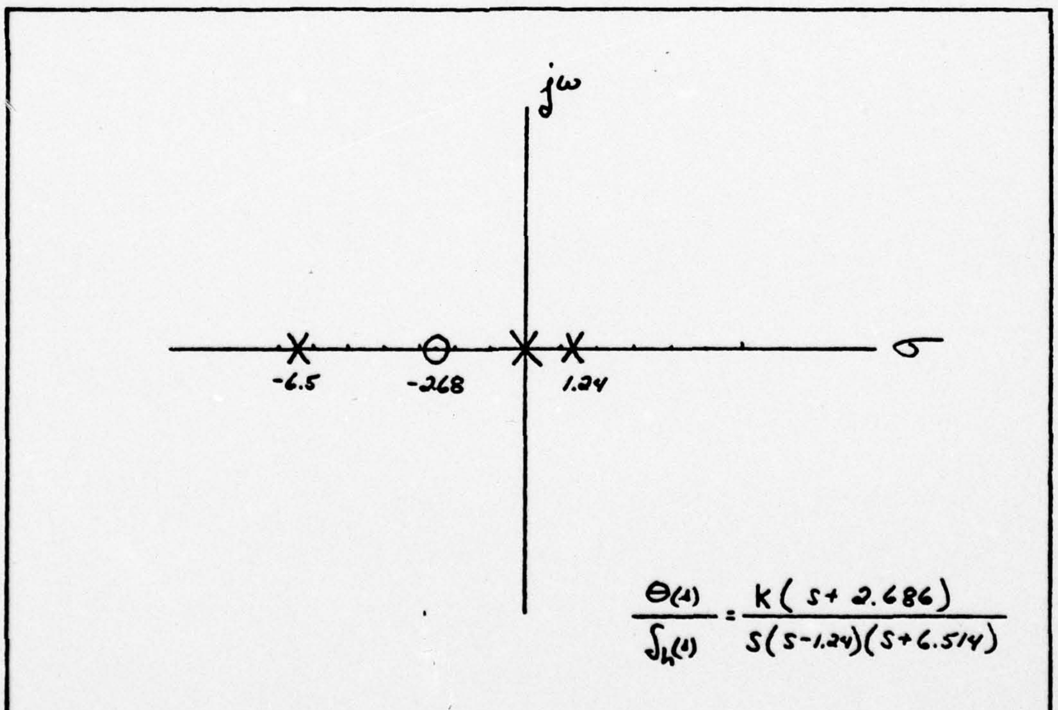

Fig. 9. Open Loop Pole-Zero Locations.

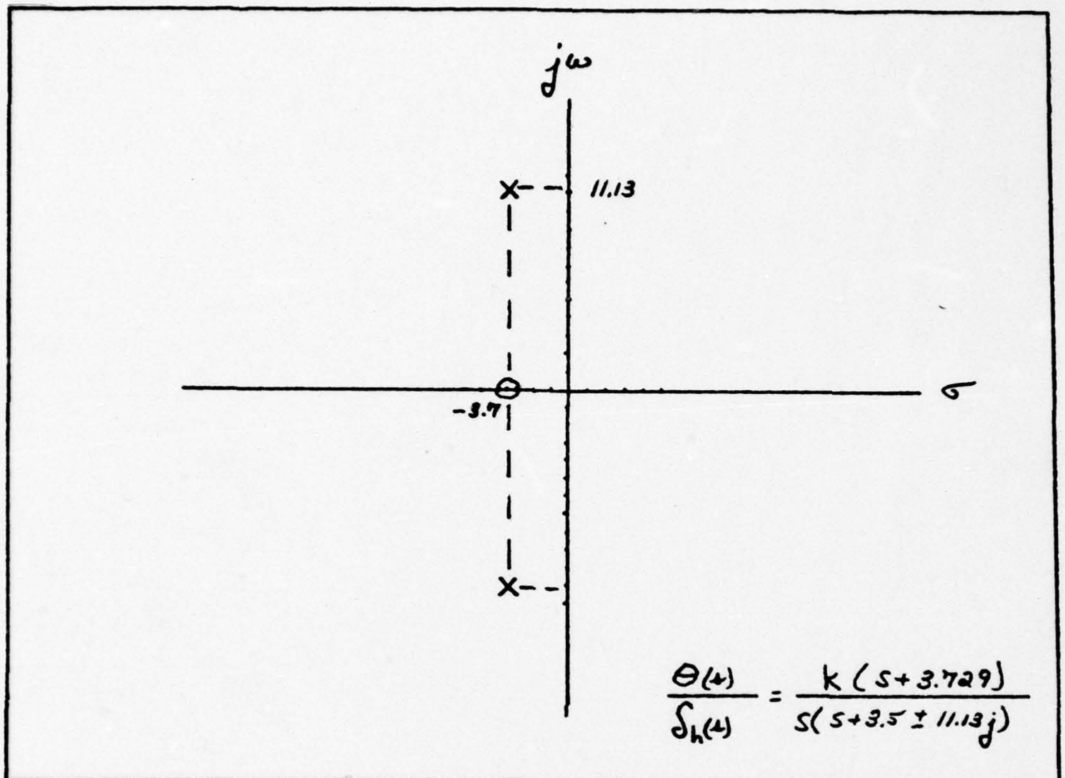

Fig. 10. Open Loop Pole Zero Locations.

Noting that F(T) represents Θ in the plots which follow, Figure 11a shows the response to a step horizontal stabilizer deflection for the M = .8 at sea level case; while, Figure 11b shows the corresponding response for the high Mach case.

The need for some type of control is clearly apparent in both cases. Figure 11a shows a very rapid parabolic divergence in the system for the M = .8 case. Figure 11b shows a lightly damped oscillation superimposed on a ramp type response. Here, although

the response to the constant step input, as expected, is ramp-like and stable, the light damping indicated by equation (73) to be $\zeta = .3$, is unsatisfactory. These response characteristics are more obvious in Figure 12. In this set of figures, the input is similar to a unit impulse. This input is given physical significance by imagining a pilot pulling back on the control stick slightly and then immediately returning the stick to neutral to null the command. Such a rapid series of commands should cause the nose to pitch-up as the aircraft attempts to begin a climb and then quickly lowering as the command is removed.

Figure 12a, reflecting the low Mach condition, is very similar to Figure 11a. Again, a rapid parabolic divergence results as the aircraft pitches up and continues to do so even when the command is removed. This phenomenon definitely reflects a dynamically unstable condition. Figure 12a, however, reflects the stable nature of the high Mach condition since the aircraft returns to a stable steady state after the perturbing command is removed. The extremely light damping ($\zeta = .3$), more evident here than in Figure 11b, remains unsatisfactory. For both flight conditions, these plots show the response of the open-loop is unacceptable. Some type of feedback control scheme is definitely necessary.

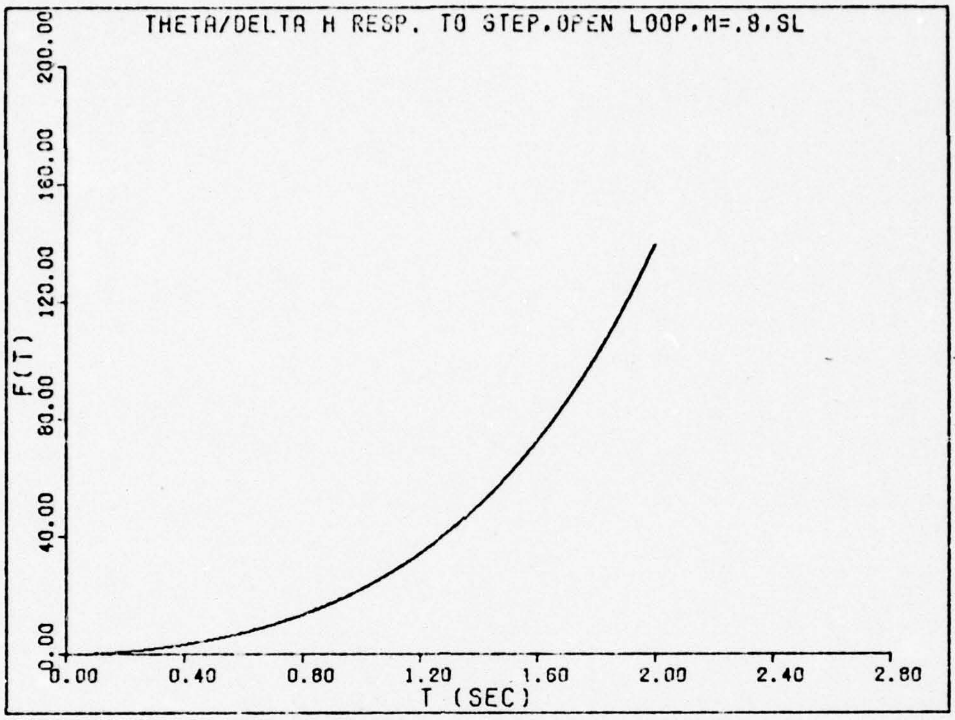

Fig. 11a. Step Response at M = .8.

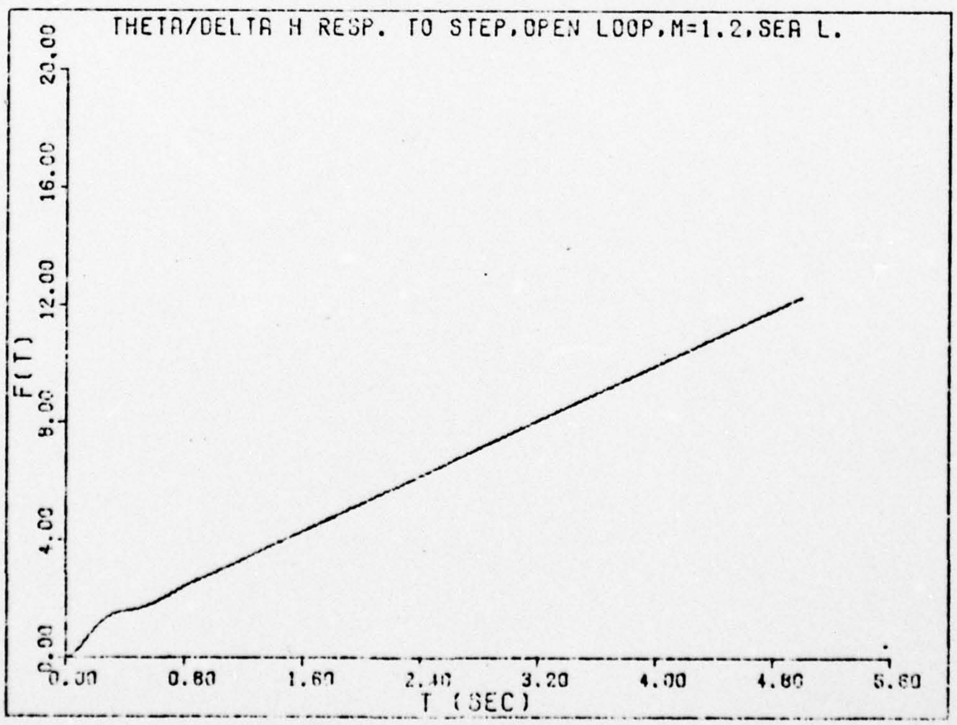

Fig. 11b. Step Response at M = 1.2.

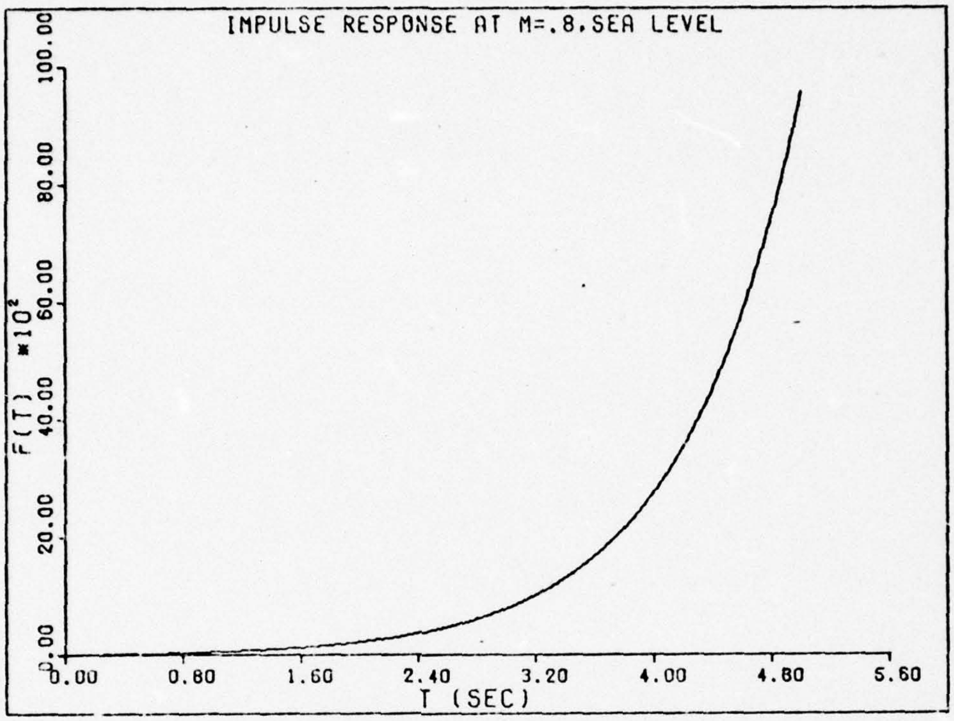

Fig. 12a. Impulse Response at M = .8.

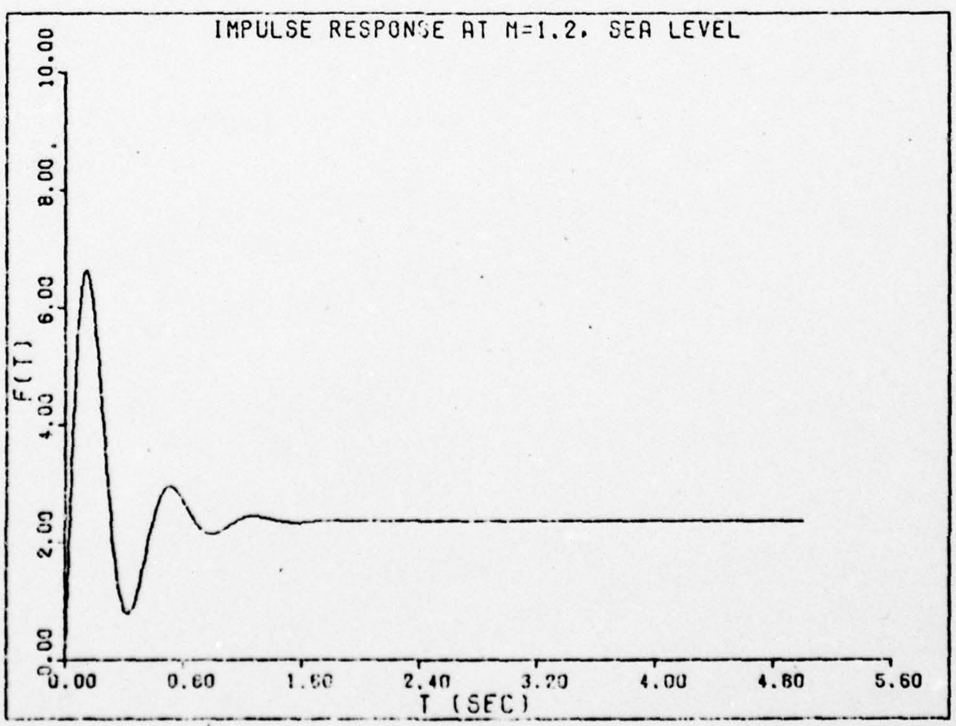

Fig. 12b. Impulse Response at M = 1.2.

Aircraft Actuator Servo

Before proceeding any further, the dynamics of the aircraft servo, which positions the horizontal stabilizer, must be considered. Reference 13 indicates that the command servo transfer function for this aircraft is:

$$\frac{\delta_{h_c}(s)}{\theta_c(s)} = \frac{(52)^2}{s^2 + 2(.7)52s + 52^2} \tag{74}$$

while that of the power actuator is:

$$\frac{\delta_h(s)}{\delta_{h_c}(s)} = \frac{20}{s + 20} \tag{75}$$

These are integrated with the aircraft dynamics as shown in Figure 13.

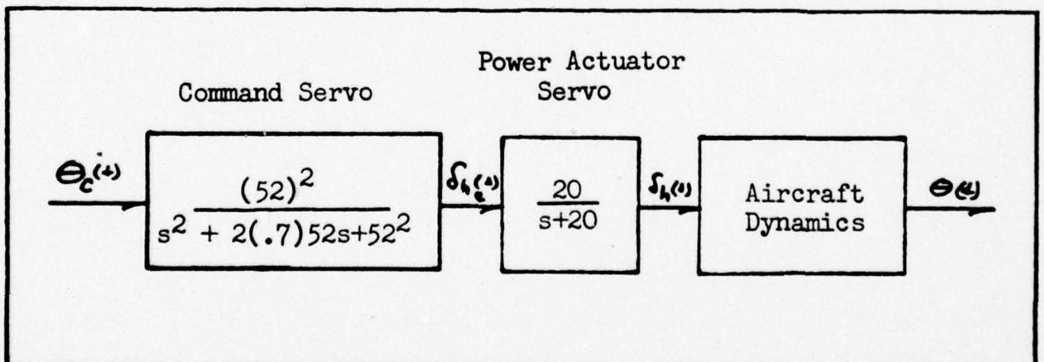

Fig. 13. Block Diagram of Servo and Aircraft.

The open loop transfer function of the cascaded network becomes:

$$\frac{\theta(s)}{\theta_c(s)} = \frac{\text{K gain (Zero of A/C Dynamics)}}{(s + 36.4 \pm 37.135j)(s + 20)(\text{Poles of A/C Dynamics})} \tag{76}$$

The conjugate roots produced by the command servo ($-36.4 \pm 37.135j$) are to the extreme left in the S-plane. Their effect on the system can be safely disregarded because of their high frequency. Their only appreciable effect would be the introduction of a small phase lag in the system. Therefore, the command servo will not be considered further in the remainder of this investigation.

Having accomplished this simplification, the system reduces to the closed loop representation shown in Figure 14.

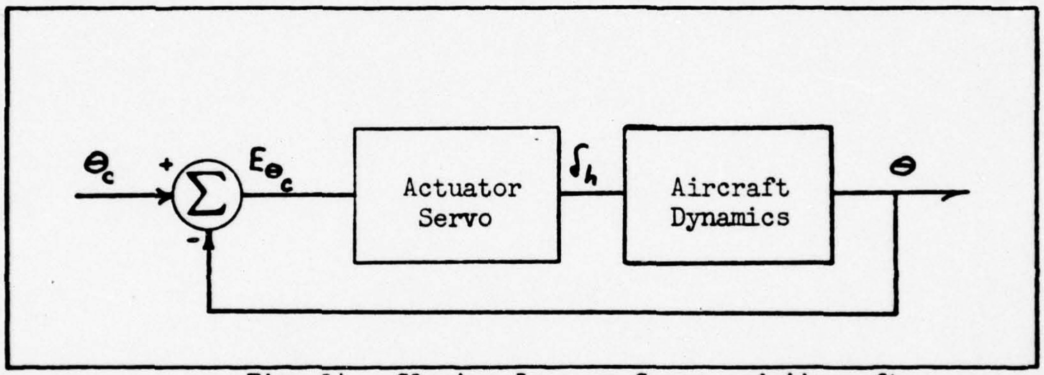

Fig. 14. Closing Loop on Servo and Aircraft.

The effect of the addition of the actuator servo to the system can now be analyzed. Use of the ROOTL computer program (Ref. 11) produces a variable gain root locus for each flight condition. The Mach .8 results appear in Figure 15 while Mach 1.2 results appear in Figure 16.

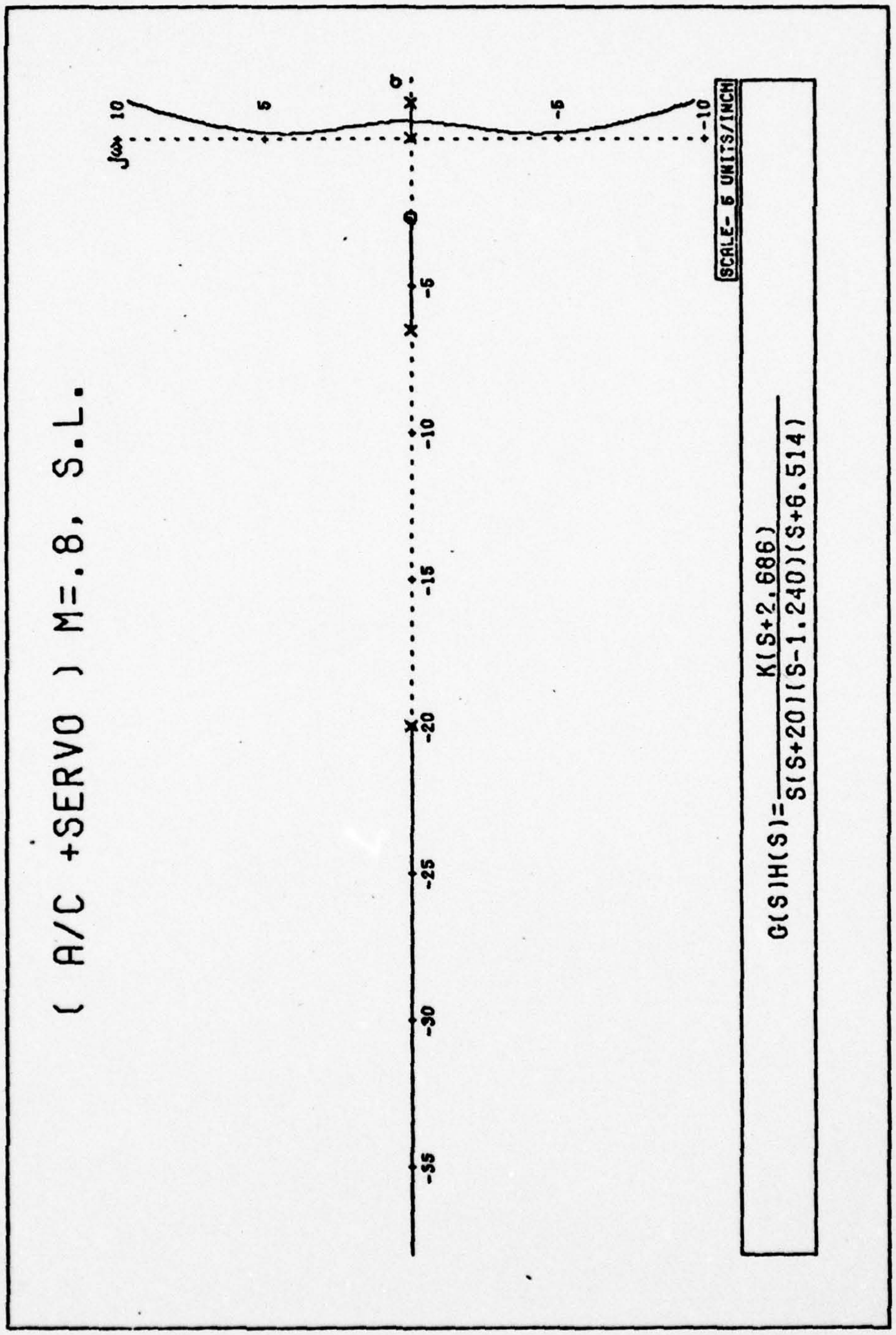

Fig. 15. Variable Gain Root Locus for Low Mach Case.

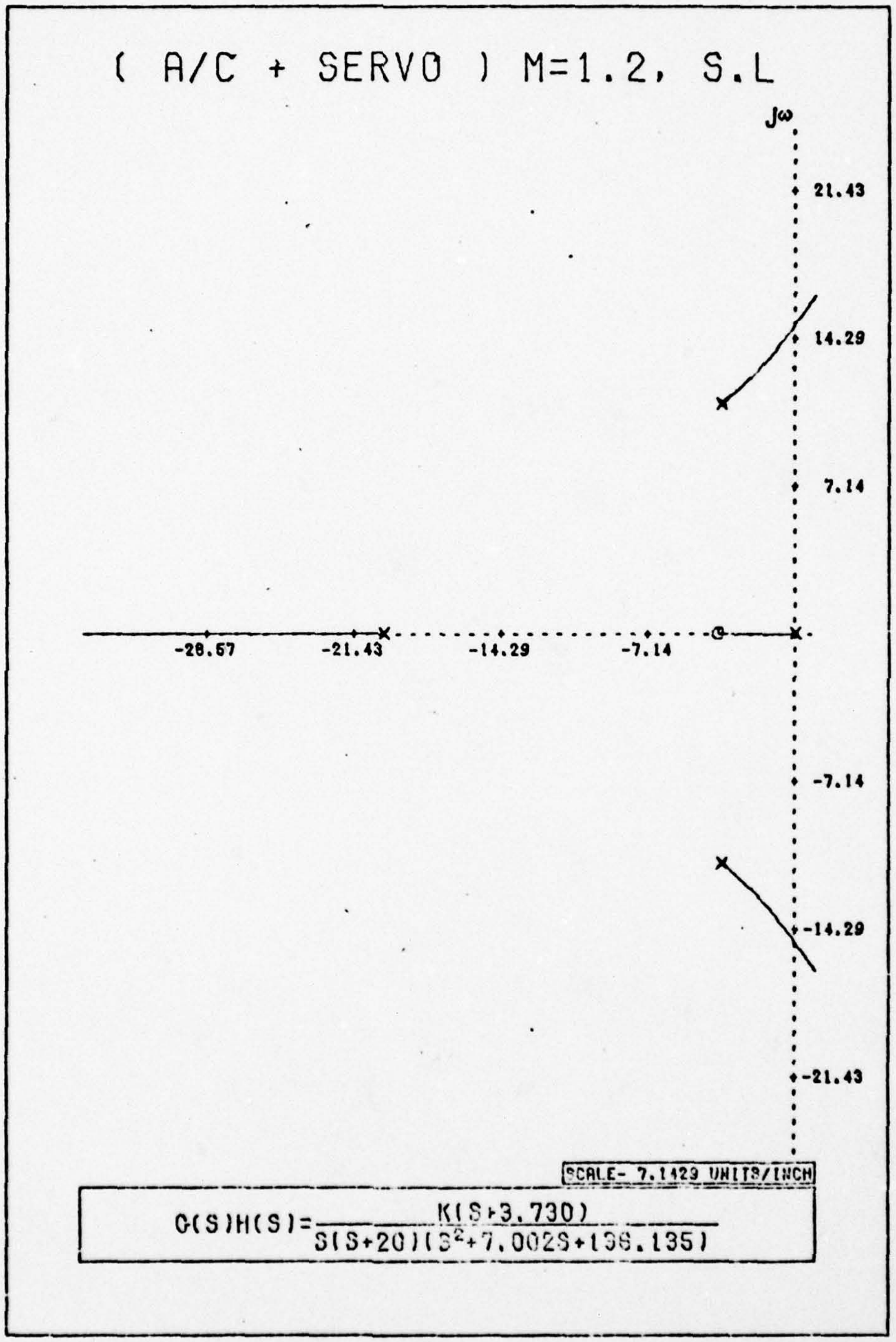

Fig. 16. Variable Gain Root Locus for High Mach Case.

The results of this root locus analysis, in which a rudimentary, unity feedback system is implemented, indicate that the high Mach case can be stabilized for a limited range of gain. Figure 15 points up a different situation. Here, no value of gain will stabilize the system. Compensation* , beyond more gain adjustment, is required for this flight condition.

Summary

This chapter, through the development and investigation of system characteristic equations and system input responses has shown the open loop dynamic character of the YF-16 modeling equations to be unsatisfactory. A short period approximation of the system, varying only slightly from a fully developed model considering both phugoid and short period oscillating modes, was shown to adequately represent the system. Additionally, a root locus analysis pointed out the need to compensate the system especially for M = .8 flight at sea level.

It is the compensation of this critical flight condition reflected in the Set A equations, which will be the focus of attention for the remainder of this investigation. The application of a classical lag compensator for analog implementation might suffice; however, as intimated earlier, investigation will focus on the implementation of a discrete optimal controller scheme specifically designed for digital computer implementation.

*Compensation: the introduction of additional equipment into a system to reshape its root locus in order to improve system performance.

IV. Control System Model and the C^* Concept

The purpose of this chapter is to present the development of a discretely controlled system model of the YF-16 incorporating in its design consideration the handling qualities response criteria C^*. First, the general form of a discrete servo control system model is presented. This is followed by a discussion of the C^* concept and its application to the proposed model.

The preceding chapter pointed out the unstable nature of Mach .8 flight at sea level for the YF-16. A requirement for some type of control system for this novel aircraft in this flight regime was repeatedly demonstrated. At this juncture, several options are available:

a. Synthesize a continuous control law using classical techniques and adapt it to a digital computer;

b. Synthesize a control law using continuous optimal control theory and again adapt it for a digital computer; or

c. Synthesize a control law using discrete regulator/servo theory (Ref. 18)

The latter approach is addressed here, due to its direct digital design nature. The theoretical approach which is implemented was first developed by Sandell (Ref. 12) and is similar to the more recent proposals of Stengel (Ref. 15) and Lee (Ref. 8). Lee points out the equivalence of his approach with that of Stengel; however, Lee's application is to a statically stable aircraft for a fixed sample rate. Here, a discrete optimal control formulation with a discrete quadratic performance index will be tested on a statically unstable

airframe for a variety of sample rates taking servo saturation effects into consideration.

As opposed to a regulator problem where perturbed states are returned to zero steady state values, this controller scheme will produce a sequence of controls to force the trajectory of the aircraft to follow some input reference signal introduced by the pilot. Pilot dynamics are not considered beyond the intimation that maneuvering commands originate with him with no time delays.

Control System Model

Recall that the continuous control system model as depicted in the state space representation of Figure 17, is based upon a continuous, linear, differential system of equations. The system is considered deterministic with no uncertainty or random inputs present while $\bar{u}$, $\bar{x}$ and $\bar{y}$, represent the control, state, and output vectors, respectively.

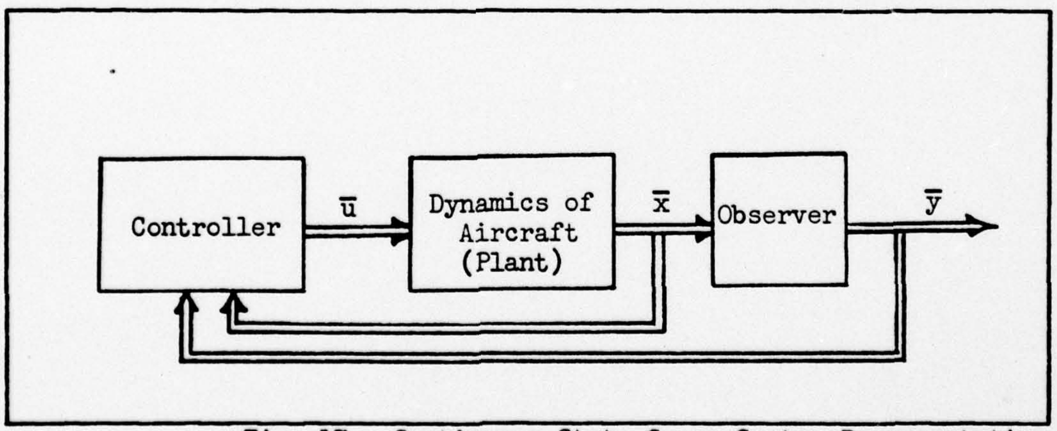

Fig. 17. Continuous State Space System Representation.

It should be noted that the observer matrix with its associated output vector $\bar{y}$ could be incorporated into the controller. However, for the purpose of clarity, it is desirable to separate the two. The above

figure, closely represents a regulator controller in that no external commands enter into the control scheme. If an external command signal is introduced into the system, the regulator problem is biased to follow that signal. The problem would then enter the realm of a servo or tracking problem. Such a situation is depicted in Figure 18.

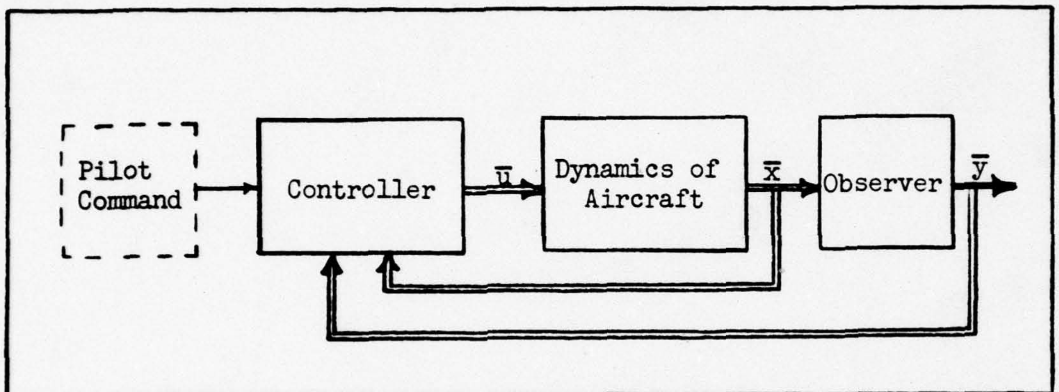

Fig. 18. Servo/Tracker System Representation with Bias Introduced to Define $\bar{x}_{s.s.}$ Other Than Zero.

Since a commitment to a discrete approach for digital computer implementation has been made, a digital equivalent of Figure 18 is necessary.

The proposed equivalent control system representation appears in Figure 19.

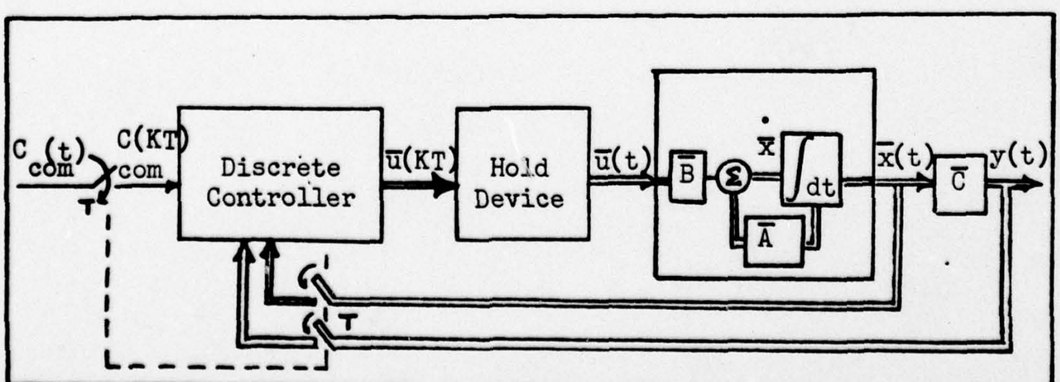

Fig. 19. Discrete System Servo Controller Scheme.

The symbolic T in Figure 19 represents the sample rate or how often samples of the continuous system are taken. The dashed line indicates that all switches close in unison. The continuous aircraft dynamic model is represented by the familiar linear equation set:

$$\dot{\bar{x}} = \overline{A}\overline{x} + \overline{B}\overline{u} \tag{77}$$

$$y = \overline{C}\overline{x} \tag{78}$$

where $\overline{A}$, $\overline{B}$, and $\overline{C}$ are the dynamics, control and observer matrix, respectively (Ref. 3). Other than determining what $\overline{A}$, $\overline{B}$, and $\overline{C}$ are, it is necessary to define the system states ($\overline{x}$), the system output ($\overline{y}$), and the nature of the input command ($C_{command}$).

C^* Concept

In 1966, Tobie, Elliott, and Malcom introduced the C^* concept as a new longitudinal performance criterion as an outgrowth of the Cornell Aeronautical Laboratory "Thumbprint" (Fig. 26), and in response to an effort of determining what levels and types of handling qualities are required by pilots (Ref. 17). The C^* criterion is an example of specifying short period handling qualities in terms of aircraft parameters familiar to a pilot ($\dot{\theta}$ and N_z) while still including the traditional short period frequency (ω_N) and damping requirements (ζ). As these authors point out:

> "It appears likely that the pilot responds to the motions that naturally tend to dominate the aircraft's characteristic response. For example, at low velocity where N_z cues are weak, pitch cues would be most important. At high velocity where very slight pitching may accompany sizable acceleration changes N_z cues would predominate. It is

postulated that the pilot then responds to a blend of pitch rate and normal acceleration, with the blend rates varying in accordance with natural variations in aircraft response. The blend of response parameters has been named C^*."

C^* is defined by the following expression:

$$C^* = K_z N_z + K_{\dot{\theta}} \dot{\theta} + K_{\ddot{\theta}} \ddot{\theta} \tag{79}$$

where the units/values of Table IV apply.

Table IV

<u>C^* Terms Defined</u>

Term	Units	Value
C^*	g's	variable
N_z	g's	variable
$\dot{\theta}$	Rad/sec	variable
$\ddot{\theta}$	Rad/sec^2	variable
K_z	g's-sec^2	1.0 (arbitrarily chosen as unity)
$K_{\dot{\theta}}$	g's-sec	$\frac{V_{co}}{32.2}$ (where $V_{co}^* = 400$ ft/sec)
$K_{\ddot{\theta}}$	g's-sec	$\frac{\text{distance to c.g. from pilot}}{\text{gravity}} = \frac{11.58}{32.2} = .36$
		*V_{co}: cross over velocity at which the normal acceleration and pitch rate give equal cues to the pilot.

The acceptable range of the C^* transient response to a step input falls within the appropriate bounds of the C^* time history envelopes of Figure 20. The four regions indicated have the following significance:

I - Optimal response (aerial combat, ground attack, and penetration);

II - Not as critical response area (air refueling, cruise);

III - Category for conditions not covered by I, II (loiter);

IV - Power approach (landing).

These regions have a direct correlation with the category system of MIL-F-8785B (Ref. 9).

With this background in the evaluation and meaning of the C^* concept as a well defined criterion on the handling qualities of an aircraft, the system model (Fig. 19) can be put into perspective.

In this study, the C^* envelope will be used to measure the response of the system with satisfactory response defined as falling within the innermost C^* boundary limit. The output of the system (y(t)) is replaced by the term C^*_{act}; $C^*_{act(t)}$ being the actual system C^* response. In this manner, the C^* response becomes a function in the performance index of the system. Additionally, the input to the system $C_{command}^{(t)}$ is replaced by $C^*_{com(t)}$ which represents the desired C^* response requested by the pilot. In a physical sense, the YF-16 model is asked to track a pilot step input command, here chosen as unity since it lies in the center of the envelope bounds. In the YF-16, using a side mount control stick, the pilot inputs a desired steady state value of the C^* parameter to the controller which is then required to have a short period response which tracks the system C^* response to the

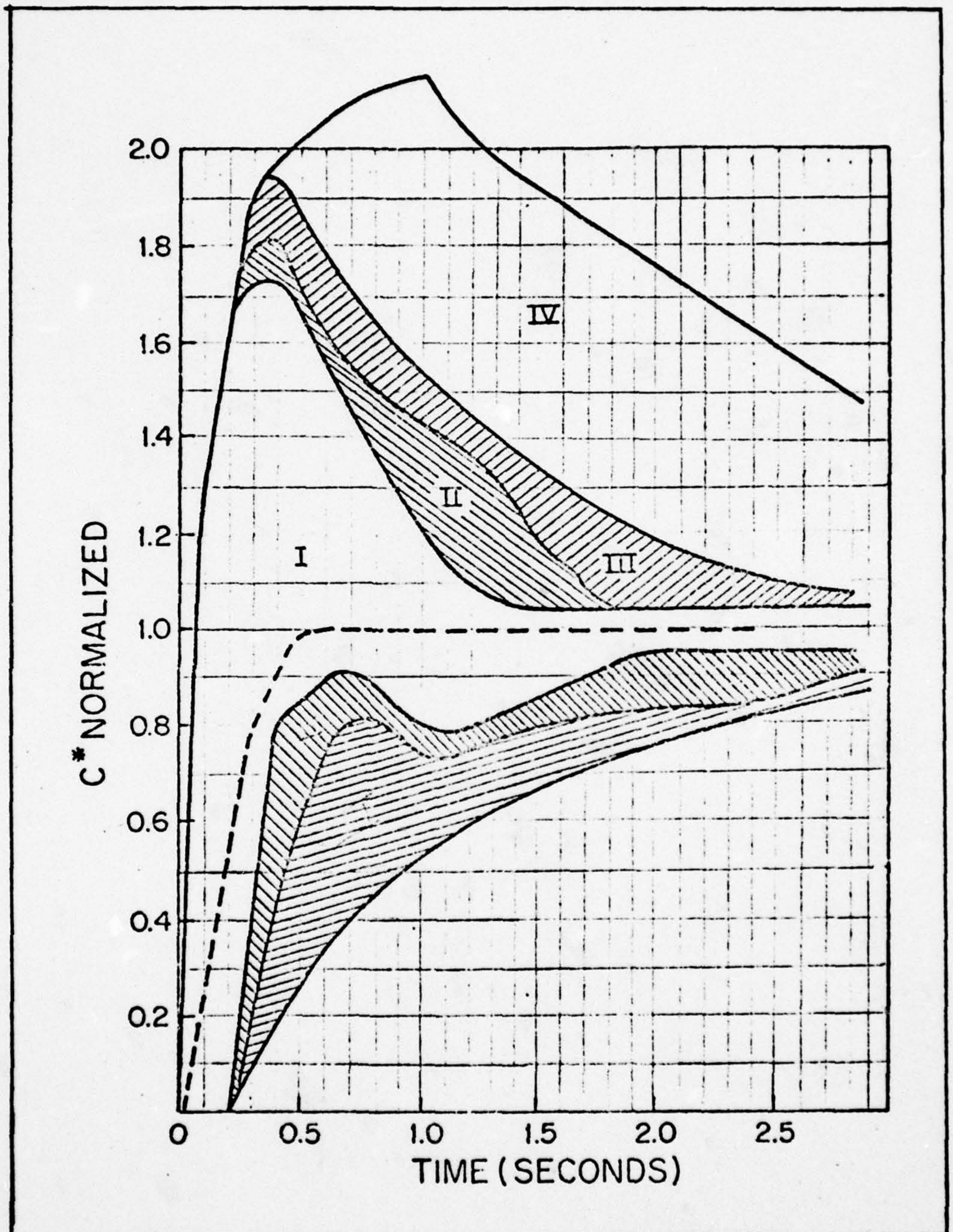

Fig. 20. C* Time History Envelope (Ref. 8)

commanded C^* value. It is apparent that the observer matrix ($\bar{C}$) must transform the system states ($\bar{x}$) into a blend of system states now redefined by equation (79) as $C^*_{act(t)}$.

The next chapter will determine the nature of this transformation matrix based upon a definition of the system states in equation (77).

V. Continuous to Discrete System Transformation

This chapter presents the transformation from a continuous sytem representation to a discrete system representation necessary to continue development toward the discrete model presented in Figure 19.

The chapter begins with the continuous system state model. Here, the nature of the observer matrix, which transforms the system states into a C^* representation, is developed. The chapter concludes with a brief discussion of the discretization process used to represent the continuous system in discrete time.

Continuous System State Model

Recall from Chapter IV that an open loop linear continuous system can be defined by the first order state variable equation set:

$$\frac{d}{dt}\ \bar{x}(t) = \bar{A}\bar{x}(T) + \bar{B}\ u(t) \tag{77}$$

$$y(t) = \bar{C}\ \bar{x}(t) \tag{78}$$

It is necessary, therefore, to transform the three original equations of motion (equations (1), (2), and (3)) into such a representation for their implementation in the controlled system model developed in the previous chapter (Fig. 19). This is done as detailed in Appendix C using the short period approximation with the resulting state variable equation being:

$$\begin{bmatrix} \dot{\alpha} \\ \ddot{\theta} \\ \dot{\delta}_h \end{bmatrix} = \begin{bmatrix} -2.603975 & 1.0 & -.260965 \\ 15.058542 & -2.682339 & -47.676367 \\ 0 & 0 & -20.0 \end{bmatrix} \begin{bmatrix} \alpha \\ \dot{\theta} \\ \delta_h \end{bmatrix} + \begin{bmatrix} 0 \\ 0 \\ 20.0 \end{bmatrix} \tag{182}$$

The resulting dynamics matrix ($\bar{A}$) is (3 x 3) while the control matrix ($\bar{B}$) is seen to be (3 x 1). A check of the controllability of the system, determined by assuring that $\left| \bar{B} \,\vdots\, \bar{A}\bar{B} \,\vdots\, \bar{A}^2\bar{B} \right| \neq 0$, shows the system is completely controllable.

Referring now to the output equation:

$$y(t) = \bar{C}\,\bar{x}(t) \tag{78}$$

We can replace the output vector y(t) by $C^*_{act}(t)$ as discussed in the previous chapter. The resulting output equation is:

$$C^*_{act}(t) = \bar{C}\,\bar{x}(t) \tag{80}$$

As shown earlier, C^* is a linear blend of N_z, $\dot{\theta}$, and $\ddot{\theta}$ expressed as:

$$C^* = K_z N_z + K_{\dot{\theta}}\dot{\theta} + K_{\ddot{\theta}}\ddot{\theta} \tag{79}$$

or equivalently as:

$$C^* = \begin{bmatrix} K_{\dot{\theta}} & K_z & K_{\ddot{\theta}} \end{bmatrix} \cdot \begin{bmatrix} \dot{\theta} \\ N_z \\ \ddot{\theta} \end{bmatrix} \tag{81}$$

It is evident that a mismatch exists between the states required to calculate C^*, indicated in equation (81) and the actual system states, developed in Appendix C, and shown in equation (182). Some transformation matrix $\bar{D}$ must be found to transform system states to

the required states needed to calculate C^*. This situation is expressed in equation (82) where some conformal, (3 x 3), $\bar{D}$ matrix is shown accomplishing the transformation.

32
$$\begin{bmatrix} \dot{\theta} \\ N_z \\ \ddot{\theta} \end{bmatrix} = \begin{bmatrix} D_{11} & D_{12} & D_{13} \\ D_{21} & D_{22} & D_{23} \\ D_{31} & D_{32} & D_{33} \end{bmatrix} \cdot \begin{bmatrix} \alpha \\ \dot{\theta} \\ \delta_h \end{bmatrix} \tag{82}$$

Three linear combinations of α , $\dot{\theta}$, and δ_h must be found which are equal to $\dot{\theta}$, N_z, and $\ddot{\theta}$, respectively.

The first expression is the trivial relationship:

33
$$\dot{\theta} = D_{11}\alpha + D_{12}\dot{\theta} + D_{13}\delta_h \tag{83}$$

34
$$\dot{\theta} = 0 + 1.0\,\dot{\theta} + 0\,\delta_h \tag{84}$$

For the next equation,

35
$$N_z = D_{21}\alpha + D_{22}\dot{\theta} + D_{23}\delta_h \tag{85}$$

recall that,

$$N_z = \frac{U}{g}\left[\dot{\theta} - \dot{\alpha}\right] = K_u\left[\dot{\theta} - \dot{\alpha}\right] \tag{86}$$

From Appendix C, equation (174) shows $\dot{\alpha}$ as:

$$\dot{\alpha} = \frac{C_{z_\alpha}}{K_1}\alpha + 1.0\,\dot{\theta} + \frac{C_{z_{\delta h}}}{K_1}\delta_h \tag{174}$$

This equation can be substituted into equation (86) leading to the following development:

$$N_z = K_u\left[\dot{\theta} - \left(\frac{C_{z_\alpha}}{K_1} + 1.0\,\dot{\theta} + \frac{C_{z_{\delta_h}}}{K_1}\delta_h\right)\right] \tag{87}$$

$$N_z = \left[-\frac{K_u}{K_1}C_{z_\alpha}\right]\alpha + \left[-\frac{K_u}{K_1}C_{z_{\delta_h}}\right]\delta_h \tag{88}$$

From this development, it is now evident that:

$$D_{21} = -\frac{K_u}{K_1}C_{z_\alpha} \tag{89}$$

$$D_{22} = 0 \tag{90}$$

$$D_{23} = -\frac{K_u}{K_1}C_{z_{\delta_h}} \tag{91}$$

Similarly, Appendix C, equation (178) shows the relationship of $\ddot{\theta}$ to α, $\dot{\theta}$, and δ_h as:

$$\ddot{\theta} = \frac{1}{K_2}\left[C_{m_\alpha} + \frac{K_3}{K_1}C_{m_{\dot{\alpha}}}C_{z_\alpha}\right]\alpha + \frac{K_3}{K_2}\left[C_{m_{\dot{\alpha}}} + C_{m_{\dot{\theta}}}\right]\dot{\theta} + \frac{1}{K_2}\left[\frac{K_3}{K_1}C_{m_{\dot{\alpha}}}C_{z_{\delta_h}} + C_{m_{\delta_h}}\right]\delta_h \tag{178}$$

which completes the development of the D matrix by defining D_{31}, D_{32}, and D_{33} as: $\frac{1}{K_2}\left[C_{m_\alpha} + \frac{K_3}{K_1}C_{m_{\dot{\alpha}}}C_{z_\alpha}\right]$, $\frac{K_3}{K_2}\left[C_{m_{\dot{\alpha}}} + C_{m_{\dot{\theta}}}\right]$

and, $\frac{1}{K_2}\left[\frac{K_3}{K_1}C_{m_{\dot{\alpha}}}C_{z_{\delta_h}} + C_{m_{\delta_h}}\right]$

respectively.

Having determined $\overline{D}$, equation (82) can be written as:

$$\begin{bmatrix} \dot{\theta} \\ N_Z \\ \ddot{\theta} \end{bmatrix} = \left[\begin{array}{c|c|c} 0 & 1.0 & 0 \\ -\frac{K_u}{K_1} C_{Z_\alpha} & 0 & -\frac{K_u}{K_1} C_{Z_{\delta_h}} \\ \frac{1}{K_2}\left[C_{m_\alpha} + \frac{K_3}{K_1} C_{m_{\dot{\alpha}}} C_{Z_\alpha}\right] & \frac{K_3}{K_2}\left[C_{m_{\dot{\alpha}}} + C_{m_q}\right] & \frac{1}{K_2}\left[\frac{K_3}{K_1} C_{m_{\dot{\alpha}}} C_{Z_{\delta_h}} + C_{m_{\delta_h}}\right] \end{array}\right] \begin{bmatrix} \alpha \\ \dot{\theta} \\ \delta_h \end{bmatrix} \tag{92}$$

Substituting this expression into equation (81), the resulting expression for C^* is:

$$C^* = \begin{bmatrix} K_{\dot{\theta}} & K_Z & K_{\ddot{\theta}} \end{bmatrix} \cdot \left[\begin{array}{c|c|c} 0 & 1.0 & 0 \\ -\frac{K_u}{K_1} C_{Z_\alpha} & 0 & -\frac{K_u}{K_1} C_{Z_{\delta_h}} \\ \frac{1}{K_2}\left[C_{m_\alpha} + \frac{K_3}{K_1} C_{m_{\dot{\alpha}}} C_{Z_\alpha}\right] & \frac{K_3}{K_2}\left[C_{m_{\dot{\alpha}}} + C_{m_q}\right] & \frac{1}{K_2}\left[\frac{K_3}{K_1} C_{m_{\dot{\alpha}}} C_{Z_{\delta_h}} + C_{m_{\delta_h}}\right] \end{array}\right] \begin{bmatrix} \alpha \\ \dot{\theta} \\ \delta_h \end{bmatrix} \tag{93}$$

This expression can be simplified to:

$$C^* = \left[\begin{array}{c|c|c} -\frac{K_Z K_u}{K_1} C_{Z_\alpha} + \frac{K_{\ddot{\theta}}}{K_2}\left(C_{m_\alpha} + \frac{K_3}{K_1} C_{m_{\dot{\alpha}}} C_{Z_\alpha}\right) & K_{\dot{\theta}} + \frac{K_{\ddot{\theta}} K_3}{K_2}\left(C_{m_{\dot{\alpha}}} + C_{m_q}\right) & -\frac{K_Z K_u}{K_1} C_{Z_{\delta_h}} + \frac{K_{\ddot{\theta}}}{K_2}\left[\frac{K_3}{K_1} C_{m_{\dot{\alpha}}} C_{Z_{\delta_h}} + C_{m_{\delta_h}}\right] \end{array}\right] \begin{bmatrix} \alpha \\ \dot{\theta} \\ \delta_h \end{bmatrix} \tag{94}$$

Substituting into this expression the appropriate values from Table III, Table IV, and the value of $K_u = \frac{u}{g} = 27.75155$ based on .8 Mach at sea level, results in the following expression:

$$C^* = \begin{bmatrix} 77.685 & 11.423 & -9.921 \end{bmatrix} \cdot \begin{bmatrix} \alpha \\ \dot{\theta} \\ \delta_h \end{bmatrix} \tag{95}$$

Equation (95) fixes the value of the $\bar{C}$ observer matrix indicated in Figure 19. It is this matrix which will transform the system states into the system scalar output C^*. Additionally, the system is found to be completely observable since the determinant of $\left[\bar{C}^T \,\vdots\, \bar{A}^T\bar{C}^T \,\vdots\, (\bar{A}^T)^2\bar{C}^T\right]$ is nonsingular.

The continuous system described by equations (182) and (95) is then completely controllable and observable which provide the sufficient conditions for the regulation of the system output.

Discrete State Model

Because of the need to implement the control system in a digital flight computer, equation set (77) and (78) must be transformed into an equivalent discrete form. When the state model of a continuous system is given by the equation set (77) and (78), the discrete state model for the same system with a piecewise constant input is given by a difference equation set of the form:

$$\bar{x}(K+1)T = \bar{A}_d\,\bar{x}(KT) + \bar{B}_d\,u(KT) \tag{96}$$

$$y(KT) = \bar{C}_d\,\bar{x}(KT) \tag{97}$$

where,

$$\bar{A}_d = e^{\bar{A}T} \tag{98}$$

$$\bar{B}_d = \int_0^T e^{\bar{A}T}\,\bar{B}\,dt \tag{99}$$

and T is the sample rate (Ref. 2).

Numerous methods are available for the calculation of the state transition matrix $\bar{A}_d$. For example, the "Solution by Functions of a

Matrix" method (Ref. 2) could be used with the values of the $\bar{A}_d$ and $\bar{B}_d$ matrices determined by hand as a general function of the variable T. Additionally, digital computer software packages are available to compute the values of $\bar{A}_d$ and $\bar{B}_d$. This is the method chosen in this study since the matrices may be determined rapidly for any specified sample rate in a call to a subroutine nested in a more complex main program.

In particular, $\bar{A}_d$ and $\bar{B}_d$ are digitally calculated in this research by use of the digital subroutine DSCRT discussed in Ref. 6. In the calculation, $\bar{B}_d$ is determined by evaluating the series:

$$\bar{B}_d = \bar{I}\delta + \frac{\bar{A}\delta^2}{2!} + \frac{\bar{A}^2\delta^3}{3!} + \cdots + \bar{A}^{NT-1}\frac{\delta^{NT}}{NT!} \qquad (100)$$

while,

$$\bar{A}_d = \bar{I} + \bar{A} \cdot \bar{B}_d \qquad (101)$$

where δ and NT are specified in the call to the subroutine (see Appendix E).

Examples of $\bar{A}_d$ and $\bar{B}_d$ for various values of T are listed in Table V.

Table V

$\bar{A}_d$ and $\bar{B}_d$ Matrices as a Function of Sample Rate

$$\bar{A}_d \qquad\qquad \bar{B}_d$$

T = 1/50 sec

$$\begin{bmatrix} .9521122 & .0189892 & -.0122758 \\ .2859504 & .9506241 & -.7653255 \\ 0 & 0 & .6703200 \end{bmatrix} \qquad \begin{bmatrix} -.0020253 \\ -.1647557 \\ .3296800 \end{bmatrix}$$

T = 1/70 sec

$$\begin{bmatrix} .9650 & .01376 & -.997504 \\ .2073 & .9639 & -.5814 \\ 0 & 0 & .7515 \end{bmatrix} \qquad \begin{bmatrix} -.0009032 \\ -.08757 \\ .2485 \end{bmatrix}$$

T = 1/100 sec

$$\begin{bmatrix} .9750 & .009742 & -.004528 \\ .1467 & .9743 & -.4265 \\ 0 & 0 & .8187 \end{bmatrix} \qquad \begin{bmatrix} -.0003916 \\ -.04427 \\ .1813 \end{bmatrix}$$

VI. ZOH, Optimal Controller and Simulation Development

This chapter presents the development of the sequence of optimal scalar controls u(KT) which will drive the system shown in Figure 19 to the commanded steady state value of C^* input by the pilot. As Figure 19 indicates, the controller accepts sampled information about the system and uses this information to construct control inputs to the system. The determination of the control law will be accomplished by minimizing an appropriate discrete penalty function with zero steady state error. The resulting controls are step-like in nature as shown in Figure 21.

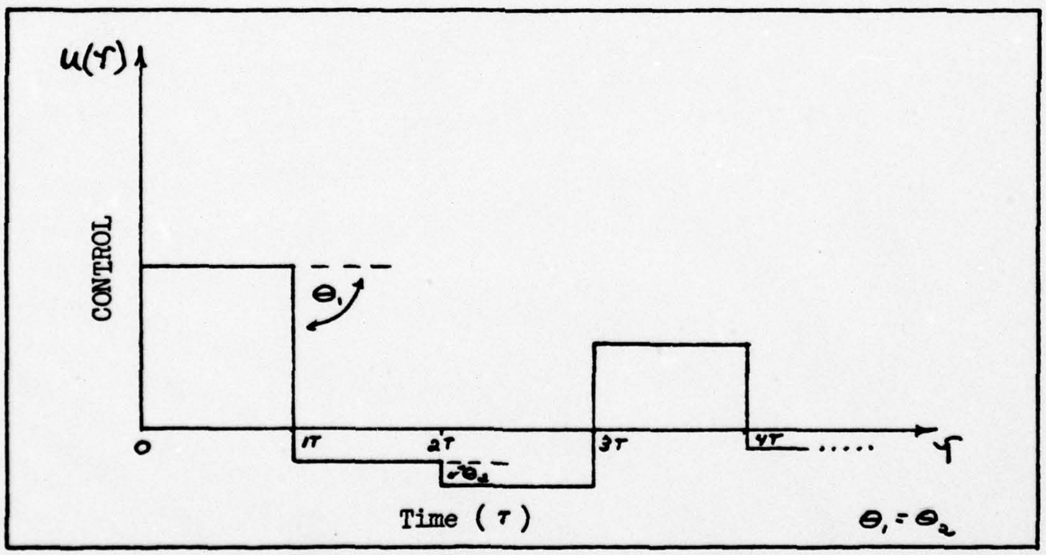

Fig. 21. Nature of Optimal Controls.

From Figure 21, it is apparent that the control u(KT) takes some constant value during the time period between samples. That is:

$$u(KT) = \text{constant} \quad \forall \; (KT) \leq \tau < (K+1)T, \; K = 0,1,2,3,\ldots N \tag{102}$$

Additionally, the sample interval (T) remains constant while the magnitude of the control is allowed to vary. This series of piecewise constant step controls corresponds to the shift-like, control stick input commands introduced by a pilot. Although a step command may not represent the most common pilot input, the step response implicitly describes the response to other inputs that a pilot uses. Additionally, Figure 21 is indicative of the output of a Zero Order Hold device.

This chapter will first discuss the general concepts of a hold device and in particular, the Zero Order Hold. Next, a discussion of the discrete penalty function selected with respect to which the performance of the system is optimized is presented. The recursive control algorithm which minimizes this cost function is then incorporated in a computer program developed for this investigation. A discussion of the structuring of this simulation program is presented. The chapter concludes with the development of the closed loop system eigenvalues. The determination of these eigenvalues is incorporated as a part of the software and used to track the migration of system roots as a function of sample rate.

Zero Order Hold Device

The type of hold device incorporated in a digital control system can play a decisive role in determining whether the system is stable especially at lower sample rates. A hold device serves to convert a discrete time sequence of numbers, separated in time by T-second intervals, into a continuous time function in order to provide a suitable input to a continuous-time component. The particular hold device chosen represents a D/A converter which constructs a piecewise

continuous control signal from a pulse sequence of numbers each of which represent a discrete control signal. For a control problem such as this, it is more appropriate to think in terms of extrapolating the present control over the time interval between samples rather than trying to reconstruct some signal which is more along the vein of a communications problem.

Between sampling instances, the hold device extrapolates between the most recent sample and the next to follow.

A power series expansion of a continuous signal $u(t)$ in the interval between sampling instant KT and (K+1)T can be expressed as:

$$u(t) = u(KT) + \frac{d\left[u(KT)\right]}{dT}\frac{(t-KT)}{1!} + \frac{d^2\left[u(KT)\right]}{dT}\frac{(t-KT)^2}{2!} + \ldots$$

$$\forall\, KT \leq t < (K+1)T \qquad (103)$$

Using the higher order derivatives of $u(t)$, for the purpose of more accurate extrapolation, can meet with serious difficulties in maintaining system stability. This is due to the fact that the higher the order of the derivative to be approximated, the larger the number of delay pulses required since one time interval must pass for each discrete control needed in the power series. The accuracy of the estimate of a derivative is then a function of the number of time delays. It is these time delays which have an adverse effect on the stability of a feedback control system. The value of the first derivative is known from the calculus to be approximated by the simple difference equation:

$$\frac{1}{T}\left[u(KT) - u(K-1)T\right] \approx \dot{u}(t) \qquad (104)$$

It is apparent that for this first derivative approximation, both the present sample value and the immediate past sample value are needed.

For higher order derivatives, the number of past control pulses required grows larger and larger. For example, the second derivative:

$$\ddot{u}(t) \approx \frac{1}{T^2}\left[u(KT) - 2u(K-1)T + u(K-2)T \right] \qquad (105)$$

requires three consecutive controls. Equation (103) can be thought of as a best-fit m^{th} order polynomial approximation of $u(t)$ which may be rewritten as:

$$u(t) = u(KT + \tau) = A_m \tau^m + A_{m-1} \tau^{m-1} + \dots A_2 \tau^2 + A_1 \tau + A_0 \qquad (106)$$

where:

$$\begin{aligned} \tau &= t-KT \\ A_0 &= u(KT) \\ A_1 &= \frac{\dot{u}(t)}{1!} \\ A_2 &= \frac{\ddot{u}(t)}{2!} \end{aligned} \qquad (107)$$

where $\dot{u}(t)$ and $\ddot{u}(t)$ are as in equations (104) and (105), respectively, and m = the order of the polynomial.

As Kuo points out (Ref. 7), when $m = 0$ the polynomial is of zero order and the ZOH extrapolator results which generates only $u(KT)$:

$$u(KT+\tau)\Big|_{m=0} = A_0 \quad , \quad \forall \quad 0 \leq \tau < T \qquad (108)$$

where A_o is equated to $u(KT)$. This makes sense since it is only natural to require the output signal $u(t)$ to have the value of the input sequence at the sample time. The Zero Order Hold is therefore expressed as:

$$u(KT + \tau) = u(KT) \tag{109}$$

As Figure 21 confirms, the effect of the ZOH is to stretch the input pulse into a series of rectangular waves of width T. Finally, it should be noted in the change in system representation from Figure 19 to Figure 23 that the ZOH effect is taken into account in the process of discretizing equation (77) into equation (96).

Penalty Function

The cost criterion selected, with respect to which the performance of the system is optimized, is of the form of the quadratic functional:

$$J = \int_0^\infty \left\{ \left[C^*_{com} - \bar{C}\,\bar{x}(t) \right]^T Q \left[C^*_{com} - \bar{C}\,\bar{x}(t) \right] + \dot{u}^T(t)\, R\, \dot{u}(t) \right\} dt \tag{110}$$

(Ref. 8)

where Q is the weighting which penalizes the trajectory deviation or difference between the C^* commanded and the C^* realized, i.e., $\overline{C}\overline{x}(t)$, and R is the weighting on the control where a penalty is exacted for large corrective control rates.

It is required to determine a discrete control sequence which will minimize a discrete equivalent of equation (110). Using the first difference equivalent of the first derivative of the control

u(t), the cost functional (J) of equation (110) can be replaced by the following equivalent discrete expression:

$$J_d = \sum_{K=0}^{\infty} \left\{ \left[C^*_{com} - \bar{C}\,\bar{x}(KT) \right]^T Q_d \left[C^*_{com} - \bar{C}\,\bar{x}(KT) \right] + \left[u(K+1)T - u(KT) \right]^T R_d \left[u(K+1)T - u(KT) \right] \right\} \quad (111)$$

or equivalently as:

$$J_d = \sum_{K=0}^{\infty} \left\{ \left[C^*_{com} - C^*_{act} \right]^T Q_d \left[C^*_{com} - C^*_{act} \right] + \left[u(K+1)T - u(KT) \right]^T R_d \left[u(K+1)T - u(KT) \right] \quad (185)$$

As pointed out in Appendix D, the control which minimizes this cost function is given by:

$$u(K+1)T - u(KT) = L_d \left(C^*_{com} - C^*_{act} \right) + \bar{N}_d \left[\bar{x}(K+1)T - \bar{x}(KT) \right] \quad (235)$$

which, when evaluated for a few values of K, i.e., K = 0, 1, 2 . . ., can be expressed by the recursive equation:

$$u(KT) = \sum_{j=0}^{K-1} L_d \left(C^*_{com} - C^*_{act} \right) + N_d \left[\bar{x}(KT) - \bar{x}(0) \right] + u(0) \quad (112)$$

where $\bar{x}(0)$ and u(0) are the initial states and control and where:

$$L_d = \left(\bar{K}_{2_d} - \bar{K}_{1_d} \left(\bar{A}_d - \bar{I} \right)^{-1} \bar{B}_d \right) \left(\bar{C}_d \left(\bar{A}_d - \bar{I} \right)^{-1} \bar{B}_d \right)^{-1} \quad . \quad (238)$$

$$N_d = (\bar{K}_{1_d} + L_d \, \bar{C}_d)(\bar{A}_d - \bar{I})^{-1} \tag{240}$$

The matrices $\bar{K}_{1_d}$, $\bar{K}_{2_d}$ are found from the positive definite solution of the algebraic matrix Ricatti equation of the form:

$$P = Q_{Ricatti} + \Phi^T P \Phi - \Phi P \Gamma \left(\Gamma^T P \Gamma + R_d \right)^{-1} \Gamma^T P \Phi \tag{219}$$

(Ref. 6)

or from Appendix D for this particular problem:

$$\begin{bmatrix} \underline{P}_{11_d} & \underline{P}_{12_d} \\ \underline{P}^T_{12_d} & \underline{P}_{22_d} \end{bmatrix} = \left[\begin{array}{c|c} \underline{C}_d^T \, \underline{Q}_d \, \underline{C}_d & \underline{0} \\ \hline \underline{0} & \underline{0} \end{array}\right] + \begin{bmatrix} \underline{A}_d^T & \underline{0} \\ \underline{B}_d^T & \underline{0} \end{bmatrix} \begin{bmatrix} \underline{P}_{11_d} & \underline{P}_{12_d} \\ \underline{P}^T_{12_d} & \underline{P}_{22_d} \end{bmatrix} \begin{bmatrix} \underline{A}_d & \underline{B}_d \\ \underline{0} & \underline{I} \end{bmatrix} - \begin{bmatrix} \underline{A}_d^T & \underline{0} \\ \underline{B}_d^T & \underline{I} \end{bmatrix} \begin{bmatrix} \underline{P}_{11_d} & \underline{P}_{12_d} \\ \underline{P}^T_{12_d} & \underline{P}_{22_d} \end{bmatrix} \cdot$$

$$\begin{bmatrix} \underline{0} \\ \underline{I} \end{bmatrix} \left[\begin{bmatrix} \underline{0} & \underline{I} \end{bmatrix} \begin{bmatrix} \underline{P}_{11_d} & \underline{P}_{12_d} \\ \underline{P}^T_{12_d} & \underline{P}_{22_d} \end{bmatrix} \begin{bmatrix} \underline{0} \\ \underline{I} \end{bmatrix} + R_d \right]^{-1} \cdot \begin{bmatrix} \underline{0} & \underline{I} \end{bmatrix} \begin{bmatrix} \underline{P}_{11_d} & \underline{P}_{12_d} \\ \underline{P}^T_{12_d} & \underline{P}_{22_d} \end{bmatrix} \begin{bmatrix} \underline{A}_d & \underline{B}_d \\ \underline{0} & \underline{I} \end{bmatrix} \tag{113}$$

(Ref. 8)

where the resulting steady state solution matrix $\begin{bmatrix} \bar{P}_{11_d} & \bar{P}_{12_d} \\ \bar{P}^T_{12_d} & \bar{P}_{22_d} \end{bmatrix}$ is used in the gain calculation equation expressed by:

$$\begin{bmatrix} \bar{K}_{1_d} & \bar{K}_{2_d} \end{bmatrix} = -\left[\Gamma^T P \Gamma + R_d \right]^{-1} \Gamma^T P \Phi \tag{218}$$

or more precisely as:

$$\begin{bmatrix} \bar{K}_{1_d} & \bar{K}_{2_d} \end{bmatrix} = -\left[\begin{bmatrix} \underline{0} & \underline{I} \end{bmatrix} \begin{bmatrix} \underline{P}_{11_d} & \underline{P}_{12_d} \\ \underline{P}^T_{12_d} & \underline{P}_{22_d} \end{bmatrix} \begin{bmatrix} \underline{0} \\ \underline{I} \end{bmatrix} + R_d \right]^{-1} \cdot \begin{bmatrix} \underline{0} & \underline{I} \end{bmatrix} \begin{bmatrix} \underline{P}_{11_d} & \underline{P}_{12_d} \\ \underline{P}^T_{12_d} & \underline{P}_{22_d} \end{bmatrix} \begin{bmatrix} \underline{A}_d & \underline{B}_d \\ \underline{0} & \underline{I} \end{bmatrix} \tag{114}$$

where $\underline{P}_{11_d}$, $\underline{P}_{12_d}$, and $\underline{P}_{22_d}$ for this application are matrices of dimension (3 x 3), (3 x 1), and (1 x 1), respectively.

Computer Program and Simulation

Equation (112) is suitable for recursive evaluation on a digital computer, along with the terms which comprise it expressed by equations (114), (219), (238), and (240). Appendix E, contains the digital computer program which follows the analytical solution to the servo problem expressed by the previous set of equations and simulates a system equivalent to Figure 19. A simplified flow diagram of the program is shown in Figure 22. The structure of the simulated closed-loop system appears in Figure 23 while its programming logic appears in Figure 24. The linear, time-invarient, continuous-time system given by equations (77) and (78), having been transformed into the equivalent discrete-time linear equation set:

$$\bar{x}(K+1)T = \bar{A}_d\,\bar{x}(KT) + \bar{B}_d\,u(KT) \tag{96}$$

$$C^*(KT) = \bar{C}_d\,\bar{x}(KT) \tag{97}$$

where $\bar{C}_d = \bar{C}$, with a quadratic cost functional used to determine u(KT), is simulated in the algorithm. All the required matrices are sequentially evaluated for a specific sampling interval with the

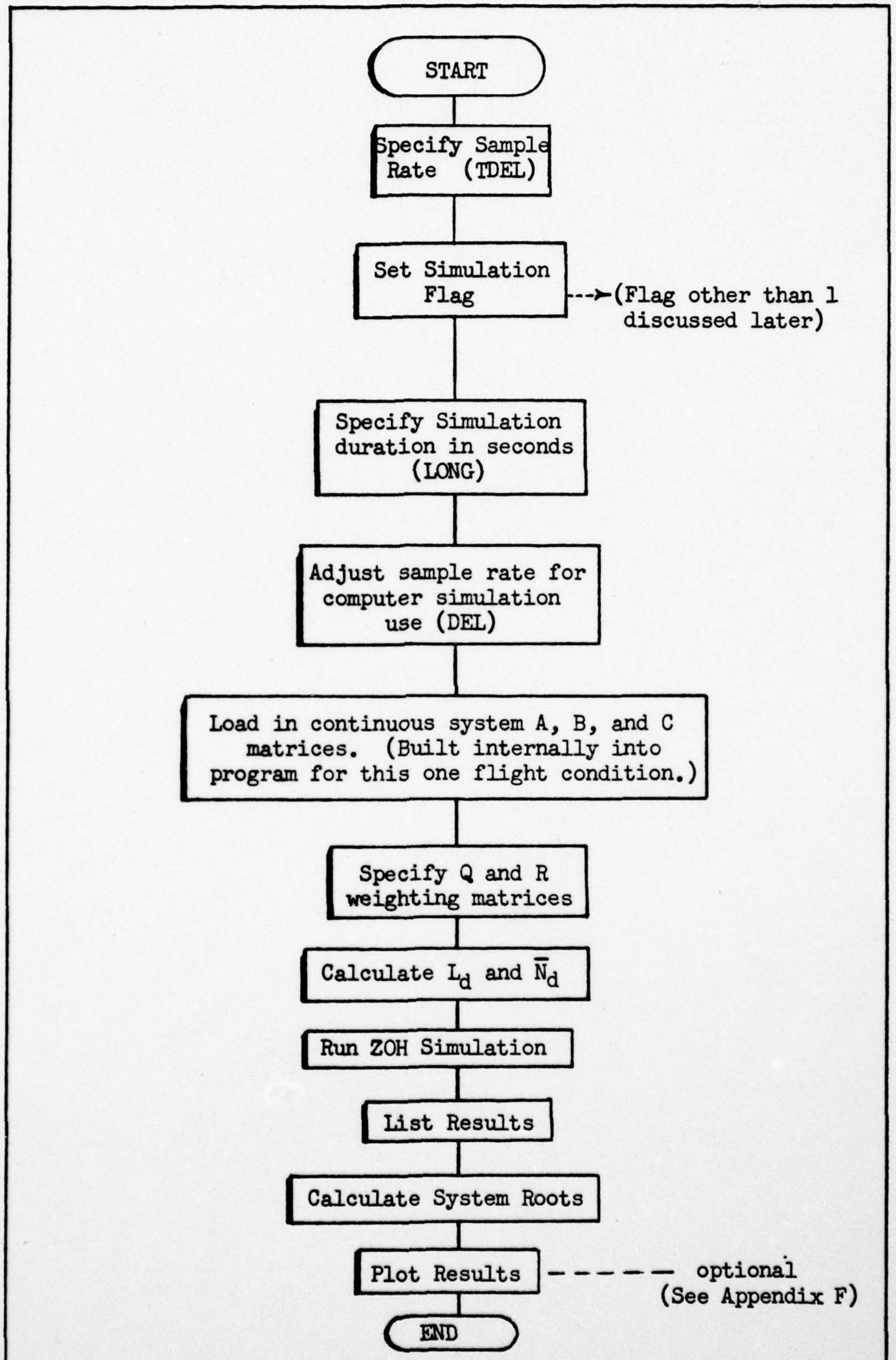

Fig. 22. Simplified Computer Program Flow Diagram.

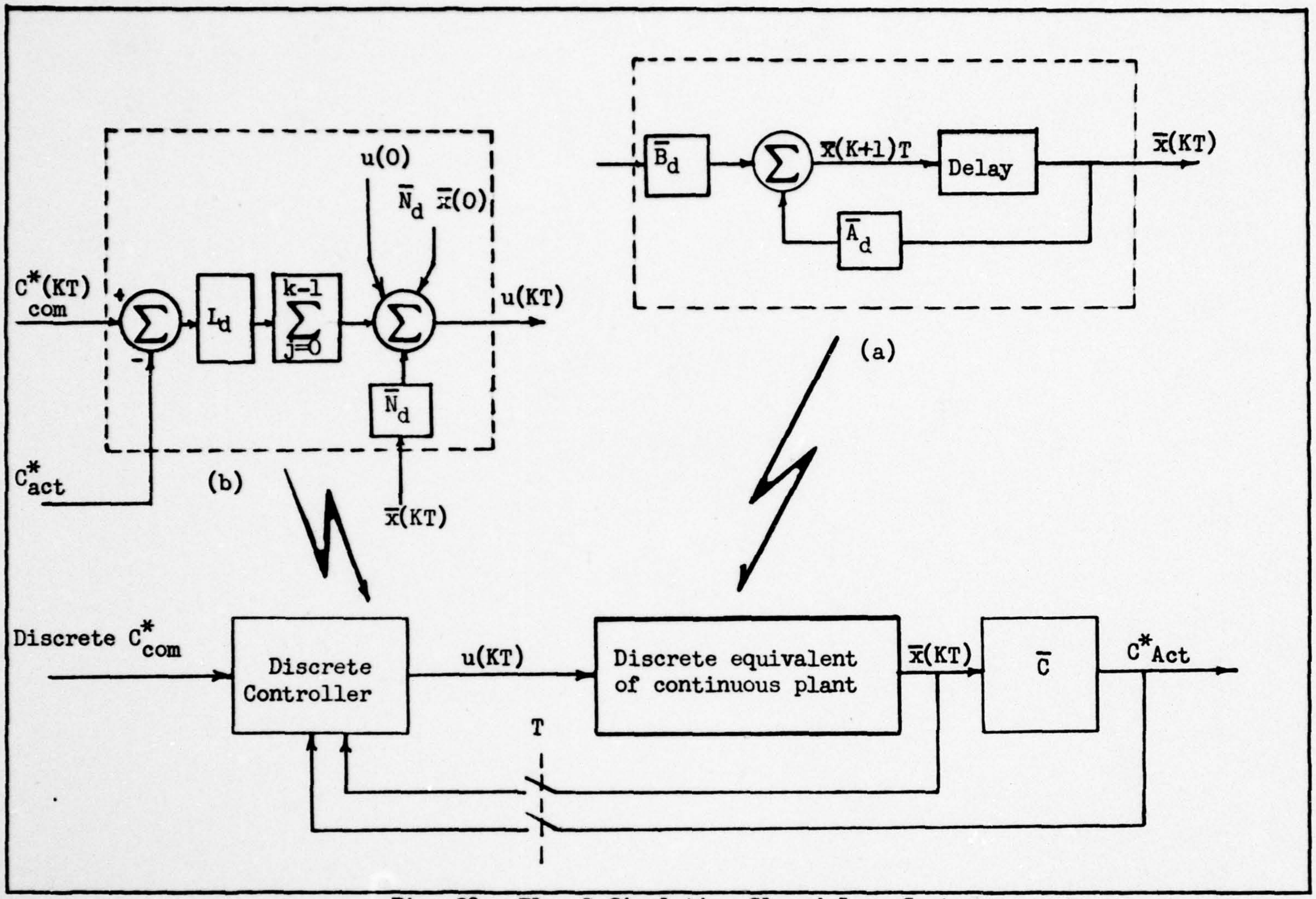

Fig. 23. Flag 1 Simulation Closed Loop System.

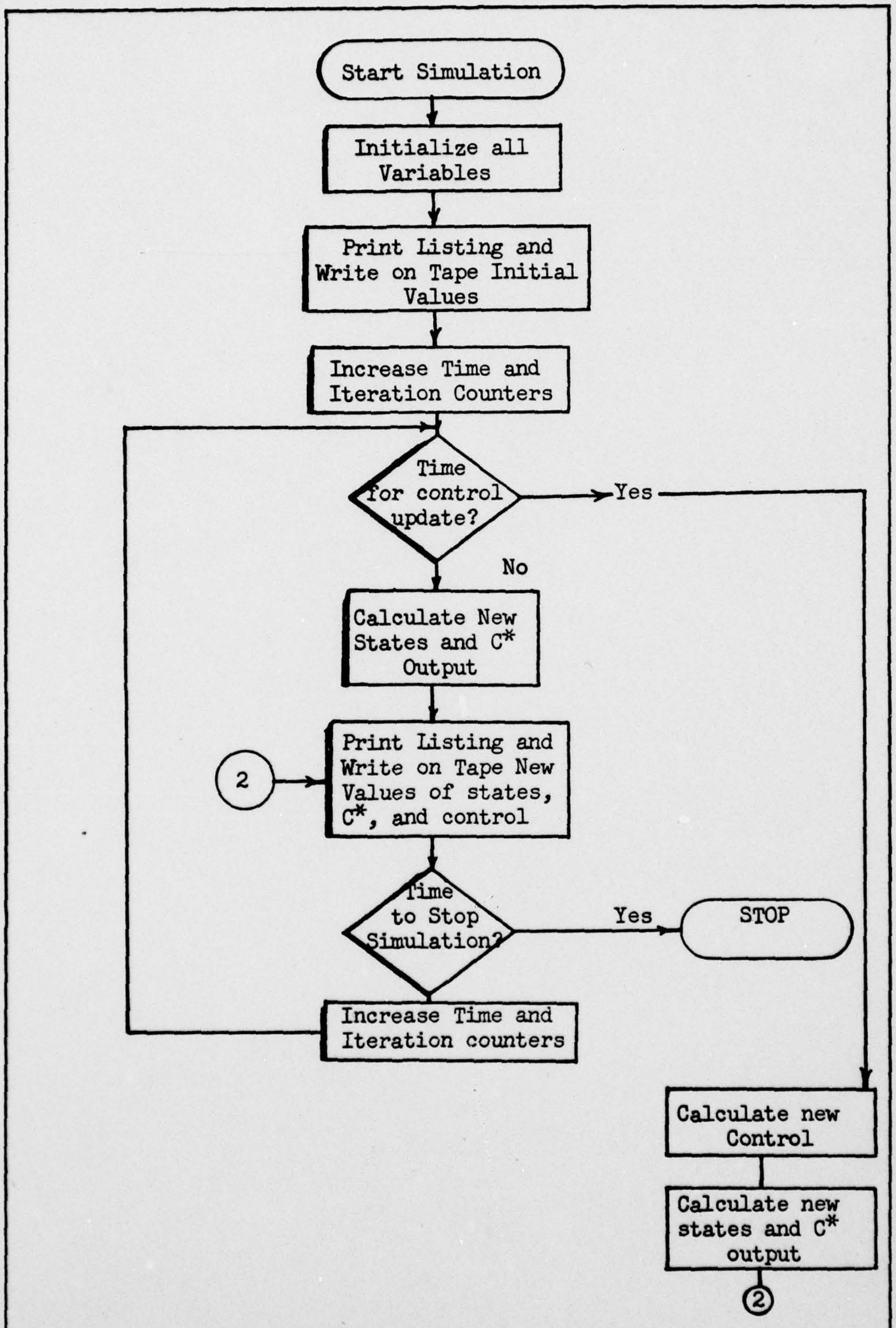

Fig. 24. Simplified Simulation Flow Design.

Ricatti matrix equation steady state solution used to calculate the matrix of feedback gains. The algorithm was programmed in Fortran IV and was tested on a CDC 6600 digital computer.

Insert (a) of Figure 23 is a breakdown of the discrete plant dynamics. Since the system being modeled is continuous, some way must be found to simulate it on a digital computer. For this problem, the continuous system was discretized at a rate of $1/500^{th}$ second. This rate of plant discretization is kept constant no matter what the sample rate specified for investigation might be. In other words, the YF-16 plant is allowed to change states every $1/500^{th}$ second. Such a fast rate allows the plant to retain an almost continuous, real-world, nature while still satisfying the requirement for discretization. It is important to realize that the sample rate specified for a particular program run is the discrete rate with which this equally discretized plant model is sampled.

Initially, the plant was discretized to a rate of some multiple of the sample rate. For example, if the sample rate was set to $T = .333$ sec., the plant was always discretized to a rate ten times faster or .033 seconds. However, to standardize the runs, thus allowing a comparison of results, and remove this factor of ten, which might influence the results, it was decided to standardize the plant discretization rate. With the "factor of ten" scheme, however, it was much simpler to determine when it was time to build a new control. For example, if the sample rate specified was $T = 1/40^{th}$ second, ten iterations of the plant ($\frac{10}{400} = \frac{1}{40}$), this time running at $1/400^{th}$ second, passed before a new control was calculated. This latest control was then implemented and retained

as the plant control for the next ten plant iterations (ZOH effect) before the cycle was repeated. It is evident that this factor of ten, while simplifying the iteration and update scheme, made the correlation of results from one sample rate to another almost impossible.

The standardization scheme, while eliminating this problem, introduced the new problem of how to determine when to update the control. The frequency of control updates now varied with the relationship of the sample rate to the $1/500^{th}$ second plant discretization rate. If a sample rate of T = 1/25 second was used, twenty plant iterations passed (20/500 = 1/25 second) before control updates.

This was simple enough for even multiples of the plant discretization rate but more complicated for non-multiple cases. The problem could be eliminated by specifying the use of only convenient multiple sample rates (i.e., T = 1/10, 1/20, 1/50, 1/100, etc.). However, to retain program flexibility in the use of any sample rate, this limitation was not implemented. Instead, the flexibility was retained but at the cost of some slight error. The Fortran function IFIX is used in conjunction with the modulo arithmatic function MOD. This is best explained by use of an example. If the sample rate is specified to be $T = 1/30^{th}$ second, which in the program is referred to as TDEL = .0333..., the program used the Fortran expressions:

```
MODI  =  IFIX (500.0 * TDEL + .5)
DEL   =  MODI/500.0
```

to come up with the adjusted sample rate of DEL = .034 seconds.

The value of DEL, in this case .034 seconds, is then used throughout the remainder of the program as the adjusted sample rate to simplify

the calculations. The amount of error introduced, in this case, the difference between .0333... and .034 seconds, is negligible. A comparison of the sample rate specified, to the actual rate selected by the algorithm for the simulation appears in Table VI. It is evident that for specified sample rates $\frac{1}{\tau}$, where $500/\tau$ equals an integer, exactness between the sample rate specified and the sample rate used is maintained.

Table VI

Specified vs Actual Sample Rates

Specified Sample Rate (DEL)	Actual Sample Rate Used (TDEL)
1/100.0	1/100.0
1/90.0	1/83.3
1/80.0	1/83.3
1/70.0	1/71.4
1/60.0	1/62.5
1/50.0	1/50.0
1/40.0	1/38.4
1/30.0	1/29.4
1/20.0	1/20.0
1/10.0	1/10.0

Additionally, the value of MODI is used to determine when a control update should occur using the Fortran modulo (MOD) arithmetic statement:

$$\text{If} \left[\text{(MOD (KK, MODI)} \right] \quad 2, 1, 2$$

Here, KK is an integer counter which keeps track of the number of system iterations. If the value of KK is divisible by MODI such that the remainder is zero, the program will jump to statement 1 where an update of the control occurs. For any other value of remainder, the program will continue using its present value of control. Such a scheme was used successfully in this study.

Insert (b) of Figure 23 is a detailed depiction of the mechanization of the discrete controller expressed by equation (96). The optimal scalar gain L_d and the (1 x 3) optimal gain matrix N_d are calculated based on the modified sample rate, DEL, just discussed. Since the control is calculated every DEL seconds, it is necessary that the gains be based on this same rate. The values of L_d and $\bar{N}_d$ are determined by sequential calls to subroutines as shown in Figure 25. Additionally, since the input to the simulation is a step of unity magnitude, a sample taken at any time will also be unity. That is:

$$C^*_{com_{discrete}} = C^*_{com_{continuous}} = 1.0. \tag{115}$$

Finally, with this unity step input driving the controller, and assuming the initial control u(0) and initial states $\bar{x}(0)$ are taken as zero, it is apparent that the first control calculated will have the value of L_d. This is the approach taken in the simulation.

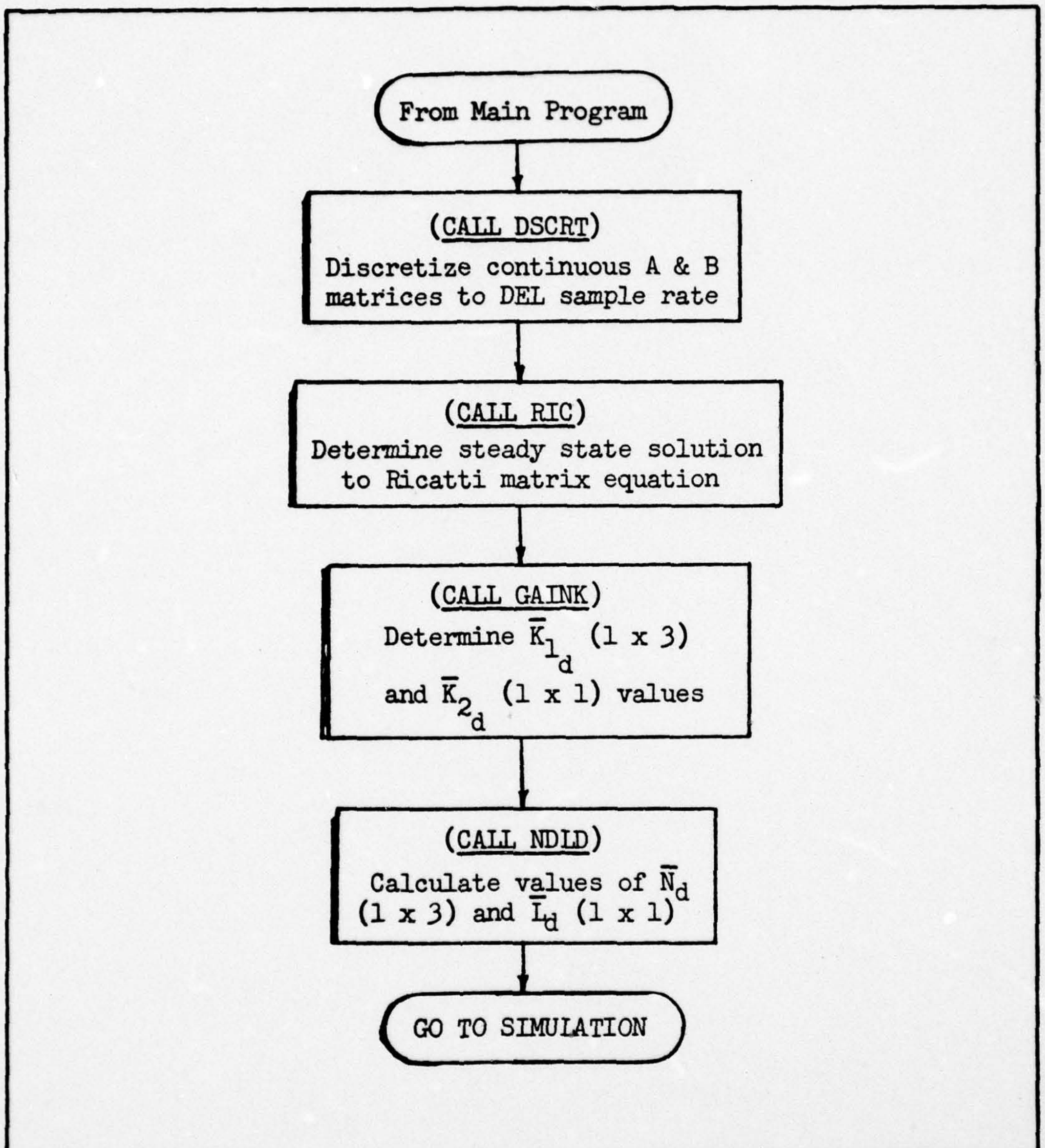

Fig. 25. Simplified Flow Diagram of $\overline{L}_d$ and $\overline{N}_d$ Calculation.

A key element in the determination of the control u(KT) is the amount of computation time required for its calculation. With the plant running at a 1/500th second state-change rate, the computation time required for both state-output and control calculations must be much less than this rate. This is especially true for the control

computation since it must be available on the next simulation iteration which occurs 1/500th second later. Such a state of affairs is true not only for this simulation but becomes even more critical when the computations are done on the type of onboard computer envisioned as the actual aircraft controller. Such computers are of much more limited capability in terms of wordlength and speed of computation than the ground based CDC computer used here. Algorithm computational time can be kept at a minimum by efficient programming, which limits the number of computer commands, and by proper sequencing of these computer commands. The most time consuming between iteration computation in this simulation is taken by the sequence of statements which calculate the new control. The calculation process has been reduced to five sequential statements by retaining information from previous control computations and, for this reason, is assumed to occur in much, much less than 1/500th second.

This assumption is reasonable in view of the amounts of time small computers require for computation purposes. Working on the micro-second (10^{-6} second) level, no time problems are envisioned in the various data manipulations (shift commands, access memory location commands, complement commands, etc.) pursuant to the calculation of $u(KT)$. By the elimination of the use of intermediate answers, as presently programmed, memory access time could be minimized even further lending greater credence to this assumption.

This assumption of negligible lapse in time for computation purposes is of additional importance when equation (112) is examined closely. From this equation, it is evident that the calculation of $u(KT)$ requires knowledge of $\bar{x}(KT)$. The $\bar{x}(KT)$ used is the most current

set of values available. The resulting u(KT) is actually u(KT^+) owing to a finite amount of computational time delay. This u(KT^+) is then used as the control u(KT) in subsequent state evaluations using equation (96).

Closed Loop System Eigenvalues

An additional feature of the program is the inclusion of a subroutine (ROOT) which calculates the characteristic roots of the closed-loop system. The location of roots inside the unit circle and their migration with changes in the sample rate is of interest. Subroutine ROOT determines these roots by solving for the eigenvalues of the dynamics matrix of an augmented state space system representation. This dynamics matrix is determined as follows. Let

$$\overline{W}(KT) \quad = \quad \sum_{j=0}^{K-1} L_d \left[C^*_{com}(KT) - C^*_{act}(KT) \right] \tag{116}$$

then,

$$\overline{W}(K+1)T \quad = \quad \overline{W}(KT) + L_d \left[C^*_{com}(KT) - C^*_{act}(KT) \right] \tag{117}$$

but,

$$C^*(KT) \quad = \quad \overline{C}_d \, \overline{x}(KT) \tag{97}$$

so,

$$\overline{W}(K+1)T \quad = \quad \overline{W}(KT) + L_d \;(C^*_{com}(KT) - \overline{C}_d \, \overline{x}(KT)) \tag{118}$$

or,

$$\overline{W}(K+1) \quad = \quad \overline{W}(KT) + L_d \; C^*_{com}(KT) - L_d \, \overline{C}_d \, \overline{x}(KT) \tag{119}$$

AD-A053 441 AIR FORCE INST OF TECH WRIGHT-PATTERSON AFB OHIO SCH--ETC F/G 1/3
INVESTIGATION OF A DISCRETE C-STAR TRANSIENT RESPONSE CONTROLLE--ETC(U).
DEC 77 P D MONICO

UNCLASSIFIED AFIT/GGC/EE/77-8 NL

2 OF 3
ADA
053441

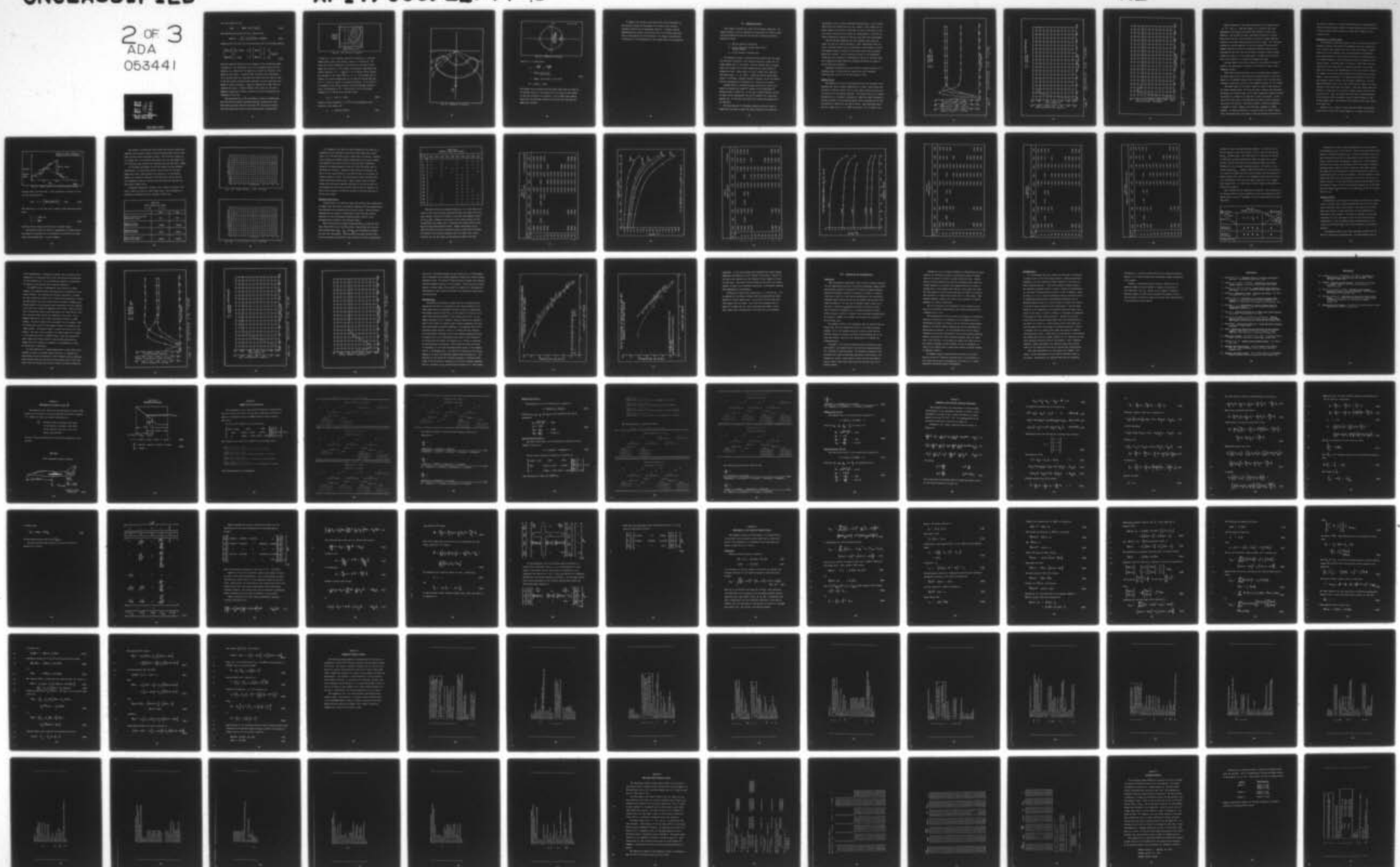

Also from equation (112):

$$u(KT) = \overline{W}(KT) + \overline{N}D \left[\overline{x}(KT) \right] \tag{120}$$

Now substituting equation (120) into equation (96):

$$\overline{x}(K+1)T = \left[\overline{A}_d + \overline{B}_d \, \overline{N}_d \right] \overline{x}(KT) + \overline{B}_d \, \overline{W}(KT) \tag{121}$$

Equations (119) and (121) are now incorporated into the following equation:

$$\begin{bmatrix} \overline{x}(K+1)T \\ \\ \overline{W}(K+1)T \end{bmatrix} = \begin{bmatrix} \overline{A}_d + \overline{B}_d \, \overline{N}D & \overline{B}_d \\ \\ -L_d\overline{C}_d & \overline{I} \end{bmatrix} \cdot \begin{bmatrix} \overline{x}(KT) \\ \\ \overline{W}(KT) \end{bmatrix} + \begin{bmatrix} 0 \\ \\ L_d \end{bmatrix} C^*_{com}(KT) \tag{122}$$

This last equation characterizes the dynamics of the closed-loop system of Figure 23. The eigenvalues of the (2 x 2) dynamics matrix of this equation, as a function of the sample rate, define the stability of the system in the Z-plane. Subroutine ROOT calculates these eigenvalues. It is desirable that the resulting short period roots not only lie within the unit circle, insuring system stability, but also that they correspondto a natural frequency ($\omega_{N_{sp}}$) and damping ratio (ζ_{sp}) that are preferred by pilots. Preferred values of ω_n verses ζ are given graphical significance in what is called the Cornell Aeronautical Lab "Thumbprint" (Fig. 26).

This particular ω_n vs ζ relationship is based on comprehensive data from several variable stability airplanes, primarily the F-94. The various ω_n values and their associated ζ values can be mapped into the S-plane and results in the "kidney-shaped" representation

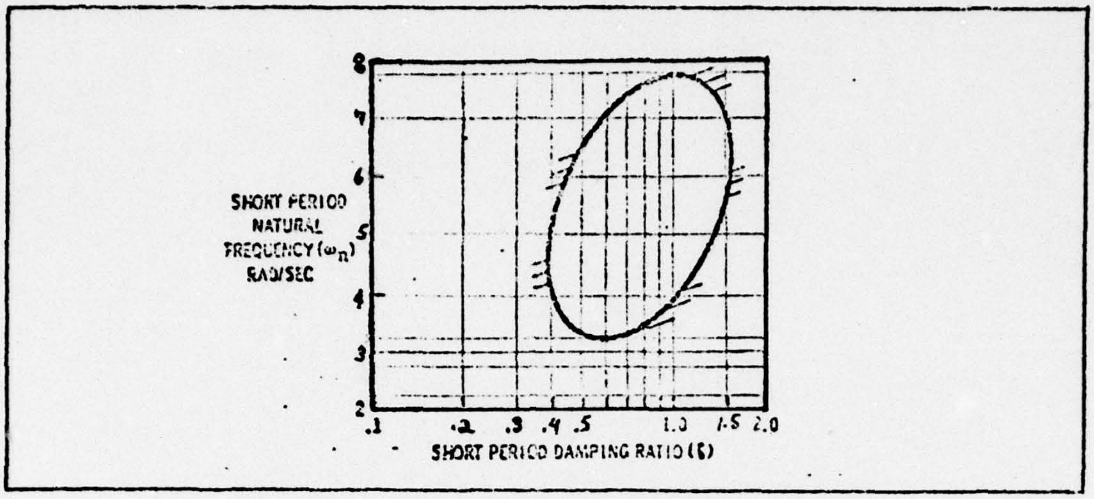

Fig. 26. CAL Thumbprint. (Ref.17)

of Figure 27. In the Z-plane, Figure 26 corresponds to a similarly shaped region, albeit much smaller, shown as I in Figure 28. The exact size of the "thumbprint" in the Z-plane is determined by the sample rate selected. As the sample rate increases, approaching continuous sampling, i.e., $T = \lim_{f \to \infty} \frac{1}{f} = 0$, the Z-plane contour shrinks and converges to the single point at u = + 1. If the sample rate is reduced, the contour expands while at the same time moving away from the u = +1 point as region II of Figure 28 depicts. If the center of the thumbprint (Fig. 26) is chosen as the most desirable operating point, corresponding to $\zeta = .707$ and $\omega_n = 5.5$, the following conjugate set of S-plane root locations result:

$$S_{1,2} = -3.89 \pm 3.389j \qquad (123)$$

Using the direct Z-transform, $Z = e^{st}$, this corresponds to pole locations in the Z-plane of:

$$Z = e^{(-3.89 \pm 3.89j)T} \qquad (124)$$

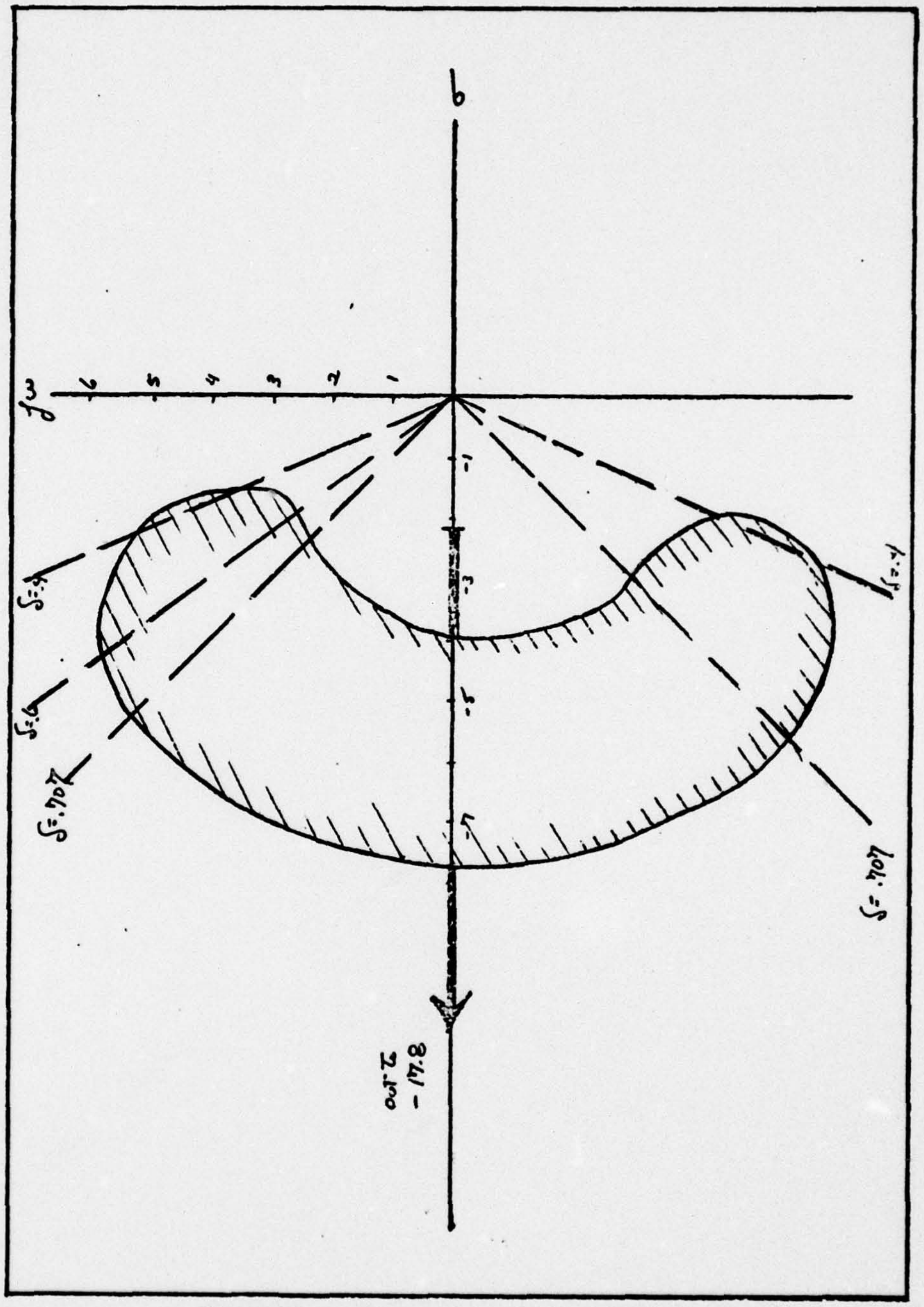

Fig. 27. Thumbprint in S-plane.

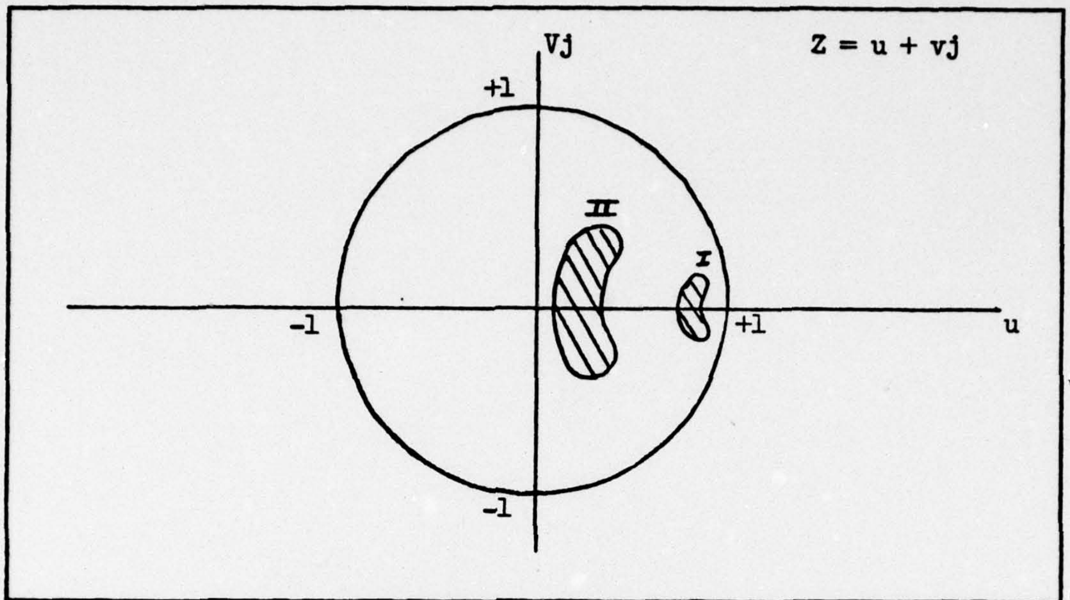

Fig. 28. Thumbprint in Z-plane.

which for T = 1/50 becomes:

$$Z = e^{\frac{-3.89}{50}} \cdot e^{\frac{+3.89j}{50}}$$

$$= .925149 \angle \pm 4.457^\circ$$

$$= .925149 \;(\cos 4.457 \pm j \sin 4.457 \qquad (125)$$

$$Z = .92235 \pm .0719j$$

The Z-plane roots resulting from subroutine ROOT, which are fixed by the optimal solution to the problem, will be looked at with respect to this most desirable root location. It is evident from equation (124) that the particular location of the roots will vary with the sample rate selected.

In summary, this chapter, which begin with a brief discussion of hold devices, showed the development of a discrete cost criterion (penalty) function and its minimizing solution. A computer program implementing this optimal solution and some of the problems associated with its development were then discussed. The chapter concluded with a discussion of the determination of the system closed loop eigenvalues.

VII. Simulation Results

This chapter presents the results of the digital simulation. The digital program, listed in Appendix E, was exercised for various sample rates and weighting factors (R & Q) with the following prioritized questions in mind:

a. Can the system be controller?

b. Is the controlled response within the C^* envelope bounds?

c. Is the solution a feasible one?

An affirmative answer to question (a) was achieved and the system was considered controlled if the system successfully tracked the 1-G climb command input to the system. This was evident when the steady state error between the C^* input command and the actual system C^* response was zero. Additionally, in such a steady state condition, the system states α , $\dot{\theta}$, and δ_h would also achieve steady state values. A divergent, undamped response as Figures 11a and 12a depict, would be unacceptable and indicative of a total lack of control.

Having achieved a controlled system, question (b) could be answered by comparing the system C^* response to the established C^* envelope bounds of Figure 20. To do this, a rescaled plastic overlay of Figure 20 was superimposed over the C^* response for a particular program run. In this way, cases which fell outside the bounds could be identified.

The final question of achieving a feasible solution, could be answered by observing the gains ($\bar{L}_d$, $\bar{N}_d$) determined as necessary by

the program, and the control deflections they produced. A set of gains which control the system and cause the response to fall within the required envelope but which are infeasible in terms of the amount of control surface deflection they require for implementation or the rate of control application (saturation effect), would also prove unacceptable.

The initial ZOH simulation runs were conducted with arbitrary values for both the Q and R weightings. After considerable trial and error, it became evident that a Q weighting of unity produced a consistent maximum response overshoot of the target value (1-G) of approximately five percent. It was convenient to think of the Q weighting (trajectory error penalty) as determining the amount of overshoot while the R weighting (energy expenditure penalty) determined the amount of control deflection employed.

Subsequent simulation runs were therefore conducted keeping the Q weighting equal to unity while the sample rate, and R weighting (affecting the ratio of Q to R) were allowed to vary.

Typical Results

ZOH simulation runs were reinitiated with both the trajectory error weighting and control penalty weighting set to unity. These values were selected to obtain an initial feel for the system response and some idea of the nature of the controls produced. The program output for a typical simulation run is contained in Appendix F. When this output information is made available to the plotting program listed in Appendix G, the output products of Figures 29, 30, and 31 result. These particular plots are for a sample rate of $T = 1/50^{th}$ second with $Q = 1.0$ and $R = 1.0$.

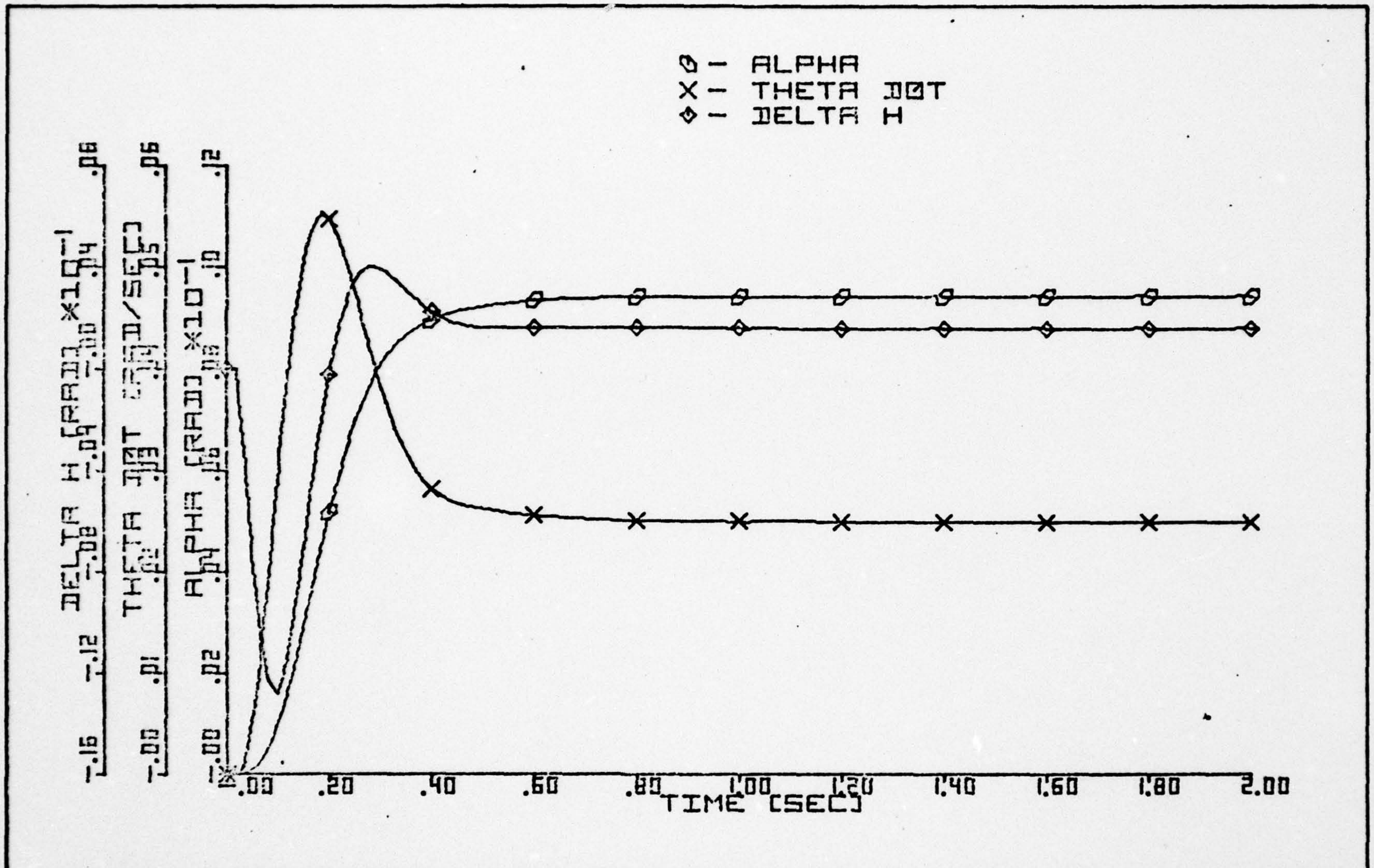

FIG 29 - STATES VS TIME

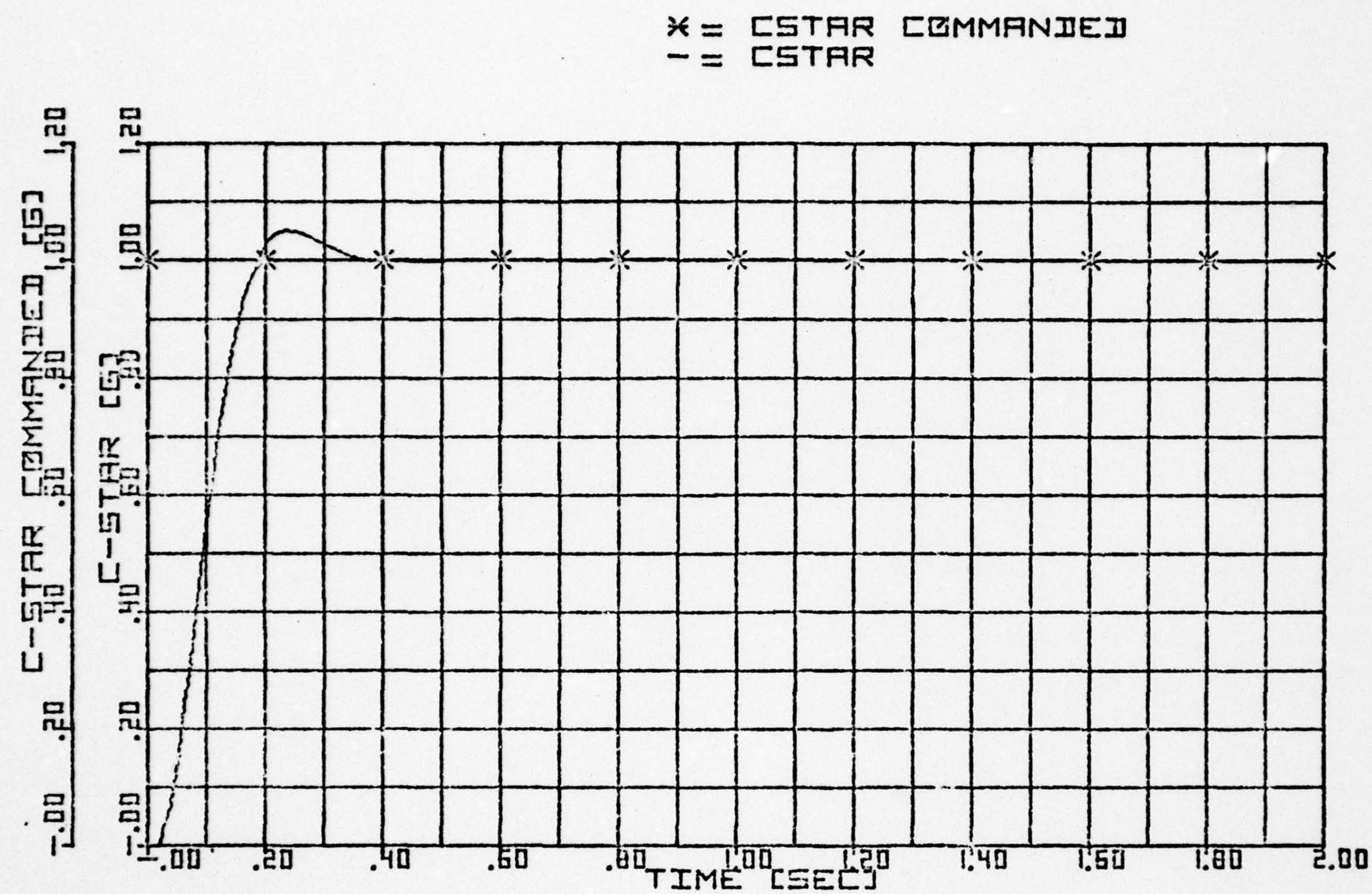

FIG 30 OUTPUT VS TIME

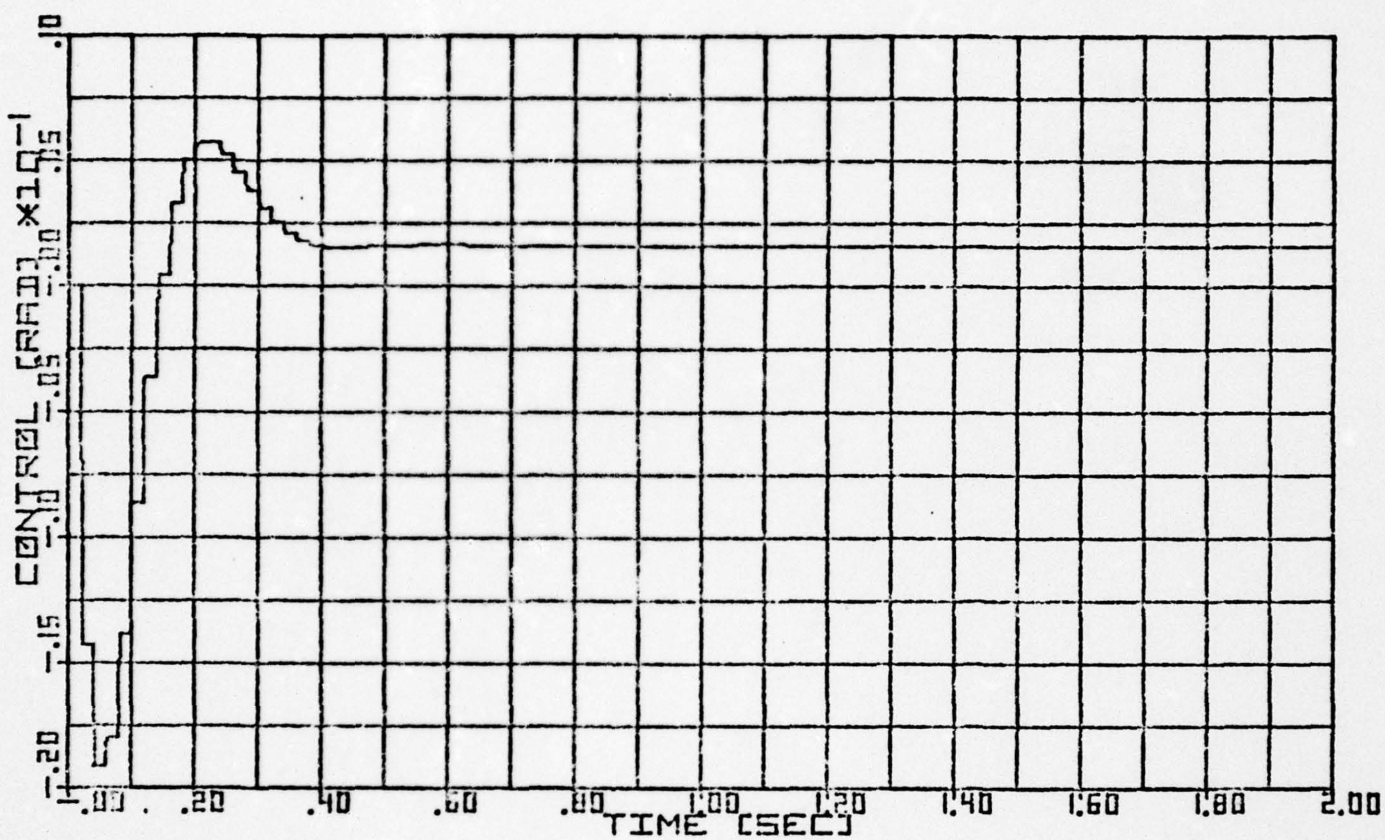

FIG $\underline{31}$ CONTROL VS TIME

Figure 29 presents a two second time history of the system states α, $\dot{\theta}$, and δ_h. From this figure, it is apparent that after approximately .80 seconds, the states have achieved a steady state condition. The initial horizontal stabilizer deflection is negative which causes the nose of the aircraft to pitch up in almost immediate response to the climb command initiated at zero seconds. The controller, sensing the reducing magnitude of the error between C^* actual and C^* command, gradually reverses the stabilizer deflection direction thus lowering both the pitch rate and the angle of attack to their eventual steady state values. In the steady state, a slightly positive deflection of the stabilizer is required to maintain the climb.

The next figure in the series, Figure 30, shows both the actual C^* output of the system and its relation, as a function of time, to the commanded response.

After some initial hesitation, due to the delay before a sample of the system states occurs, the controller responds rapidly to drive the system to the commanded response with an overshoot of 5.1 percent before reaching a steady state lock-on to the commanded response in .556 seconds.

The final figure in the series, Figure 31, shows a time history of the controls which produce the state and output responses just discussed. Initially, the controls remain at zero until enough time (sample interval) has passed for a sample to be taken and a control calculated. In this case, this occurs after .02 seconds with the initial control equaling the value of the gain $\bar{L}_d$. The control surface is deflected negatively a maximum of .01911 radians, then positively a maximum of .005695 radians. It finally stabilizes to a positive value of .001571 radians after .80 seconds which corresponds to the same elapsed time needed for

the states to stabilize. The Zero Order Hold effect of maintaining the controls constant between samples is clearly evidenced by those portions of the plot which remain constant over time before jumping to a new constant value.

Modification of Control Scheme

In an effort to reduce the amount of time it took for the actual C^* response to achieve and maintain C^* commanded, with zero steady state error, shown in this example (Fig. 30) to take .556 seconds, a modification to the hold technique used in the simulation was undertaken. From observing numerous control time history plots, of which Figure 31 is a typical example, it was felt that time could be conserved in the control scheme. Conserving time, in this case, could reduce the time required to reach steady state to something less than .556 seconds. After the calculation and implementation of the first non-zero control, for example, the controls remain negative and constant until the next update. At the next update, it is apparent from Figure 31 that a yet more negative control results from the update computation. It would appear advantageous then to use some of the time the controls are held constant to move toward this new control. This would appear especially helpful in saving time on the positive, upward sloped, portion of the plot (Fig. 31). Here, the control deflection has reversed and begins to move positive until reaching its peak of .005695 radians at .202 seconds elapsed time. The scheme of the modified control would appear as in Figure 32.

Figure 32 is, in effect, a First Order Hold (FOH) representation of the control, where the control changes at a constant rate between

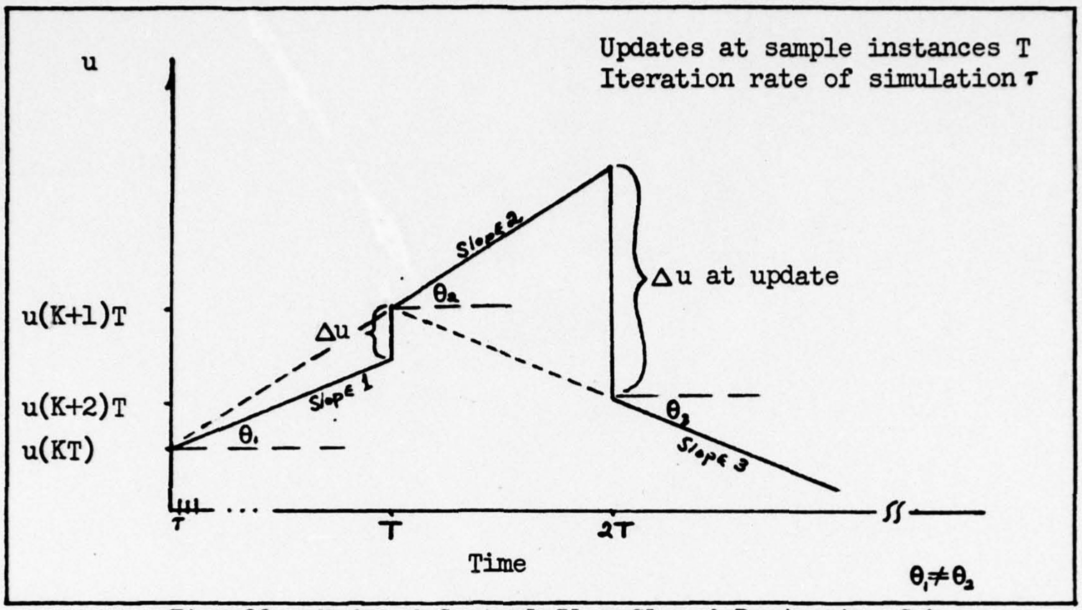

Fig. 32. Updated Control Plus Sloped Projection Scheme.

discrete update intervals (KT). On any particular iteration, the control can be expressed as:

$$u(KT + \tau) = \left[\frac{u(KT) - u(K-1)T}{T}\right]\tau + u(KT) \qquad (126)$$

This expression is in the same form as equation (106) discussed earlier where:

$$A_o = u(KT) \text{ and,}$$
$$A_1 = \frac{\dot{u}(t)}{1!} \qquad (107)$$

and where $\dot{u}(t)$ has again been defined as in equation (104).

This modified scheme of control is mechanized as the FOH option of the program in Appendix E and is substituted for the ZOH in the simulation by specifying FLAG = 2 in the program.

The results of introducing a First Order Hold into the problem are expressed by two typical control time history plots which follow. Both plots are for Q and R weightings of unity. The first plot, Figure 33, is a sample rate of .01 seconds while Figure 34 is for the sample rate of .02 seconds, just discussed in connection with the ZOH control scheme.

It is evident from Figure 33 that the control has been smoothed considerably. To some extent, this is also the case for the lower sample rate control time history plot, Figure 34. In this figure, however, the "sawtooth" character of the FOH can be seen as the control propagates along the constant slope then abruptly jumps when the next control update occurs.

Of greater significance, however, is the effect of the FOH on the time it takes the system to reach steady state. This information is presented in comparative form to the ZOH, in Table VII.

Table VII

ZOH vs FOH Control Scheme

T = .02 R = Q = 1

	ZOH	FOH
Time to achieve controlled steady state (sec)	.556	.630
Maximum positive deflection (Rad)	.005695	.005054
Maximum negative deflection (Rad)	.01911	.02718
Final control value at steady state (Rad)	.001571	.001571

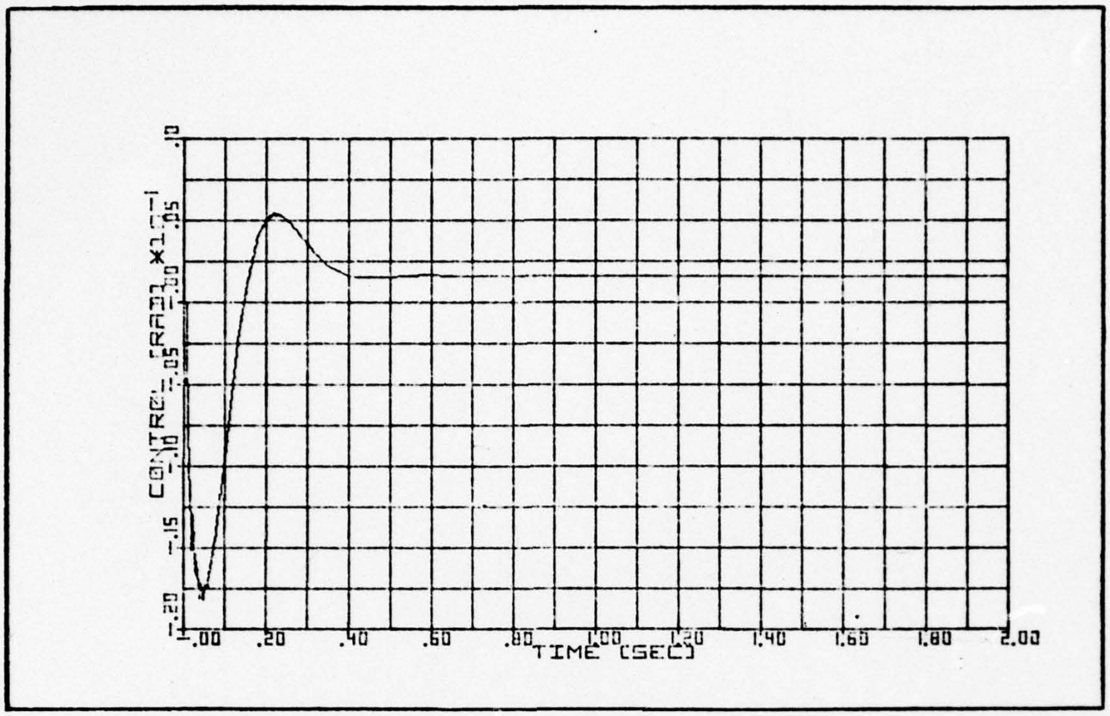

FIG – 33. CONTROL VS TIME

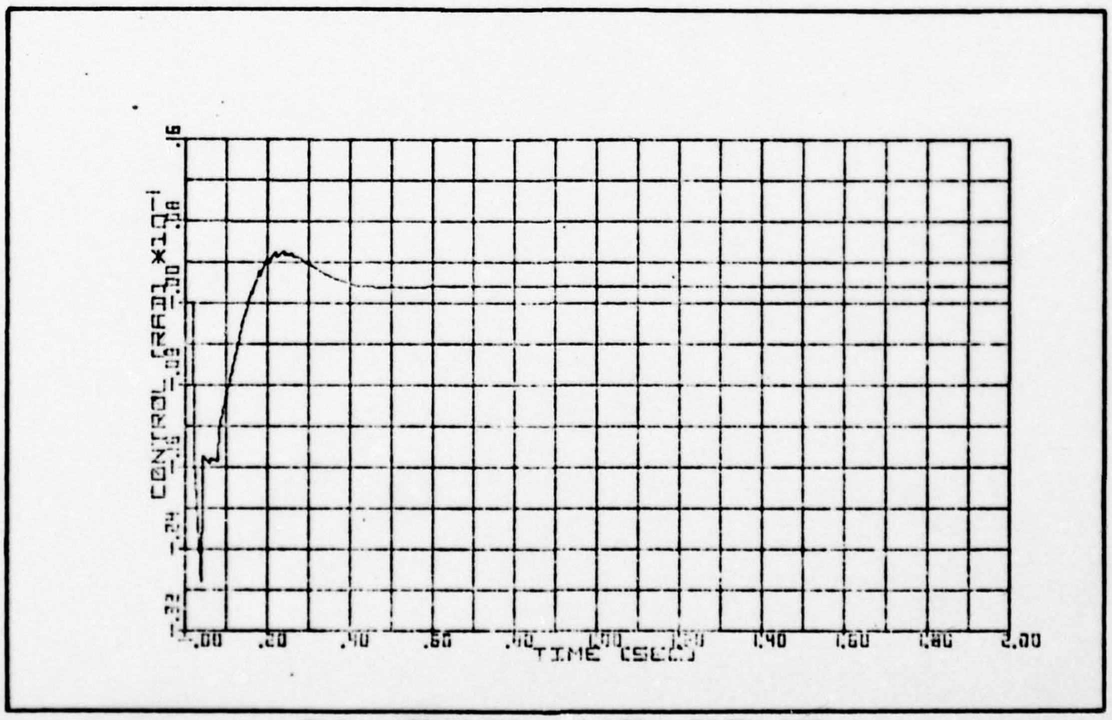

FIG – 34. CONTROL VS TIME

It is apparent from Table VII that although both hold devices, as mechanized in the simulation, achieve the same steady state control value, it is the ZOH which achieves steady state the fastest. Additionally, although the maximum positive deflections of the control surface are comparable (the same at least for the first three significant figures), the maximum negative excursion of the FOH exceeds that of the ZOH by 29.7 percent. Though the same results are achieved, the FOH is not as energy efficient as the ZOH in light of the greater deflection needed to control the aircraft and in view of the fact that surface deflections produce drag. Longer elapsed times to achieve steady state and greater negative excursions of the control were the case whenever the First Order and Zero Order Holds were compared. In view of this situation, the ZOH was retained as the most efficient of the two hold schemes.

Simulation Observations

Concentrating on the ZOH then, Table VIII presents those combinations of sample rates and control rate penalty weightings (R) investigated while the trajectory error weighting (Q) was held at unity. These particular combinations were chosen in consideration of the time and resources available for this investigation,weighed against a desire to get reasonably good coverage of the available regime.

Table IX presents the optimal feedforward gains L_d found for each case, while Tables X, XI, and XII present, respectively, the three optimal feedback gains N_{d_α}, N_{d_θ}, and $N_{d_{\delta_h}}$ also determined as optimal for each case investigated. Selected points from Table IX and X have also been presented in graphical form in Figures 35 and 36, respectively.

Table VIII
Summary of Cases Investigated

R \ T	1/100	1/90	1/80	1/70	1/60	1/50	1/40	1/30	1/20	1/10
1	x		x			x		x	x	x
25	x		x			x		x	x	x
50	x	x	x	x	x	x	x	x	x	x
75	x		x		x	x		x		x
100	x		x			x	x	x	x	
125						x	x	x		
150						x	x	x		
175						x	x	x		
200						x	x	x	x	
225						x	x	x	x	
300	x		x			x	x	x	x	x
400	x		x			x	x	x	x	x
500	x		x			x	x	x	x	x

From Table IX and its associated Figure 35, it is seen that an increase in the control penalty weighting (R) while the sample rate (T) is held constant, produces an increase in the value (less negative value) of the L_d gain. However, if the value of the control penalty is held constant while the sample rate is decreased, the optimal value of this gain decreases (more negative value). Similar observations can be taken from Table X with its associated Figure 36 and Tables XI and XII. An increase in the penalty weighting, while the sample rate is held constant, has the same effect as decreasing the sample rate while

Table IX

Optimal L_d Gains

* = information plotted

	R \ T	1/100	1/90	1/80	1/70	1/60	1/50	1/40	1/30	1/20	1/10
*	1	-.00846		-.00982			-.10430		-.01920	-.02148	-.01803
*	25	-.00184		-.00216			-.00337		-.00508	-.00650	-.00842
*	50	-.00131	-.00155	-.00155	-.00178	-.00201	-.00244	-.00303	-.11373	-.00487	-.00669
*	75	-.00108		-.00128		-.00166	-.00201		-.00311		-.00580
*	100	-.00094		-.00111			-.00176	-.00220	-.00273	-.00362	
	125						-.00158	-.00198	-.00247		
	150						-.00145	-.00182	-.00227		
	175						-.00135	-.00169	-.00211		
	200						-.00126	-.00159	-.00199	-.00267	
	225						-.00120	-.00150	-.00188	-.00254	
	300	-.00055		-.00065			-.00104	-.00131	-.00165	-.00223	-.00344
	400	-.00048		-.00057			-.00091	-.00115	-.00144	-.00196	-.00307
*	500	-.00043		-.00051			-.00081	-.00103	-.00130	-.00177	-.00280

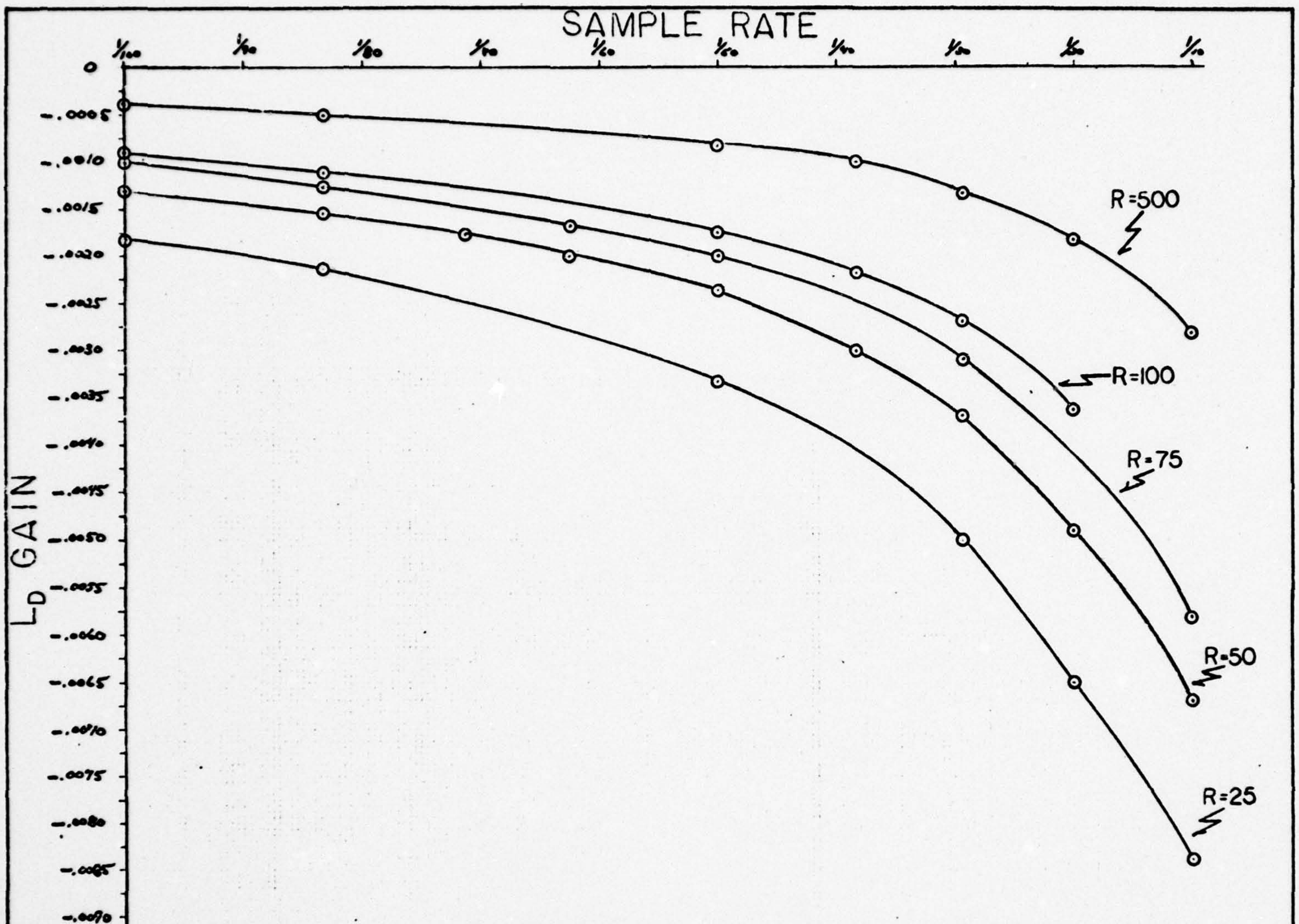

FIG 35/SAMPLE RATE vs L_D GAIN (Q=1, VAR. R)

Table X

Optimal N_{d_α} Gains

* = plotted

	R \ T	1/100	1/90	1/80	1/70	1/60	1/50	1/40	1/30	1/20	1/10
	1	5.8568		5.7997			5.5609		5.1118	4.5732	2.9931
*	25	2.3764		2.3656			2.3210		2.2385	2.1389	1.8084
*	50	1.9604	1.9528	1.9528	1.9451	1.9374	1.9216	1.8974	1.8642	1.7951	1.5644
	75	1.7534		1.7472		1.7346	1.7218		1.6753		1.4324
*	100	1.6208		1.6154			1.5935	1.5765	1.5533	1.5052	
	125						1.5010	1.4859	1.4652		
	150						1.4230	1.4159	1.3971		
	175						1.3724	1.3596	1.3421		
	200						1.3247	1.3128	1.2964	1.2626	
	225						1.2842	1.2729	1.2575	1.2256	
*	300	1.2069		1.2037			1.1909	1.1811	1.1677	1.1401	1.0483
	400	1.1191		1.1164			1.1052	1.0967	1.0850	1.0610	.9815
*	500	1.0561		1.0537			1.0436	1.0359	1.0254	1.0039	.9326

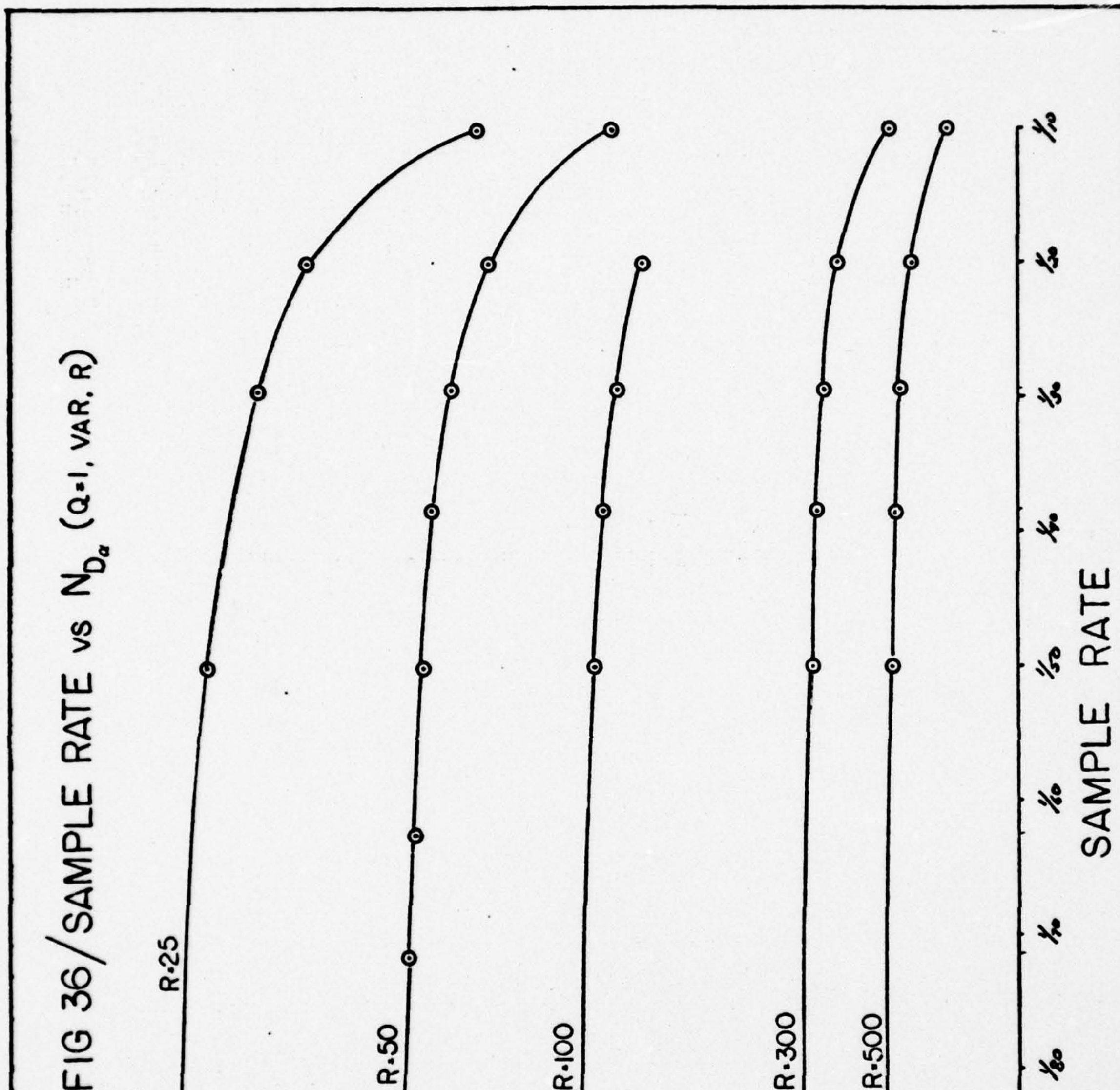

FIG 36/SAMPLE RATE vs N_{D_α} (Q=1, VAR. R)

Table XI

Optimal $N_{d_{\dot{\theta}}}$ Gains

R \ T	1/100	1/90	1/80	1/70	1/60	1/50	1/40	1/30	1/20	1/10
1	1.0003		.9904			.9492		.8734	.7840	.5262
25	.4491		.4468			.4377		.4212	.4017	.3398
50	.3799	.3782	.3782	.3765	.3749	.3715	.3664	.3594	.3453	.3001
75	.3448		.3435		.3407	.3378		.3278		.2783
100	.3222		.3210			.3160	.3122	.3071	.2968	
125						.3001	.2967	.2921		
150						.2878	.2846	.2804		
175						.2779	.2749	.2709		
200						.2695	.2667	.2629	.2553	
225						.2624	.2597	.2562	.2489	
300	.2499		.2491			.2460	.2436	.2404	.2339	.2134
400	.2341		.2334			.2307	.2286	.2257	.2200	.2018
500	.2227		.2221			.2196	.2176	.2150	.2098	.1933

Table XII
Optimal $N_{d_{\delta_h}}$ Gain

R \ T	1/100	1/90	1/80	1/70	1/60	1/50	1/40	1/30	1/20	1/10
1	-1.5812		-1.5637			-1.4886		-1.3599	-1.2175	-.8351
25	- .8316		- .8262			- .8044		- .7665	- .7238	-.5985
50	- .7233	-.7192	- .7192	-.7150	-.7108	- .7025	-.6900	- .6734	- .6405	-.5430
75	- .6667		- .6631		-.6560	- .6489		- .6239		-.5116
100	- .6293		- .6261			- .6133	-.6037	- .5910	- .5657	
125						- .5871	-.5783	- .5666		
150						- .5666	-.5584	- .5474		
175						- .5998	-.5421	- .5317		
200						- .5357	-.5283	- .5185	- .4990	
225						- .5235	-.5165	- .5071	- .4884	
300	- .5056		- .5035			- .4951	-.4888	- .4803	- .4636	-.4128
400	- .4778		- .4759			- .4683	-.4626	- .4551	- .4400	-.3943
500	- .4573		- .4556			- .4486	-.4434	- .4364	- .4225	-.3804

Table XIII
Summary of Times to Reach Steady State

R \ T	1/100	1/90	1/80	1/70	1/60	1/50	1/40	1/30	1/20	1/10
1	.554		.554			.556		.560	.564	.906
25	1.084		1.086			1.088		1.094	1.102	1.122
50	1.1258	1.258	1.258	1.258	1.260	1.262	1.264	1.268	1.276	1.298
75	1.372		1.372		1.374	1.376		1.382		1.412
100	1.460		1.462			1.466	1.468	1.472	1.480	
125						1.538	1.542	1.546		
150						1.602	1.606	1.608		
175						1.658	1.662	1.664		
200						1.708	1.712	1.716	1.724	
225						1.754	1.758	1.762	1.770	
300	1.870		1.870			1.874	1.876	1.880	1.888	1.912
400	1.998		1.998			>2.00	>2.00	>2.00	>2.00	>2.00
500	>2.00		>2.00			>2.00	>2.00	>2.00	>2.00	>2.00

holding the control penalty weighting constant. The result is an effective decrease in the value of gain. This is true for both the N_{d_α} and $N_{d_{\dot\theta}}$ feedback gains. From Table XII, it is seen that an increase in the control penalty weighting (R), while the sample rate is held constant, has the same effect as decreasing the sample rate, while holding the control penalty weighting constant. The effect is to increase the gain $N_{d_{\delta_h}}$. Finally, Table XIII presents the time required, as a function of sample rate and control penalty, for the simulation to achieve steady state lock-on to the commanded response with zero error. It is interesting to note that for higher sample rates (i.e., sample rates greater than $T = 1/50$) there is little change in this amount of elapsed time required.

These observations are summarized in Table XIV. Also included are the observed effects of these operations on the time required for the C^* system output to match C^* commanded, with zero steady state error, from Table XIII.

Table XIV
Summary of Gain Effects

▲= increase ▼= decrease

Gain Values / Operation	L_d	N_d	$N_{d_{\dot\theta}}$	N_d	Gain Values / * Time Required for C^* act= C^* com
Increase R (T Constant)	▲	▼	▼	▲	▲
Decrease T (R Constant)	▼	▼	▼	▲	▲

* From Table XIII

Increasing the control penalty weighting R then, has the effect of decreasing the size of the controls. This has the same effect on the system as increasing the sample rate. These are reasonable effects in that increasing the penalty on using excessive control rate results in smaller controls, while decreasing the sample rate, or the frequency with which new controls are introduced, forces the system to adjust by producing larger controls in order to keep the system under control. The sample rate can effectively be traded off against the control penalty weighting (R) to control the response. The time required to reach steady state with zero error increases in one case due to the use of smaller controls. In the other instance, with decreasing sample rates, the increase in time is due to the associated greater drop in the feedback gains N_{d_α} and $N_{d_{\dot{\theta}}}$ verses the rise in gain $N_{d_{\delta_h}}$ and the use of larger values of L_d.

<u>Saturation Effect</u>

Observations on the nature of the controls, especially the initial control, indicate that a possible problem may exist due to the large initial jump that occurs in the control. This jump in the control might very often be too fast and lead to the rate saturation of a "real-world" servo actuator. The effect of the ZOH, as can be seen from Figure 31, is to introduce a series of steps in the control. Consequently, a series of impulses would be characteristic of the control rate ($\dot{u}$) which might lead to rate saturation of the control actuator.

The maximum movement rate of the horizontal stabilizer for the YF-16 is currently 60 degrees/seconds. In radian measure, this is

1.047 radians/second. Realizing, of course, that the nature of the simulation is a constraint here in that .002 second was decided upon for its iteration rate, it is nevertheless valuable to characterize the nature of this possible flaw using the simulation.

In $1/500^{th}$ second, a displacement of the surface of .00209 radians or .12 degrees becomes the limiting rate of movement for this control surface. This limiting rate becomes significant. Consider the case in which the sample rate is slowed down considerably. During the time interval that the aircraft model is allowed to change states between updates, the plant may diverge considerably from that required to null the error between C^* commanded and C^* actual. When a new control is calculated, based on existing states, the result may be a control correction which exceeds the capability of the servo. As an example, consider the case in which the present control is -.0085 radians. The control update rate is assumed to be $1/\tau$ seconds. After $1/\tau$ seconds have passed, the new updated control is calculated to be +.0065 radians. The absolute range of control can be seen to be .015 radians. The servo of the aircraft is in effect being told to supply a .015 radian correction in $1/500^{th}$ second. Since this exceeds the servo limit, this control cannot be supplied indicating that the sample rate of $1/\tau$ seconds is infeasible. The possibility of such an effect must be considered.

For this simulation, it became apparent that a limit would be approached in terms of a minimum sample rate where the response just falls within the most restrictive of the C^* response criteria envelopes using controls which are just below the saturation limit of the servo. Such a point was reached, the results of which are shown in Figure 37,

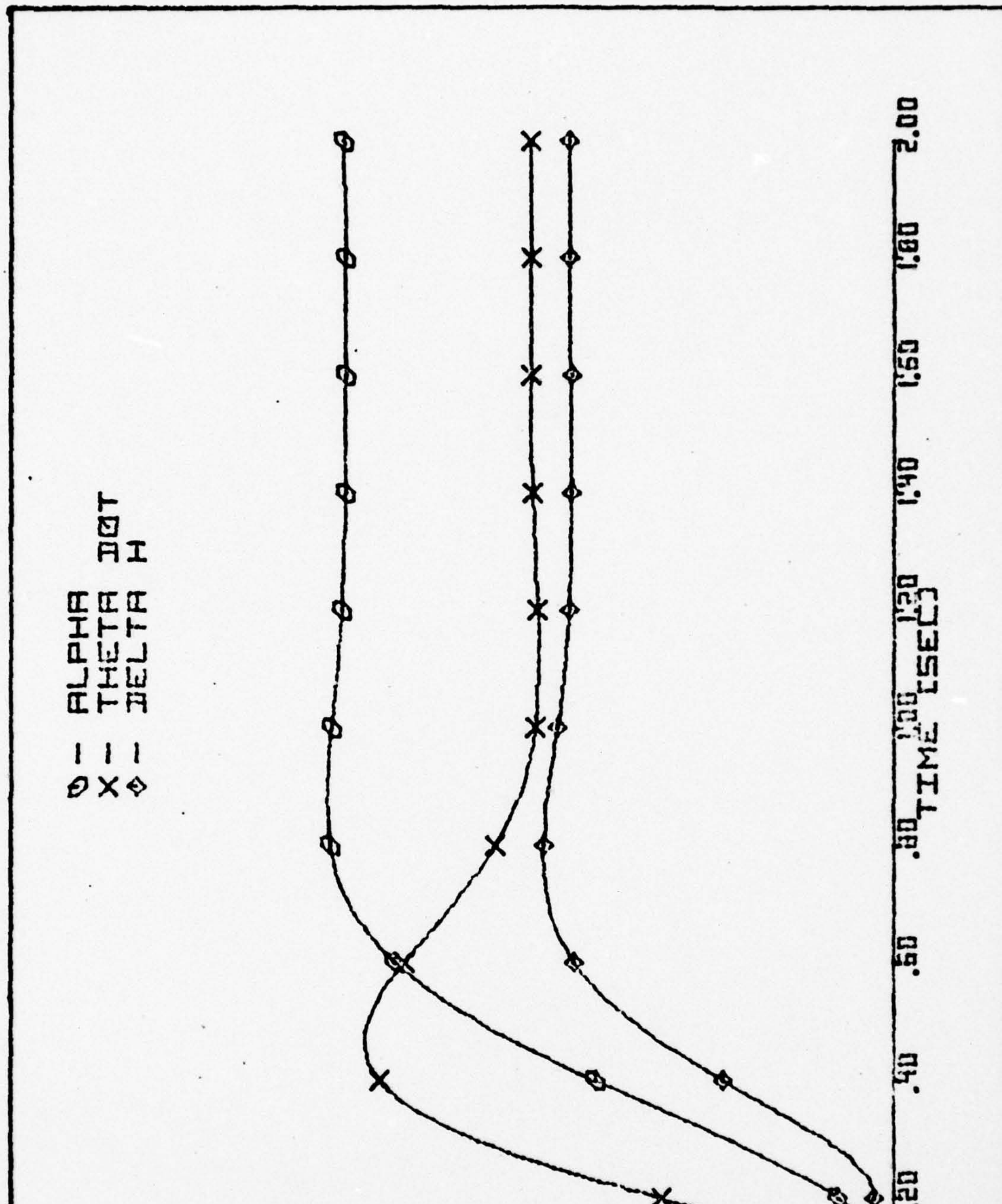

FIG - 37. STATES VS TIME

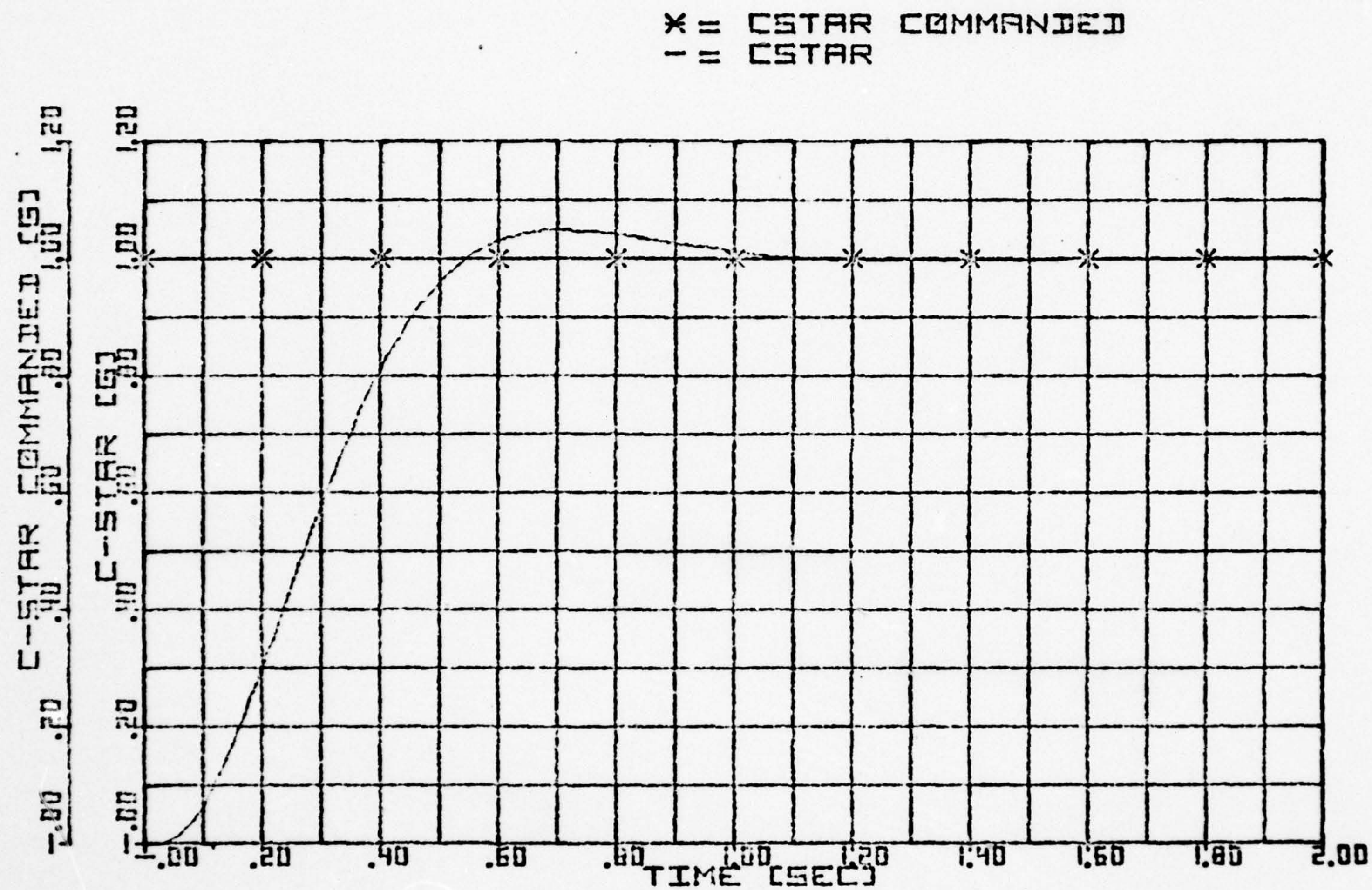

FIG - 38. OUTPUT VS TIME

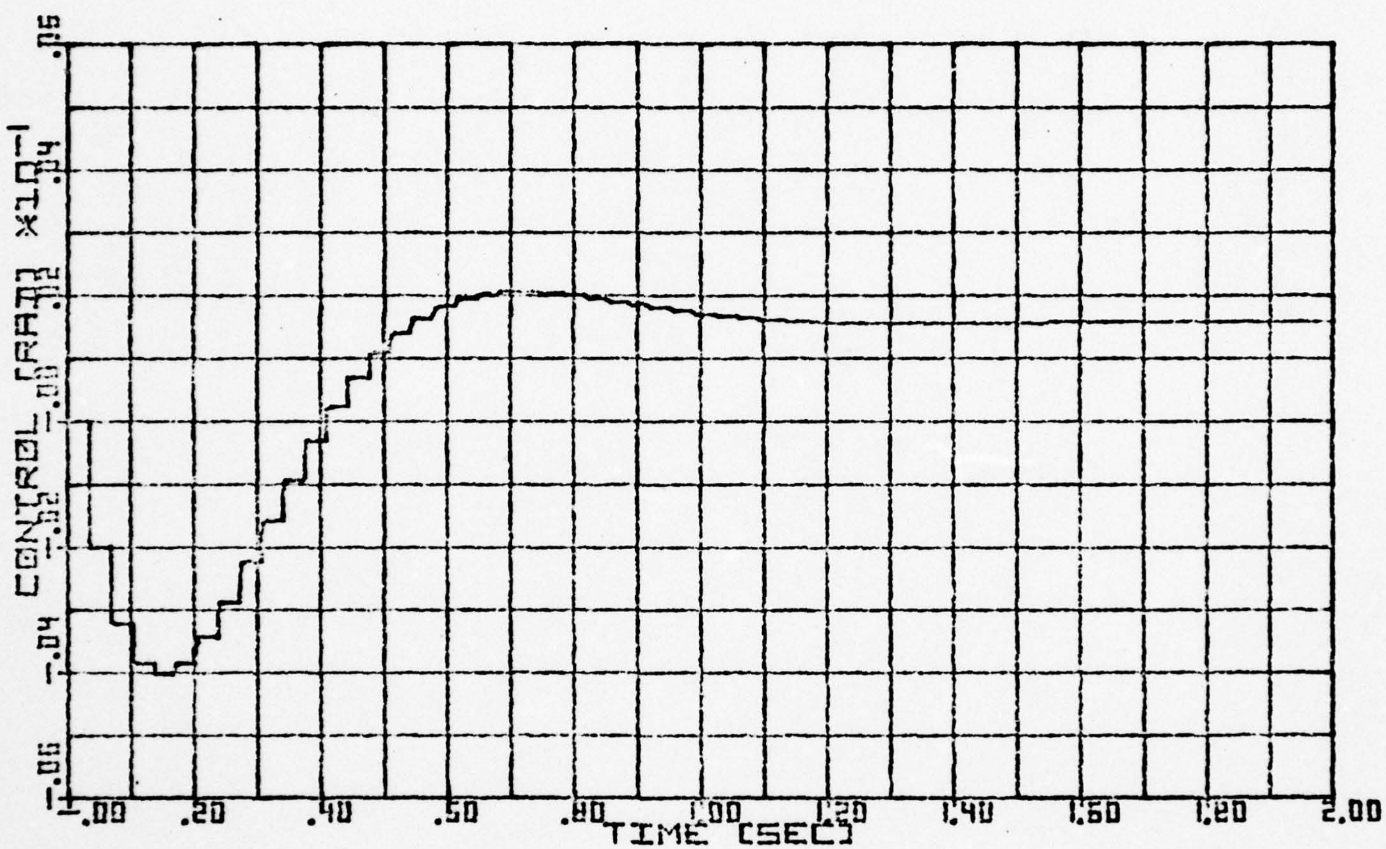

FIG - 39. CONTROL VS TIME

38, and 39. The minimum sample rate was found to be $T = 1/30$ seconds with a trajectory error penalty weighting of unity and a control penalty weighting of 200. The system C^* output achieved a steady state match-up with the commanded response in 1.716 seconds. Greater values of control penalty or slower sample rates caused the response to be stretched out sufficiently to fall outside the bounds of the envelope at some time in its time history.

Root Migrations

The effects of variation in sample rate for a constant control penalty and the effects of variation in the control penalty for constant sample rates are presented in Figures 40 and 41, respectively. Both figures portray limited data, for the purpose of clarity, in the upper right (positive) quadrant of the Z-plane unit circle. A conjugate counterpart root is assumed. Figure 40 depicts the concentric nature of the curves of constant control penalty weighting; the innermost curve having the greater weighting. It is apparent that for one particular sample instance, such as $T = 1/100$, the root locations vary considerably depending on the control penalty weighting selected. It appears, due to the consistency in the nature of the overshoot of the output, that the amount of overshoot (i.e., $f(\zeta)$) is controlled by the trajectory error penalty. With Q fixed at unity, the system is operating in a less than critically damped region, in the neighborhood of a .69 damping ratio. The effect of a variation in the control penalty is to alter the particular damped natural frequency ω_n. The direction of this variation in natural frequency is inversely proportional to the direction of variation in the control penalty weighting; that is, a decrease in ω_n results from an increase in R. This appears

FIG 40/CURVES OF CONSTANT R, VAR. SAMPLE RATES
LOCATING ROOTS IN UNIT CIRCLE

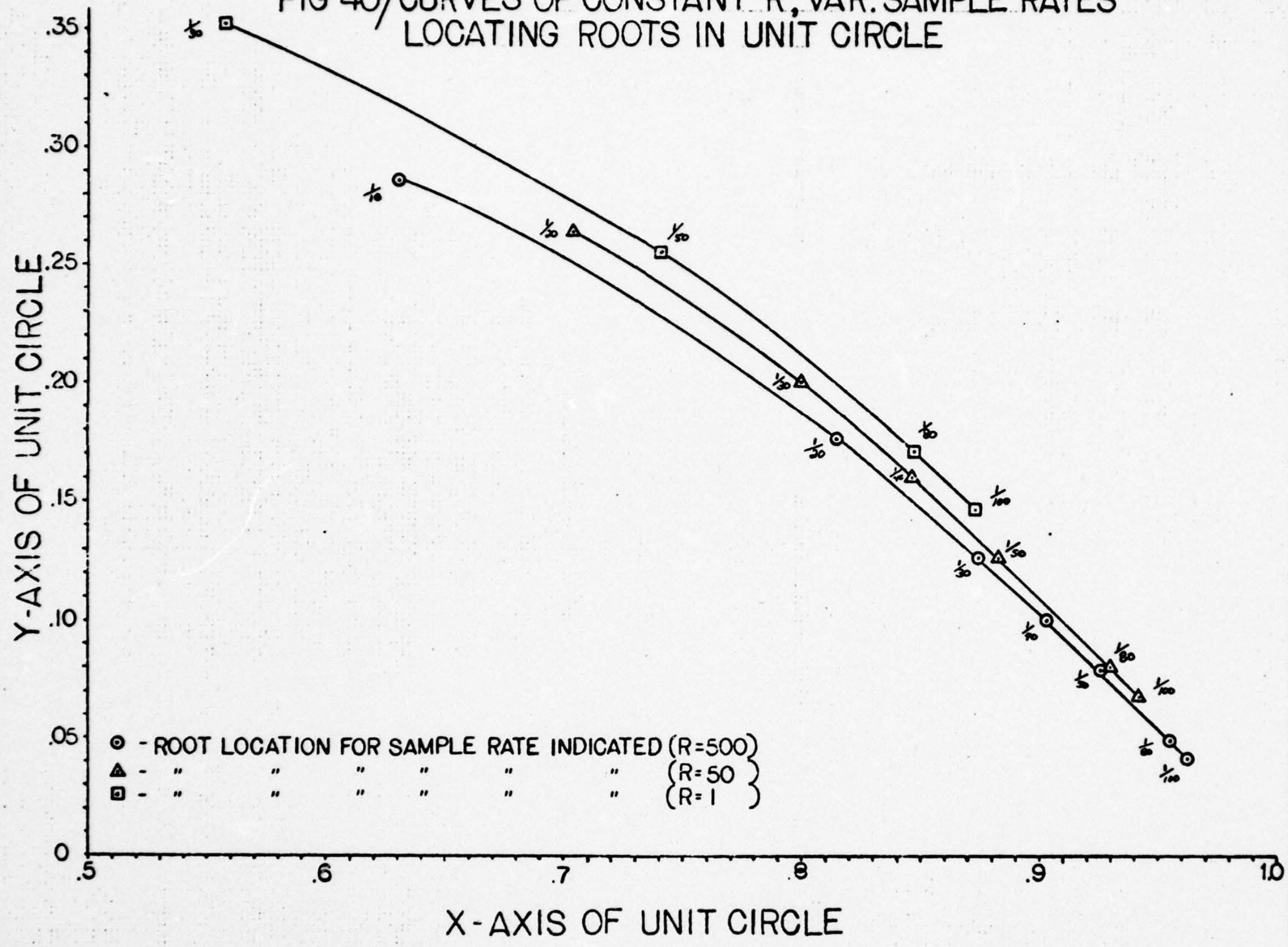

FIG 41/ ROOT CURVES OF CONST. SAMPLE RATE BUT VARIABLE R vs TGT ROOT VALUES

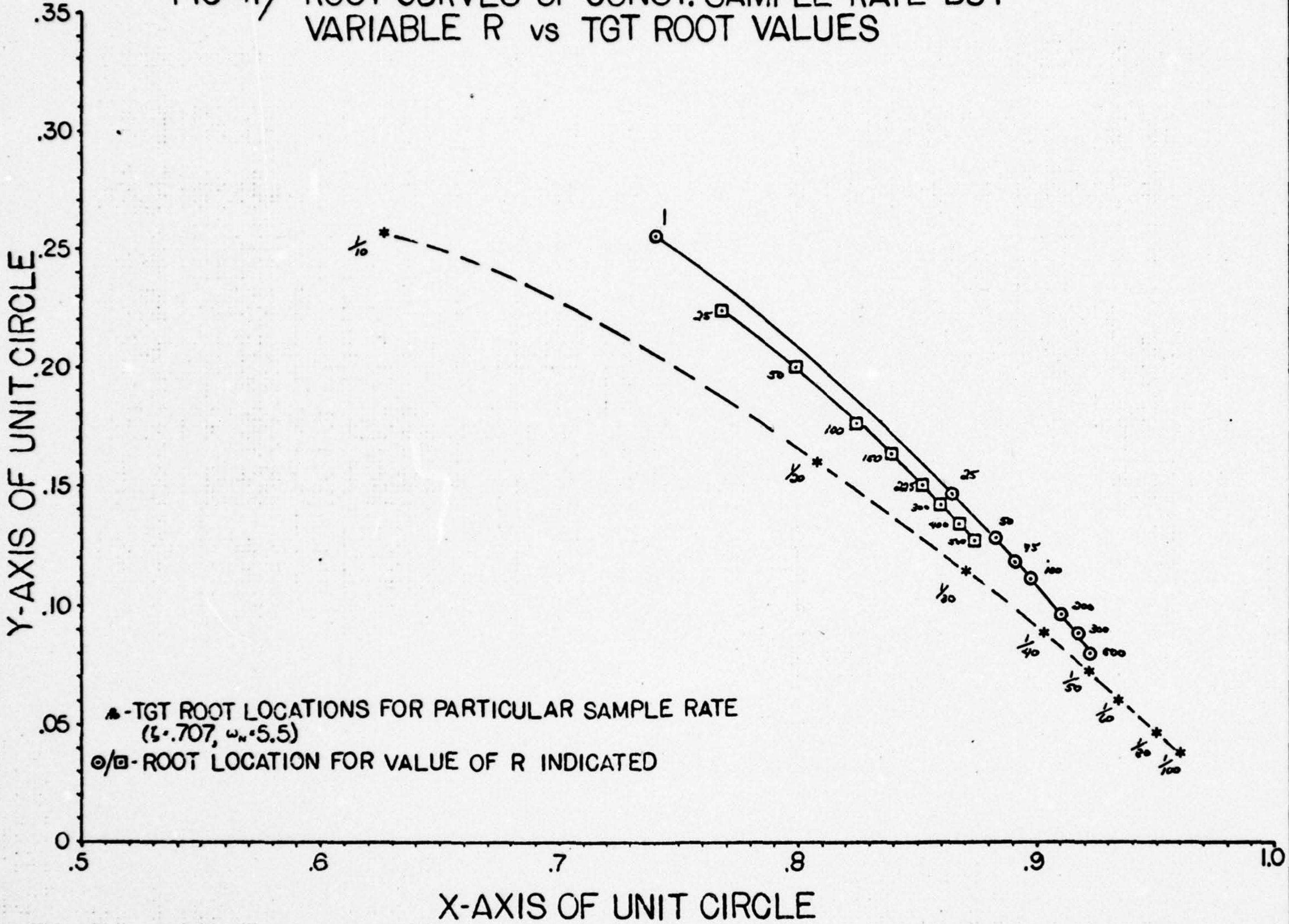

reasonable. It was noted earlier that increasing the control penalty weighting "stretched-out" the C^* response of the system. Such an effect would also increase the time required for the response to reach its peak (t_p). Peak time, directly related in this way to the control penalty, is known to be inversely proportional to the natural frequency thus completing the relationship.

In Figure 41, target roots, based upon a $\zeta = .707$ and $\omega_n = .5.5$ as presented in the previous chapter have been calculated and superimposed for various sample rates. The locus of roots for two particular sample rates are shown. Due to the direct mapping nature of Figure 27 to Figure 28, the roots, being above the target in each case, confirm that a damping factor less than .707 is in operation.

VIII. Conclusions and Recommendations

Conclusions

This investigation demonstrates that a discrete optimal controller for the longitudinal pitch axis of the YF-16 Lightweight Fighter Prototype aircraft, based on the proposed C^* transient response handling qualities performance criteria, is possible at .8 Mach. A reduced state model, based on a short period approximation, was successfully developed using stability derivatives calculated from available wind tunnel information. For the case of subsonic flight at Mach .8 at sea level, a positive C_{m_α} stability derivative was shown to exist. Such a situation is indicative of a statically unstable aircraft. In this respect, the YF-16 is unique. Once disturbed from equilibrium by a pitch up command, for instance, the aircraft will continue to pitch up (Fig. 12a).

The design is based on the requirement that the aircraft successfully track, with zero steady state error, a 1-G climb step input command. Due to its unstable character, results confirm that the aircraft attempts to continue its pitch up necessitating the use of nose down elevator control, in the steady state, to continue the climbing maneuver.

In answer to the series of questions which introduced the previous chapter, the system could be controlled and controlled within the innermost C^* envelope bounds. The everpresent problem of rate saturation was shown as presenting limitations to the concept. The tendency for initial, large jumps in control position was shown to lead to control rates which could exceed the movement rate of the control surface.

Through the use of a digital simulation, a ZOH approach was found superior to a FOH control scheme in reducing the amount of elapsed time for the system to achieve a steady controlled state. Investigation of various sample rates using the simulation model showed the optimal approach to a solution only slightly effected, in terms of elapsed time to reach steady state lock-on, to the sample rate used. The time required to reach steady state was also shown to be appreciably uneffected at sample rates greater than $T = 1/50$ second. More frequent sampling, however, did result in the production of smaller magnitudes of control deflections.

Use of a trajectory error weighting of unity produced an overshoot in the response of approximately five percent associated with a damping ratio of .69.

The investigation of system closed loop conjugate root migrations showed the trajectory error weighting to be the dominant factor in determining the amount of overshoot and the effective system damping. Likewise, the control penalty weighting was seen as determining the system natural frequency. This relationship held that the natural frequency was inversely proportional to the control penalty weighting. Finally, increasing the control penalty weighting, while the sample rate is held constant, or decreasing the sample rate, while the control penalty weighting is held constant, is seen as causing an increase in the elapsed time to steady state lock-on of system response to commanded response.

In summary, digital longitudinal pitch control of the YF-16 using the discrete C^* approach presented here, as an alternative to the present analog control configuration of the YF-16, is a viable possibility warranting further investigation.

Recommendations

It is recommended that this research be broadened to incorporate a larger portion of the YF-16 flight envelope. Stability derivative information for three additional flight conditions is presented for future research purposes. A full scale analysis of major subsonic and supersonic operating points is urged to confirm the applicability of a discrete C^* controller and the nature of the C^* response. Quite possibly, the use of a system of modeling stability derivatives based on simplifying assumptions and approximations different from the Blakelock approach used here, could be useful to confirm the validity of the YF-16 model developed in this investigation. From the small variation in the magnitude of the controller gains with sample rate, noted in this study, it would be valuable to investigate the magnitude of the gains for other flight conditions. Relatively close gain results between operating regions might foster the identification of one fixed set of gains or a limited range of gain values which control the system over a broad range of operating conditions. Failure to identify such "all purpose gains" might necessitate an adaptive controlling gain scheme. Additionally, the feasibility of substituting the optimal gains from one flight condition for its equivalent at some other operating condition should be investigated. Such a "mismatch analysis", though suboptimal in its approach, might still provide control of the system and aid in an all purpose gain identification.

This study concentrated on a step input pilot command to the system. Future investigations should address alternate inputs to the system. Additionally, the approach taken here was completely

deterministic. Attention should be given to the discrete stochastic aspects of a C^* control design which incorporates random disturbances to the system.

Finally, a sensitivity analysis should be conducted on the effective change in system response to changes in the values of the coefficients $K_{\dot{\theta}}$, K_Z , and $K_{\ddot{\theta}}$ in the original C^* equation. Different weights to these terms, effecting the blending of pitch rate and normal acceleration, might yield among other characteristics, a more responsive control system.

Bibliography

1. Blakelock, John H. Automatic Control of Aircraft and Missiles. New York: John Wiley and Sons, Inc., 1965.

2. Cadzow , J. A. and H. R. Martens. Discrete-Time and Computer Control Systems. New Jersey: Prentice-Hall, Inc., 1970.

3. D'Azzo, J. J. and C. H. Houpis. Linear Control System Analysis and Design. New York: McGraw-Hill Book Company, Inc., 1975.

4. Etkins, B. Dynamics of Flight: Stability and Control. New York: John Wiley and Sons, Inc., 1959.

5. Horwitz, David L. Development of a "Gyro-Less" Digital Flight Director. Research and Technical Report ECOM-0084-S-2, Prepared for Army Electronics Command, Ohio University, 1972.

6. Kleinman, D. L. A Description of Computer Programs Useful in Linear System Studies. Report No. TR-754, University of Connectifut, October 1975.

7. Kuo, B. C. Analysis and Synthesis of Sampled Data Control Systems. New Jersey: Prentice-Hall, Inc., 1963.

8. Lee, W. H., M. Athans, D. Costanon, F. Bacchioloni. Tracking Systems with Applications to Aircraft Control System Design. Nasa Langley Research Grant No. ESL-R-720, MIT, January 1977.

9. MIL-F-8785B. Military Specifications - Flying Qualities of Piloted Airplanes. 7 August 1969.

10. PARTL - Heavierside Partial Fraction Expansion and Time Response Program. Unpublished User's Guide to Computer Program. Ohio: Air Force Institute of Technology, December 1974.

11. ROOTL User's Manual. Unpublished User's Guide to Computer Program. Ohio: Air Force Institute of Technology, January 1976.

12. Sandell, N. R. Jr. Optimal Linear Tracking Systems. S.M. Thesis, MIT, 1971.

13. Stability and Flight Control. YF-16 Aerodynamic Data Summary, Vol. III. General Dynamics Convair Aerospace Division. November 1973.

14. Stability and Flight Control. YF-16 Flight Simulator Program/Data. General Dynamics Convair Aerospace Division, January 1973.

Bibliography

15. Stengel, R. F., J. R. Broussard, P. W. Berry. The Design of Digital-Adaptive Controllers for VTOL Aircraft. NASA CR 144912. March 1976.

16. TRANFUN - Transfer Function Program. Unpublished User's Guide to Computer Program. Ohio: Air Force Institute of Technology, 1974.

17. Tobie, H. N. and E. M. Elliot. New Short Period Handling Qualities Criterion for Fighter Aircraft. Boling Document No. D6-17841 T/N, September 1965.

18. Whitbeck, Richard F. Final Report on Multi-Rate Digital Flight Control. Calspan Report No. AK-5505-E-1, Air Force Office of Scientific Research, Air Force Systems Command, January 1975.

19. Zeta Plotter User's Manual. Compatible Plotting Subroutines. Calif: Zeta Research Incorporated, May 1973.

Appendix A

Determination of Length to Tail ℓ_t

This appendix first defines and then determines the value of ℓ_t needed in the evaluation of various stability derivatives in Chapter II. Dimensional values are taken from Reference 13.

ℓ_t = distance between the quarter chord point of the wing mean aerodynamic chord (MAC) and the quarter chord point of the horizontal stabilizer MAC.

The value of ℓ_t was determined from the physical dimensions of the aircraft.

Side View

YF-16 Lightweight Fighter Prototype

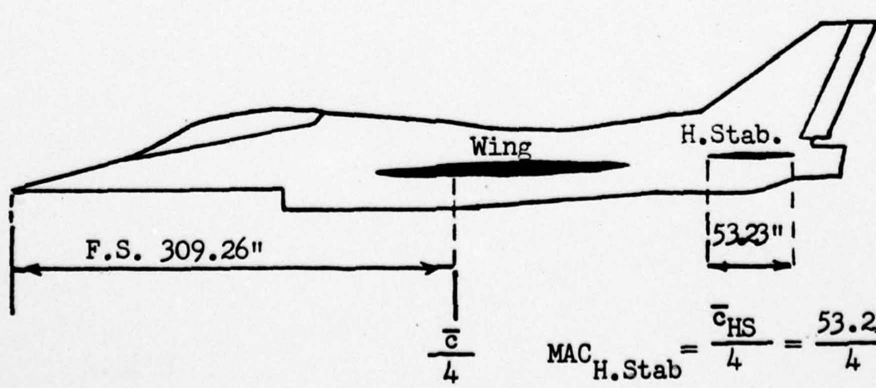

$$MAC_{H.Stab} = \frac{\bar{c}_{HS}}{4} = \frac{53.23}{4}$$

$= 13.31"$ in from leading edge (127)

Top View of
Horizontal Stabilizer

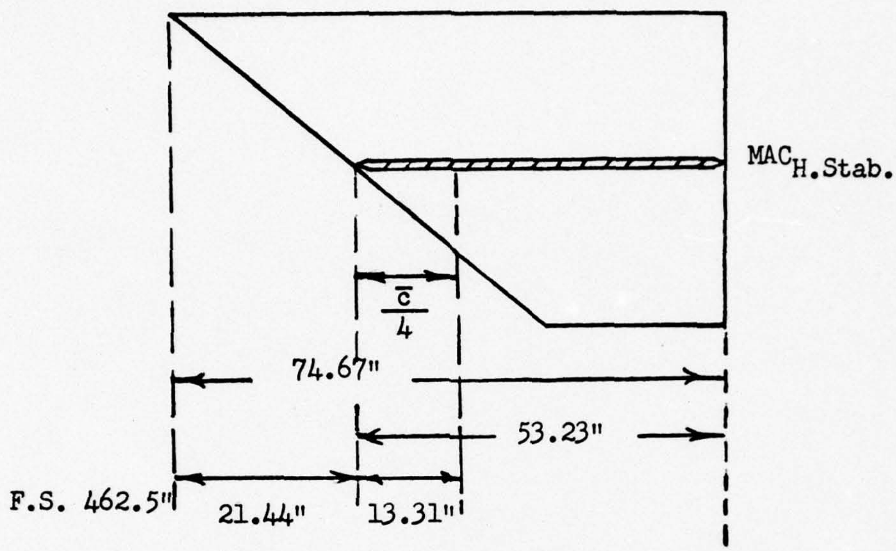

$$F.\,S. = 462.5'' + 21.44'' + 13.31'' = 497.25'' \tag{128}$$

$$\ell_t = 497.25'' - 309.26'' = 187.99'' = 15.666'$$

$$\ell_t = 15.666' \tag{129}$$

Appendix B

TRANFUN Program Input/Output

The determination of the characteristic equations, characteristic roots and transfer functions from the three longitudinal equations of motion is accomplished using the TRANFUN digital computer program (Ref. 16).

For Set A, the equations can be expressed as:

$$\begin{bmatrix} 1.726s + .0656 & .0005 & .0621 \\ .1882 & 1.7325s + 4.4942 & -1.7073s \\ 0 & .0093s - .1788 & .0135s^2 + .0268s \end{bmatrix} \begin{bmatrix} \frac{u}{\delta_h} \\ \frac{\alpha}{\delta_h} \\ \frac{\theta}{\delta_H} \end{bmatrix} = \begin{bmatrix} 0 \\ -.4504 \\ -.6452 \end{bmatrix} \quad (130)$$

This information is input into TRANFUN in the following manner:

```
ENTER $ABC INPUT DATA
$ABC A(2)=1.726,.0656,B(3)=.0005,C(3)=.0621$

ENTER $DEF INPUT DATA
$DEF D(3)=.1882,E(2)=1.7325,4.4942,F(2)=-1.7073$

ENTER $GHP INPUT DATA
$GHP G(3)=0.0,H(2)=.0093,-.1788,P(1)=.0135,.0268$

ENTER $FORCE INPUT DATA
$FORCE FORC1(3)=0.0,FORC2(3)=-.4504,FORC3(3)=-.6452$
```

The following results are forthcoming:

YF-16 MACH=.9 ALPHA=.73 SEA LEVEL

CHARACTERISTIC EQUATION

S6	S5	S4	S3
0.	0.	.40368983E-01	.21379880E+00

S2	S1	S0
-.31093424E+00	-.12018067E-01	-.20996749E-02

ROOTS ARE

REAL	IMAG
.1223932E+01	0.
-.2093674E-01	.7804015E-01
-.2093674E-01	-.7804015E-01
-.6478175E+01	.6967083E-30

TRANSFER FUNCTION A

NUMERATOR EQUATION

S6	S5	S4	S3
0.	0.	0.	0.

S2	S1	S0
.30402000E-05	.69712630E-01	.18506976E+00

GAIN = 1.72689

ZEROES AT

REAL	IMAG
-.2654752E+01	0.

POLES AT

REAL	IMAG
.1223932E+01	0.
-.2093674E-01	.7804015E-01
-.2093674E-01	-.7804015E-01
-.6478175E+01	.6967083E-30

TRANSFER FUNCTION B

NUMERATOR EQUATION

S6	S5	S4	S3
0.	0.	0.	-.10494770E-01

S2	S1	S0
-.19225082E+01	-.73053517E-01	-.75405943E-02

GAIN = -.25997

ZEROES AT

REAL	IMAG
-.1899276E-01	-.5965549E-01
-.1899276E-01	.5965549E-01
-.1831493E+03	-.2969072E-35

POLES AT

REAL	IMAG
.1223932E+01	0.
-.2093674E-01	.7804015E-01
-.2093674E-01	-.7804015E-01
-.6478175E+01	.6967081E-30

```
TRANSFER FUNCTION C

NUMERATOR EQUATION

      S6                  S5                  S4                  S3
 0.                  0.                  0.                  0.

              S2                  S1                  S0
        -.19221086E+01      -.52168603E+01      -.19543971E+00

                          GAIN =          -47.61350
           ZEROES AT                                   POLES AT
    REAL                 IMAG              REAL                 IMAG
 -.3799498E-01       0.                 .1223932E+01        0.
 -.2676139E+01       0.                -.2093674E-01         .7804015E-01
                                       -.2093674E-01        -.7804015E-01
                                       -.6478175E+01         .6567083E-30
```

The results determine the system transfer functions which can be expressed as:

$$\frac{u}{\delta_h} = \frac{.0000030402s^2 + .06971263s + .18506976}{.040368983s^4 + .2137988s^3 - .31093424s^2 - .012018067s - .0020896749} \qquad (131)$$

$$\frac{\alpha}{\delta_h} = \frac{-.25997\ (s + .01899276 \pm .05968549j)\ (s + 183.1493)}{(s - 1.223932)\ (s + .02093674 \pm .07804015j)\ (s + 6.478175)} \qquad (132)$$

$$\frac{\theta}{\delta_h} = \frac{-47.6135\ (s + .03799498)\ (s + 2.676139)}{(s - 1.223932)\ (s + .02093674 \pm .07804015j)\ (s + 6.478175)} \qquad (133)$$

Phugoid Roots (Set A)

The phugoid factor of the characteristic equation is:

$$s + .02093674 \pm .07804015j \tag{134}$$

From this ω_n, ω_d, ζ_{ph}, and T_{ph} for this oscillatory mode can be determined:

$$\begin{aligned}
\omega_n &= \sqrt{\sigma^2 + \omega_d^2} &&= .0808 \\
\omega_d &= .07804 && \\
\zeta_{ph} &= \frac{\sigma}{\omega_n} &&= .25912 \\
T_{ph} &= \frac{2\pi}{\omega_n} &&= 77.762 \text{ sec}
\end{aligned} \tag{135}$$

Short Period Root (Set A)

The short period factor of the characteristic equation for this unstable situation is:

$$s^2 + 5.254243s - 7.928845684 = 0 \tag{136}$$

For Set B, the equations can likewise be expressed as:

$$\begin{bmatrix} 1.1506s + .1033 & .0813 & .0276 \\ .1200 & 1.1465s + 4.8132 & -1.11862s \\ 0 & -.00164s + .7392 & .006s^2 + .01855s \end{bmatrix} \begin{bmatrix} \frac{u}{\delta_h} \\ \frac{\alpha}{\delta_h} \\ \frac{\theta}{\delta_h} \end{bmatrix} = \begin{bmatrix} 0 \\ -.361 \\ -.5157 \end{bmatrix} \tag{137}$$

This information is input into TRANFUN as:

```
ENTER $ABC INPUT DATA
$ABC A(2)=1.1506,.1033,B(3)=.0818$C(3)=.0276$

ENTER $DEF INPUT DATA
$DEF D(3)=.12,E(2)=1.1465,4.8132,F(2)=-1.11862$

ENTER $GHP INPUT DATA
$GHP G(3)=0.0,H(2)=-.00164,.7392,P(1)=.006,.01855$

ENTER $FORCE INPUT DATA
$FORCE FORC1(3)=0.0,FORC2(3)=-.361,FORC3(3)=-.5157$
```

The following output information results:

```
               YF-16 MACH=1.2 ALPHA=1.3 SEA LEVEL
*********************************************************************

                     CHARACTERISTIC EQUATION

     S6                 S5                 S4                 S3
 0.                 0.                 .79149774E-02      .56298662E-01

          S2                 S1                 S0
     .10590759E+01      .94453828E-01      .24482304E-02

        ROOTS ARE
     REAL               IMAG
  -.4474255E-01      .1790868E-01
  -.4474255E-01     -.1790868E-01
  -.3511721E+01      .1099289E+02
  -.3511721E+01     -.1099289E+02
*********************************************************************
*********************************************************************

                     TRANSFER FUNCTION A

                     NUMERATOR EQUATION

     S6                 S5                 S4                 S3
 0.                 0.                 0.                 0.

          S2                 S1                 S0
     .17609580E-03      .63778992E-01      .61142723E-01

                     GAIN =               .02225
        ZEROES AT                                 POLES AT
     REAL               IMAG                REAL               IMAG
  -.9612166E+00      0.                -.4474255E-01      .1790868E-01
  -.3612223E+03      0.                -.4474255E-01     -.1790868E-01
                                       -.3511721E+01      .1099289E+02
                                       -.3511721E+01     -.1099289E+02
*********************************************************************
```

```
TRANSFER FUNCTION B

NUMERATOR EQUATION

     S6                S5                S4                S3
0.                0.                0.                -.24921996E-02

            S2                S1                S0
      -.67167811E+00    -.60282666E-01    -.17079994E-02

                        GAIN =            -.31487
           ZEROES AT                                    POLES AT
     REAL                IMAG                REAL                IMAG
  -.4488490E-01       -.2300164E-01       -.4474255E-01       .1790868E-01
  -.4488490E-01        .2300164E-01       -.4474255E-01      -.1790868E-01
  -.2694224E+03       -.2447436E-21       -.3511721E+01       .1099289E+02
                                          -.3511721E+01      -.1099289E+02
```

```
TRANSFER FUNCTION C

NUMERATOR EQUATION

     S6                S5                S4                S3
0.                0.                0.                0.

            S2                S1                S0
      -.68097351E+00    -.26100799E+01    -.22351098E+00

                        GAIN =            -86.03606
           ZEROES AT                                    POLES AT
     REAL                IMAG                REAL                IMAG
  -.8775803E-01       0.                  -.4474255E-01       .1790868E-01
  -.3745108E+01       0.                  -.4474255E-01      -.1790868E-01
                                          -.3511721E+01       .1099289E+02
                                          -.3511721E+01      -.1099289E+02
```

The resulting system transfer functions are:

$$\frac{u}{\delta_h} = \frac{(s + .9612166)\ (s + 361.2223)}{.0079149774s^4 + .056298662s^3 + 1.0590759s^2 + .094453828s + .0024482304} \quad (138)$$

$$\frac{\alpha}{\delta_h} = \frac{-.31487\ (s + .0448849\ \pm .02300164j)\ (s + 269.4224)}{(s + .04474255 \pm .01790868j)\ (s + 3.511721 \pm\ 10.99289j)} \quad (139)$$

$$\frac{\theta}{\delta_h} =$$

$$\frac{-86.03606\ (s + .08775803)\ (s + 3.745108)}{(s + .04474255 \pm .01790868j)\ (\ s + 3.511721 \pm 10.99289j)} \tag{140}$$

Phugoid Roots (Set B)

The phugoid factor of the characteristic equation is:

$$s + .0447255 \pm .01790868j = 0 \tag{141}$$

From this ω_n , ω_d , δ_{ph} , T_{ph} are found to be:

$$\begin{aligned}
\omega_n &= \sqrt{\sigma^2 + \omega_d^2} = .0482 \\
\omega_d &= .0179 \\
\delta_{ph} &= \frac{\sigma}{\omega_n} = .9279 \\
T_{ph} &= \frac{2\pi}{\omega_n} = 130.357
\end{aligned} \tag{142}$$

Short Period Root (Set B)

The short period factor of the characteristic equation is:

$$s + 3.511721 \pm 10.99289j = 0 \tag{143}$$

From this ω_n , ω_d , δ_{sp} , and T_{sp} are determined to be:

$$\begin{aligned}
\omega_n &= \sqrt{\sigma^2 + \omega_d^2} = 11.540 \\
\omega_d &= 10.99289 \\
\delta_{sp} &= \frac{\sigma}{\omega_n} = .3043 \\
T_{sp} &= \frac{2\pi}{\omega_n} = .544 \text{ sec}
\end{aligned} \tag{144}$$

Appendix C

Continuous State Variable Equation Development

This appendix details the development of a state variable representation of the longitudinal equations of motion. Such a development is needed in order to model the YF-16 as a linear system of the form $\dot{\bar{x}} = \bar{A}\,\bar{x} + \bar{B}\,u$ for implementation of the controlled system model represented in Figure 19.

Returning to the original equations shown previously in Chapter II:

$$\frac{mU}{S_q}\dot{u}' - C_{x_u}u' - \frac{\bar{c}}{2U}C_{x_{\dot{\alpha}}}\dot{\alpha}' - C_{x_\alpha}\alpha' - \frac{\bar{c}}{2U}C_{x_q}\dot{\theta} - C_W\cos\Theta\,\theta = C_{x_{\delta_h}}\delta_h \qquad (1)$$

$$-C_{z_u}u' + \frac{mU}{S_q}\dot{\alpha}' - \frac{\bar{c}}{2U}C_{z_{\dot{\alpha}}}\dot{\alpha}' - C_{z_\alpha}\alpha' - \frac{mU}{S_q}\dot{\theta} - \frac{\bar{c}}{2U}C_{z_q}\dot{\theta} - C_W\sin\Theta\,\theta = C_{z_{\delta_h}}\delta_h \qquad (2)$$

$$-C_{m_u}u' - \frac{\bar{c}}{2U}C_{m_{\dot{\alpha}}}\dot{\alpha}' - C_{m_\alpha}\alpha' + \frac{I_{yy}}{S_q\bar{c}}\ddot{\theta} - \frac{\bar{c}}{2U}C_{m_q}\dot{\theta} = C_{m_{\delta_h}}\delta_h \qquad (3)$$

and letting

$$k_1 \triangleq \frac{mU}{S_q} \qquad\qquad k_3 \triangleq \frac{\bar{c}}{2U}$$

$$k_2 \triangleq \frac{I_{yy}}{S_q\bar{c}} \qquad\qquad k_4 \triangleq k_1 - k_3 C_{z_{\dot{\alpha}}} \qquad (145)$$

while neglecting the following terms by setting them equal to zero for the reasons explained in Chapter II:

$$C_{x_{\dot{\alpha}}} = C_{x_q} = C_{m_u} = C_{x_{\delta_h}} = \Theta = 0 \qquad (146)$$

the equations of motion can now be written as:

$$K_1 \acute{\dot{u}} - C_{x_u}\acute{u} - C_{x_\alpha}\acute{\alpha} - C_w \Theta = 0 \qquad = f(u,\dot{u},\alpha,\theta) \qquad (147)$$

$$-C_{z_u}\acute{u} + K_1\acute{\dot{\alpha}} - K_3 C_{z_{\dot{\alpha}}}\acute{\dot{\alpha}} - C_{z_\alpha}\acute{\alpha} - K_1\dot{\theta} - K_3 C_{z_q}\dot{\theta} = C_{z_{\delta_h}}\delta_h \qquad = f(u,\alpha,\dot{\alpha},\dot{\theta}) \qquad (148)$$

$$-K_3 C_{m_{\dot{\alpha}}}\acute{\dot{\alpha}} - C_{m_\alpha}\acute{\alpha} + K_2\ddot{\theta} - K_3 C_{m_q}\dot{\theta} = C_{m_{\delta_h}}\delta_h \qquad = f(\alpha,\dot{\alpha},\dot{\theta},\ddot{\theta}) \qquad (149)$$

Dropping the primes and defining the following state variables:

$$\bar{x} = \begin{bmatrix} x_1 = u \\ x_2 = \alpha \\ x_3 = \theta \\ x_4 = q \end{bmatrix} \qquad (150)$$

The equations become:

$$K_1\dot{x}_1 - C_{x_u}x_1 - C_{x_\alpha}x_2 - C_w x_3 = 0 \qquad (151)$$

$$-C_{z_u}x_1 + K_1\dot{x}_2 - K_3 C_{z_{\dot{\alpha}}}\dot{x}_2 - C_{z_\alpha}x_2 - K_1 x_4 - K_3 C_{z_q}x_4 = C_{z_{\delta_h}}\delta_h \qquad (152)$$

$$-K_3 C_{m_{\dot{\alpha}}}\dot{x}_2 - C_{m_\alpha}x_2 + K_2\dot{x}_4 - K_3 C_{m_q}x_4 = C_{m_{\delta_h}}\delta_h \qquad (153)$$

Dividing equation (151) by K, yields:

$$\dot{x}_1 - \frac{C_{x_u}}{K_1}x_1 + \frac{C_{x_\alpha}}{K_1}x_2 - \frac{C_w}{K_1}x_3 = 0 \qquad (154)$$

or,

$$\dot{X}_1 = \frac{C_{x_u}}{k_1} X_1 + \frac{C_{x_\alpha}}{k_1} X_2 + \frac{C_w}{k_1} X_3 \tag{155}$$

Similarly, equation (152) can be rewritten as:

$$-C_{z_u} X_1 + \left[k_1 - k_3 C_{z_{\dot\alpha}}\right]\dot{X}_2 - C_{z_\alpha} X_2 - k_1 X_4 - k_3 C_{z_q} X_4 = C_{z_{\delta_h}} \delta_h \tag{156}$$

or after expanding:

$$-C_{z_u} X_1 + k_4 \dot{X}_2 - C_{z_\alpha} X_2 - k_1 X_4 - k_3 C_{z_q} X_4 = C_{z_{\delta_h}} \delta_h \tag{157}$$

Solving for $\dot{x}_2$

$$k_4 \dot{X}_2 = C_{z_u} X_1 + C_{z_\alpha} X_2 + k_1 X_4 + k_3 C_{z_q} X_4 + C_{z_{\delta_h}} \delta_h \tag{158}$$

$$\dot{X}_2 = \frac{C_{z_u}}{k_4} X_1 + \frac{C_{z_\alpha}}{k_4} X_2 + \frac{k_1}{k_4} X_4 + \frac{k_3}{k_4} C_{z_q} X_4 + \frac{C_{z_{\delta_h}}}{k_4} \delta_h \tag{159}$$

or finally as:

$$\dot{X}_2 = \frac{C_{z_u}}{k_4} X_1 + \frac{C_{z_\alpha}}{k_4} X_2 + \left[\frac{k_1 + k_3 C_{z_q}}{k_4}\right] X_4 + \frac{C_{z_{\delta_h}}}{k_4} \delta_h \tag{160}$$

Since $\dot\theta = q$, then:

$$\dot{x}_3 = x_4 \tag{161}$$

The final equation results by dividing equation (153) by K_2 :

$$-\frac{k_3}{k_2} C_{m_{\dot\alpha}} \dot{x}_2 - \frac{C_{m_\alpha}}{k_2} x_2 + \frac{k_2}{k_2} \dot{x}_4 - \frac{k_3}{k_2} C_{m_\gamma} x_4 = \frac{C_{m\delta_h}}{k_2} \delta_h \quad (162)$$

Which, when solving for $\dot{x}_4$ becomes:

$$\dot{x}_4 = \frac{k_3}{k_2} C_{m_{\dot\alpha}} \dot{x}_2 + \frac{C_{m_\alpha}}{k_2} x_2 + \frac{k_3}{k_2} C_{m_\gamma} x_4 + \frac{C_{m\delta_h}}{k_2} \delta_h \quad (163)$$

Substituting in the previous expression for $\dot{x}_2$:

$$\dot{x}_4 = \frac{k_3}{k_2} C_{m_{\dot\alpha}} \left[\frac{C_{z_u}}{k_4} x_1 + \frac{C_{z_\alpha}}{k_4} x_2 + \left(\frac{k_1 + k_3 C_{z_\gamma}}{k_4} \right) x_4 + \frac{C_{z\delta_h}}{k_4} \delta_h \right] +$$

$$\frac{C_{m_\alpha}}{k_2} x_2 + \frac{k_3}{k_2} C_{m_\gamma} x_4 + \frac{C_{m\delta_h}}{k_2} \delta_h \quad (164)$$

Multiplying through each term:

$$\dot{x}_4 = \left[\frac{k_3}{k_2 k_4} C_{m_{\dot\alpha}} C_{z_\alpha} \right] x_1 + \left[\frac{k_3}{k_2 k_4} C_{m_{\dot\alpha}} C_{z_\alpha} \right] x_2 + \left[\frac{k_3}{k_2 k_4} (k_1 + k_3 C_{z_\gamma}) C_{m_{\dot\alpha}} \right] x_4 +$$

$$\left[\frac{k_3}{k_2 k_4} C_{m_{\dot\alpha}} C_{z\delta_h} \right] \delta_h + \frac{C_{m_\alpha}}{k_2} x_2 + \frac{k_3}{k_2} C_{m_\gamma} x_4 + \frac{C_{m\delta_h}}{k_2} \delta_h \quad (165)$$

or finally:

$$\dot{x}_4 = \left[\frac{k_3}{k_2 k_4} C_{m_{\dot\alpha}} C_{z_u} \right] x_1 + \left[\frac{k_3}{k_2 k_4} C_{m_{\dot\alpha}} C_{z_\alpha} + \frac{C_{m_\alpha}}{k_2} \right] x_2 +$$

$$\left[\frac{k_3}{k_2 k_4} (k_1 + k_3 C_{z_\gamma}) C_{m_{\dot\alpha}} + \frac{k_3}{k_2} C_{m_\gamma} \right] x_4 + \left[\frac{k_3}{k_2 k_4} C_{m_{\dot\alpha}} C_{z\delta_h} + \frac{C_{m\delta_h}}{k_2} \right] \delta_h \quad (166)$$

Summarizing, the four state variable equations corresponding to $\dot{u}$, $\dot{\alpha}$, $\dot{\theta}$, and $\ddot{\theta}$ are respectively:

155

$$\dot{x}_1 = \frac{C_{x_u}}{k_1} x_1 + \frac{C_{x_\alpha}}{k_1} x_2 + \frac{C_w}{k_1} x_3 \qquad (155)$$

60

$$\dot{x}_2 = \frac{C_{z_u}}{k_4} x_1 + \frac{C_{z_\alpha}}{k_4} x_2 + \left[\frac{k_1 + k_3 C_{z_{\dot\theta}}}{k_4}\right] x_4 + \frac{C_{z\delta_h}}{k_4} \delta_h \qquad (160)$$

161

$$\dot{x}_3 = 1.0\, x_4 \qquad (161)$$

$$\dot{x}_4 = \left[\frac{k_3}{k_2 k_4} C_{m_{\dot\alpha}} C_{z_u}\right] x_1 + \left[\frac{k_3}{k_2 k_4} C_{m_{\dot\alpha}} C_{z_\alpha} + \frac{C_{m_\alpha}}{k_2}\right] x_2 +$$

166

$$\left[\frac{k_3}{k_2 k_4}(k_1 + k_3 C_{z_{\dot\theta}}) C_{m_{\dot\alpha}} + \frac{k_3}{k_2} C_{m_{\dot\theta}}\right] x_4 + \left[\frac{k_3}{k_2 k_4} C_{m_{\dot\alpha}} C_{z_{\delta_h}} + \frac{C_{m\delta_h}}{k_2}\right] \delta_h \qquad (166)$$

Now, δ_h is introduced as the new state x_5, since:

75

$$\frac{\delta_h}{\delta_{h_c}} = \frac{20}{S + 20} \qquad (75)$$

where δ_{h_c} is the commanded deflection in the horizontal stabilizer, then:

167

$$20\, \delta_{h_c} = \dot{\delta}_h + 20\, \delta_h \qquad (167)$$

and solving for $\dot{\delta}_h$:

68

$$\dot{\delta}_h = -20\, \delta_h + 20\, \delta_{h_c} \qquad (168)$$

133

or finally that:

9 $$\dot{x}_5 = -20x_5 + 20\delta_{h_e} \tag{169}$$

the new forcing function u(t) become δ_{h_e}(t).

Now the system modeling equations of motion in the form of

77 equation (77) become:

$$\begin{bmatrix} \dot{x}_1 \\ (\dot{u}) \\ \dot{x}_2 \\ (\dot{\alpha}) \\ \dot{x}_3 \\ (\dot{\theta}) \\ \dot{x}_4 \\ (\ddot{\theta}) \\ \dot{x}_5 \\ (\dot{\delta}_h) \end{bmatrix} = \begin{bmatrix} \frac{C_{x_u}}{K_1} & \frac{C_{x_\alpha}}{K_1} & \frac{C_w}{K_1} & 0 & 0 \\ \frac{C_{z_u}}{K_4} & \frac{C_{z_\alpha}}{K_4} & 0 & \frac{K_1+K_3C_{z_q}}{K_4} & \frac{C_{z_{\delta_h}}}{K_4} \\ 0 & 0 & 0 & 1.0 & 0 \\ \frac{K_3}{K_2K_4}C_{m_{\dot\alpha}}C_{z_u} & \frac{K_3}{K_2K_4}C_{m_{\dot\alpha}}C_{z_\alpha}+\frac{C_{m_\alpha}}{K_2} & 0 & \frac{K_3}{K_2K_4}(K_1+K_3C_{z_q})C_{m_{\dot\alpha}}+\frac{K_3C_{m_q}}{K_2} & \frac{K_3}{K_2K_4}C_{m_{\dot\alpha}}C_{z_{\delta_h}}+\frac{C_{m_{\delta_h}}}{K_2} \\ 0 & 0 & 0 & 0 & -20.0 \end{bmatrix} \begin{bmatrix} x_1 \\ x_2 \\ x_3 \\ x_4 \\ x_5 \end{bmatrix} + \begin{bmatrix} 0 \\ 0 \\ 0 \\ 0 \\ -20.0 \end{bmatrix} \delta_{h_c} \qquad (170)$$

When the appropriate terms are extracted from Table III, and substituted into this latest expression, the following equation results:

$$\begin{bmatrix} \dot{x}_1 \\ \dot{x}_2 \\ \dot{x}_3 \\ \dot{x}_4 \\ \dot{x}_5 \end{bmatrix} = \begin{bmatrix} -.03800914 & -.99928970 & -.03598122 & 0 & 0 \\ -.10863579 & -2.5942135 & 0 & .985425739 & -.25998704 \\ 0 & 0 & 0 & 1.0 & 0 \\ .07495323 & 15.0520989 & 0 & -2.6725778 & -47.677365 \\ 0 & 0 & 0 & 0 & -20.0 \end{bmatrix} \begin{bmatrix} x_1 \\ x_2 \\ x_3 \\ x_4 \\ x_5 \end{bmatrix} + \begin{bmatrix} 0 \\ 0 \\ 0 \\ 0 \\ 20.0 \end{bmatrix} \delta_{h_c} \tag{171}$$

which is positionally equivalent to the terms of $\dot{\bar{x}} = \bar{A}\,\bar{x} + \bar{B}\,\bar{u}$.

Equation (171) can be simplified in terms of the number of states by using a short period approximation. Such a simplification is justified since the interest here is in the transient response of the aircraft. Additionally, the coefficients of the velocity state (u) in the A matrix above, have only a minor contribution on the short period transient response. The velocity state (u) can therefore be eliminated without degrading the short period performance of the aircraft.

Again, referring to the short period approximation equations of motion from Chapter III:

$$\left[\frac{mU}{Sq}s - C_{z_\alpha}\right]\alpha(s) + \left[-\frac{mU}{Sq}s - C_w(\sin\Theta)\right]\theta(s) = C_{z_{\delta_h}}\delta_h(s) \tag{61}$$

$$\left[-\frac{\bar{c}}{2u} C_{m_{\dot{\alpha}}} s - C_{m_{\alpha}}\right]\alpha'(s) + \left[\frac{I_{yy}}{S_q \bar{c}} s^2 - \frac{\bar{c}}{2u} C_{m_q} s\right]\theta(s) = C_{m_{\delta_h}} \delta_h(s) \qquad (62)$$

and eliminating the primes and s's, equation (61) becomes:

72 $$\frac{mu}{S_q} \dot{\alpha} - C_{z_{\alpha}} \alpha - \frac{mu}{S_q} \dot{\theta} = C_{z_{\delta_h}} \delta_h \qquad (172)$$

solving for $\dot{\alpha}$:

73 $$\dot{\alpha} = \frac{C_{z_{\alpha}}}{mu/S_q} + 1.0\, \dot{\theta} + \frac{C_{z_{\delta_h}}}{mu/S_q} \delta_h \qquad (173)$$

or equivalently,

74 $$\dot{\alpha} = \frac{C_{z_{\alpha}}}{k_1} \alpha + 1.0\, \dot{\theta} + \frac{C_{z_{\delta_h}}}{k_1} \delta_h \qquad (174).$$

Likewise, equation (62) becomes:

75 $$-\frac{\bar{c}}{2u} C_{m_{\dot{\alpha}}} \dot{\alpha} - C_{m_{\alpha}} \alpha + \frac{I_{yy}}{S_q \bar{c}} \ddot{\theta} - \frac{\bar{c}}{2u} C_{m_q} \dot{\theta} = C_{m_{\delta_h}} \delta_h \qquad (175)$$

or,

76 $$-k_3 C_{m_{\dot{\alpha}}} \dot{\alpha} - C_{m_{\alpha}} \alpha + k_2 \ddot{\theta} - k_3 C_{m_q} \dot{\theta} = C_{m_{\delta_h}} \delta_h . \qquad (176)$$

and solving for $\ddot{\theta}$ becomes:

$$\ddot{\theta} = \frac{C_{m_\alpha}}{k_2}\alpha + \frac{k_3}{k_2}C_{m_{\dot{\alpha}}}\dot{\alpha} + \frac{k_3}{k_2}C_{m_\delta}\dot{\theta} + \frac{C_{m_{\delta_h}}}{k_2}\delta_h \qquad (177)$$

Now, if the expression just found for $\dot{\alpha}$ is substituted into this newest expression, $\ddot{\theta}$ becomes:

$$\ddot{\theta} = \frac{1}{k_2}\left[C_{m_\alpha} + \frac{k_3}{k_1}C_{m_{\dot{\alpha}}}C_{z_\alpha}\right]\alpha + \frac{k_3}{k_2}\left[C_{m_{\dot{\alpha}}} + C_{m_\delta}\right] +$$

$$\frac{\delta_h}{k_2}\left[\frac{k_3}{k_1}C_{m_{\dot{\alpha}}}C_{z_{\delta_h}} + C_{m_{\delta_h}}\right] \qquad (178)$$

The remaining state equations remain the same. Specifically:

$$\dot{\theta} = q \qquad (179)$$

and

$$\dot{\delta}_h = -20.0\,\delta_h + 20.0\,\delta_{h_e} \qquad (168)$$

In state variable format, equations (168), (174), (178), and (179) can be expressed as:

$$
\begin{bmatrix} \dot{x}_1 \\ (\dot{\alpha}) \\ \dot{x}_2 \\ (\dot{\theta}) \\ \dot{x}_3 \\ (\ddot{\theta}) \\ \dot{x}_4 \\ (\dot{\delta}_h) \end{bmatrix}
=
\begin{bmatrix}
\frac{C_{z_\alpha}}{k_1} & 0 & 1.0 & \frac{C_{z_{\delta_h}}}{k_1} \\
0 & 0 & 1.0 & 0 \\
\frac{1}{k_2}\left[C_{m_\alpha} + \frac{k_3}{k_1} C_{m_{\dot{\alpha}}} C_{z_\alpha}\right] & 0 & \frac{k_3}{k_2}\left[C_{m_{\dot{\alpha}}} + C_{m_q}\right] & \frac{1}{k_2}\left[\frac{k_3}{k_1} C_{m_{\dot{\alpha}}} C_{z_{\delta_h}} + C_{m_{\delta_h}}\right] \\
0 & 0 & 0 & -20.0
\end{bmatrix}
\begin{bmatrix} x_1 \\ (\alpha) \\ x_2 \\ (\theta) \\ x_3 \\ (\dot{\theta}) \\ x_4 \\ (\delta_h) \end{bmatrix}
+
\begin{bmatrix} 0 \\ 0 \\ 0 \\ 20.0 \end{bmatrix} \delta_{h_c}
\tag{180}
$$

As the highlighted area of this matrix equation indicates, a trivial state relationship exists, i.e., the derivative of a state equals its derivative and this state makes no contribution to the remaining state expressions. The θ state can therefore be eliminated, reducing the state matrix equation even further. The resulting reduced short period approximation state variable equation which models the YF-16 longitudinal dynamics is:

$$
\begin{bmatrix} \dot{x}_1 \\ \dot{x}_2 \\ \dot{x}_3 \end{bmatrix}
=
\begin{bmatrix} \dot{\alpha} \\ \ddot{\theta} \\ \dot{\delta}_h \end{bmatrix}
=
\begin{bmatrix}
\frac{C_{z_\alpha}}{k_1} & 1.0 & \frac{C_{z_{\delta_h}}}{k_1} \\
\frac{1}{k_2}\left[C_{m_\alpha} + \frac{k_3}{k_1} C_{m_{\dot{\alpha}}} C_{z_\alpha}\right] & \frac{k_3}{k_2}\left[C_{m_{\dot{\alpha}}} + C_{m_q}\right] & \frac{1}{k_2}\left[\frac{k_3}{k_1} C_{m_{\dot{\alpha}}} C_{z_{\delta_h}} + C_{m_{\delta_h}}\right] \\
0 & 0 & -20.0
\end{bmatrix}
\begin{bmatrix} \alpha \\ \theta \\ \delta_h \end{bmatrix}
+
\begin{bmatrix} 0 \\ 0 \\ 20.0 \end{bmatrix} \delta_{h_c}
\tag{181}
$$

which, when the appropriate values from Table III for M = .8 at sea level are substituted, becomes:

$$\begin{bmatrix} \dot{\alpha} \\ \ddot{\theta} \\ \dot{\delta}_h \end{bmatrix} = \begin{bmatrix} -2.603975 & 1.0 & -.260965 \\ 15.058542 & -2.682339 & -47.676367 \\ 0 & 0 & -20.0 \end{bmatrix} \begin{bmatrix} \alpha \\ \dot{\theta} \\ \delta_h \end{bmatrix} + \begin{bmatrix} 0 \\ 0 \\ 20.0 \end{bmatrix} \delta_{h_c} \tag{182}$$

Appendix D

Development of the Recursive Optimal Control

This appendix presents the development of the expression for the recursive discrete optimal control u(KT) used to control the system. The development is a combination of the approaches presented in References 8, 12, and 15.

Development

Given the discrete system of equations:

$$\bar{x}(K+1)\,T = \bar{A}_d\,\bar{x}\,(KT) + \bar{B}_d\,u(KT) \qquad (96)$$

$$y\,(KT) = \bar{C}_d\,\bar{x}\,(KT) \qquad (97)$$

it is necessary to find the sequence of controls that minimize the discrete equivalent of the continuous quadratic functional which follows:

$$J_{(u)} = \int_0^{\infty} \left\{ \left[Z_o - y(t)\right]^T Q \left[Z_o - y(t)\right] + \dot{u}(t)^T R\, u(t) \right\} dt \qquad \text{(Ref. 12)} \qquad (183)$$

where Z_o is an arbitrary step input ($Z_o = C^*{}_{com}$). This continuous cost functional can be replaced by the following equivalent discrete expression where $\sum$ and ΔT replace $\int$ and dt, respectively, and $\dot{u}(t)$ is replaced by its first difference equivalent. Note that an infinite time cost functional is used because it results in a constant gain control law. The discrete cost function becomes:

$$J(u)_d = \sum_{K=0}^{\infty} \left\{ \left(\left[Z_o - y(KT) \right]^T \frac{Q_d}{\Delta T} \left[Z_o - y(KT) \right] \right) \Delta T + \right.$$

$$\left. \left(\left[\frac{u(K+1)T - u(KT)}{\Delta T} \right] R_d \cdot \Delta T \left[\frac{u(K+1)T - u(KT)}{\Delta T} \right] \right) \Delta T \right\} \quad (184)$$

or equivalently for this particular problem:

$$J(u)_d = \sum_{K=0}^{\infty} \left\{ \left(C^*_{com} - C^*_{act} \right)^T Q_d \left(C^*_{com} - C^*_{act} \right) + \right.$$

$$\left. \left[u(K+1)T - u(KT) \right]^T R_d \left[u(K+1)T - u(KT) \right] \right\} \quad (185)$$

Let x_o be the solution of equation (96), that is, $\bar{x}(KT) = \bar{x}(K+1)T$ in the steady state. Then, equation (96) becomes:

$$\bar{x}(K+1)T = \bar{x} \; KT = \bar{A}_d \, \bar{x}(KT) + \bar{B}_d \, u(KT) \quad (186)$$

or,

$$\bar{x}(KT)(\bar{I} - \bar{A}_d) = \bar{B}_d \, u(KT) \quad (187)$$

Now, if $\bar{x}_o \triangleq \lim_{k \to \infty} \bar{x}(KT)$ and $u_o \triangleq \lim_{k \to \infty} u(KT)$, equation (187) becomes:

$$\bar{x}_o \left[\bar{I} - \bar{A}_d \right] = \bar{B}_d \, u_o \quad (188)$$

or,

$$\bar{x}_o = - \left[\bar{A}_d - \bar{I} \right]^{-1} \bar{B}_d \, u_o \quad (189)$$

which is the unique solution of:

$$\bar{x}_o = \bar{A}_d \, \bar{x}_o + \bar{B}_d \, u_o \tag{190}$$

This implies that:

$$\bar{x}_o - \bar{A}_d \, \bar{x}_o = \bar{B}_d \, u_o \tag{191}$$

Additionally, using equation (97), if $Z_o = y(KT)$, then by equation (189):

$$\begin{aligned} Z_o &= \bar{C}_d \left\{ -\left[\bar{A}_d - \bar{I} \right]^{-1} \bar{B}_d \, u_o \right\} \\ &= \bar{C}_d \, \bar{x}_o \end{aligned} \tag{192}$$

Solving for u_o:

$$u_o = - \left[\bar{C}_d \left(\bar{A}_d - \bar{I} \right)^{-1} \bar{B}_d \right]^{-1} Z_o \tag{193}$$

The development continues by defining the following error variables. Letting the transient in the control be defined as:

$$\tilde{v}(KT) \triangleq u(K+1)T - u(KT) \tag{194}$$

then the transient is u(KT) is defined as:

$$\tilde{u}(KT) \triangleq u(KT) - u_o \tag{195}$$

which implies that:

$$u_o = u(KT) - \tilde{u}(KT) \tag{196}$$

Finally, the transient part of $\bar{x}(KT)$ is defined as:

$$\bar{x}(KT) \triangleq \bar{x}(KT) - \bar{x}_o \tag{197}$$

This allows the definition of $\tilde{\bar{x}}(K+1)T$ as follows:

$$\tilde{\bar{x}}(K+1)T \triangleq \bar{x}(K+1)T - \bar{x}_o \tag{198}$$

and, $\tilde{u}(K+1)T$ as:

$$\tilde{u}(K+1)T \triangleq u(K+1)T - u_o \tag{199}$$

which, from equation (196), becomes:

$$\tilde{u}(K+1)T = u(K+1)T - \Big[u(KT) - \tilde{u}(KT)\Big] \tag{200}$$

Regrouping the terms:

$$\tilde{u}(K+1)T = \tilde{u}(KT) + \Big[u(K+1)T - u(KT)\Big] \tag{201}$$

and using equation (194), this becomes:

$$\tilde{u}(K+1)T = \tilde{u}(KT) + \tilde{v}(KT) \tag{202}$$

Finally, let $\tilde{v}(K+1)T$ be defined as:

$$\tilde{v}(K+1)T \triangleq u(K+1)T - u(KT) \tag{203}$$

Subtracting $\bar{x}_o$ from both sides of the identity $\bar{x}(K+1)T = \bar{x}(K+1)T$, equation (96) can be written as:

$$\begin{aligned} \bar{x}(K+1)T - \bar{x}_o &= \bar{x}(K+1)T - \bar{x}_o \\ &= \bar{A}_d\, \bar{x}(KT) + \bar{B}_d\, u(KT) - \bar{x}_o \end{aligned} \tag{204}$$

190 Substituting equation (190) for the $\bar{x}_o$ on the right side of

204 equation (204):

$$\bar{x}(K+1)T - \bar{x}_o = \bar{A}_d\,\bar{x}(KT) + \bar{B}_d\,u(KT) - \left[\bar{A}_d\,\bar{x}_o + \bar{B}_d\,u_o\right]$$

205

$$= \bar{A}_d\left[\bar{x}(KT) - \bar{x}_o\right] + \bar{B}_d\left[u(KT) - u_o\right] \tag{205}$$

198 but, $\bar{x}(K+1)T - \bar{x}_o = \tilde{x}(K+1)T$ by equation (198), or

206

$$\tilde{x}(K+1)T = \bar{A}_d\left[\bar{x}(KT) - \bar{x}_o\right] + \bar{B}_d\left[u(KT) - u_o\right] \tag{206}$$

195, 197 Now substituting in equations (195) and (197), the result becomes:

207

$$\tilde{x}(K+1)T = \bar{A}_d\,\tilde{x}(KT) + \bar{B}_d\,\tilde{u}(KT) \tag{207}$$

202, 207 Equations (202) and (207) can be expressed in state space notation as:

208

$$\begin{bmatrix} \tilde{x}(K+1)T \\ \tilde{u}(K+1)T \end{bmatrix} = \begin{bmatrix} \bar{A}_d & \bar{B}_d \\ \bar{0} & \bar{I} \end{bmatrix}\begin{bmatrix} \tilde{x}(KT) \\ \tilde{u}(KT) \end{bmatrix} + \begin{bmatrix} \bar{0} \\ \bar{I} \end{bmatrix} \cdot \tilde{v}(KT) \tag{208}$$

Let the matrix $\begin{bmatrix} \bar{A}_d & \bar{B}_d \\ \bar{0} & \bar{I} \end{bmatrix} \triangleq \Phi$ and the matrix $\begin{bmatrix} \bar{0} \\ \bar{I} \end{bmatrix} \triangleq \Gamma$

then,

207

$$\begin{bmatrix} \tilde{x}(K+1)T \\ \tilde{u}(K+1)T \end{bmatrix} = \Phi\begin{bmatrix} \tilde{x}(KT) \\ \tilde{u}(KT) \end{bmatrix} + \Gamma \cdot \tilde{v}(KT) \tag{209}$$

184 Realizing that equation (184) can be expressed as:

210

$$J(u)_d = \sum_{K=0}^{\infty}\Big\{\left[Z_o - y(KT)\right]^T Q_d\left[Z_o - y(KT)\right] + \left[u(K+1)T - u(KT)\right]^T R_d\left[u(K+1)T - u(KT)\right]\Big\} \tag{210}$$

145

and recalling from equation (97) that:

$$y(KT) = \bar{C}_d \, \bar{x}(KT) \tag{97}$$

and from equation (192) that:

$$Z_o = \bar{C}_d \, \bar{x}_o \tag{192}$$

then,

$$Z_o - y(KT) = \bar{C}_d \left[\bar{x}_o - \bar{x}(KT) \right] = \bar{C}_d \left[-\tilde{x}(KT) \right] \tag{211}$$

and the cost functional, equation (184), can be rewritten as:

$$\begin{aligned} J(u)_d = \sum_{K=0}^{\infty} \Big\{ & \left(\bar{C}_d \left[-\tilde{x}(KT) \right] \right)^T Q_d \left(\bar{C}_d \left[-\tilde{x}(KT) \right] \right) + \\ & \left[u(K+1)T - u(KT) \right]^T R_d \left[u(K+1)T - u(KT) \right] \Big\} \end{aligned} \tag{212}$$

Equation (194) can then be substituted into equation (212) with the result:

$$\begin{aligned} J(u)_d = \sum_{K=0}^{\infty} \Big\{ & \left(-\bar{C}_d \, \tilde{x}(KT) \right)^T Q_d \left(-\bar{C}_d \, \tilde{x}(KT) \right) + \\ & \tilde{v}(KT)^T R_d \, \tilde{v}(KT) \Big\} \end{aligned} \tag{213}$$

$$= \sum_{K=0} \tilde{x}^T (KT) \, \bar{C}_d{}^T Q_d \, \bar{C}_d \, \tilde{x}(KT) + \tilde{v}^T(KT) \, R_d \, \tilde{v}(KT) \tag{214}$$

or,

$$\begin{aligned} J(u)_d = \sum_{K=0}^{\infty} & \left[\tilde{x}^T(KT) \; \tilde{u}^T(KT) \right] \left[\begin{array}{c|c} \bar{C}_d{}^T Q_d \, \bar{C}_d & \bar{0} \\ \hline \bar{0} & \bar{0} \end{array} \right] \left[\begin{array}{c} \tilde{x}(KT) \\ \tilde{u}(KT) \end{array} \right] + \\ & \tilde{v}^T(KT) \, R_d \, \tilde{v}(KT) \end{aligned} \tag{215}$$

where,

$$\left[\begin{array}{c|c} \bar{C}_d^{\,-T} \quad Q_d \quad \bar{C}_d & \bar{0} \\ \hline \bar{0} & \bar{0} \end{array}\right] \triangleq Q_{Ricatti} \tag{216}$$

The control $\hat{v}(KT)$ which minimizes this cost functional is of the form:

$$\begin{aligned} \hat{v}_K &= \bar{K}_{1_d} \cdot \hat{x}(KT) + \bar{K}_{2_d} \cdot \hat{u}(KT) \\ &= \begin{bmatrix} \bar{K}_{1_d} & \bar{K}_{2_d} \end{bmatrix} \cdot \begin{bmatrix} \hat{x}(KT) \\ \hat{u}(KT) \end{bmatrix} \end{aligned} \tag{217}$$

where $\bar{K}_{1_d}$ and $\bar{K}_{2_d}$ are the gains obtained using the positive definite steady state solution (P) of the discrete Ricatti equation in the expression:

$$\left[\begin{array}{c|c} \bar{K}_{1_d} & \bar{K}_{2_d} \end{array}\right] = -\left[\Gamma^T P \Gamma + R_d\right]^{-1} \cdot \Gamma^T P \Phi \tag{218}$$

The discrete Ricatti equation used is of the form:

$$P = Q_{Ricatti} + \Phi^T P \Phi - \Phi^T P \Gamma \left[\Gamma^T P \Gamma + R_d\right]^{-1} \cdot \Gamma^T P \Phi \tag{219}$$

The final expression for the control law is obtained by manipulating equation (217). Assume that there exists a matrix W such that:

$$\bar{\bar{W}}B_d = \bar{I} \tag{220}$$

Using equation (207), repeated here:

$$\hat{x}(K+1)T = \bar{A}_d \hat{x}(KT) + \bar{B}_d \hat{u}(KT) \tag{207}$$

it follows that:

$$\bar{B}_d \, \hat{u}(KT) \quad = \quad \hat{x}(K+1)T - \bar{A}_d \, \hat{x}(KT) \tag{221}$$

multiplying through by $\bar{W}$ and thereby employing equation (220):

$$\bar{W}\bar{B}_d \quad \hat{u}(KT) = \quad \bar{W} \, \hat{x}(K+1)T - \bar{W} \, \bar{A}_d \, \hat{x}(KT) \tag{222}$$

or,

$$\hat{u}(KT) \quad = \quad \bar{W} \, \hat{x}(K+1)T - \bar{W} \, \bar{A}_d \, \hat{x}(KT) \tag{223}$$

When equation (223) is substituted into equation (217), the result is:

$$\hat{v}(KT) \;=\; \bar{K}_{1_d} \, \hat{x}(KT) + \bar{K}_{2_d} \left[\bar{W} \, \hat{x}(K+1)T - \bar{W} \, \bar{A}_d \, \hat{x}(KT) \right] \tag{224}$$

$$= \left[\bar{K}_{1_d} - \bar{K}_{2_d} \, \bar{W} \, \bar{A}_d \right] \hat{x}(KT) + \bar{K}_{2_d} \, \bar{W} \, \hat{x}(K+1)T \tag{225}$$

Adding and subtracting $\bar{K}_{2_d} \, \bar{W} \, \hat{x}(KT)$ to the right side of equation (225), results in:

$$\hat{v}(KT) \;=\; \left[\bar{K}_{1_d} - \bar{K}_{2_d} \, \bar{W} \, \bar{A}_d \right] \hat{x}(KT) + \bar{K}_{2_d} \, \bar{W} \, \hat{x}(KT) \;+$$

$$\bar{K}_{2_d} \, \bar{W} \, \hat{x}(K+1)T \;-\; \bar{K}_{2_d} \, \bar{W} \, \hat{x}(KT) \tag{226}$$

or,

$$\hat{v}(KT) \;=\; \left[\bar{K}_{1_d} - \bar{K}_{2_d} \, \bar{W}\left(\bar{A}_d - I\right) \right] \hat{x}(KT) \;+$$

$$\bar{K}_{2_d} \, \bar{W} \left[\hat{x}(K+1)T - \hat{x}(KT) \right] \tag{227}$$

Equation (227) can be simplified by defining $\bar{I}_d$ such that:

$$-\bar{I}_d \, \bar{C}_d = \bar{K}_{1_d} \;-\; \bar{K}_{2_d} \, \bar{W} \, (\bar{A}_d - \bar{I}) \tag{228}$$

Now equation (227) becomes:

$$\hat{v}(KT) = -\bar{L}_d \, \bar{C}_d \, \hat{x}(KT) + \bar{K}_{2_d} \, \bar{W} \left[\hat{x}(K+1)T - \hat{x}(KT) \right]$$

$$= -L_d \left\{ \bar{C}_d \left[\bar{x}(KT) - \bar{x}_o \right] \right\} + \bar{K}_{2_d} \, \bar{W} \left[\hat{x}(K+1)T - \hat{x}(KT) \right] \tag{229}$$

but from equations (97) and (192):

$$\bar{C}_d \, \bar{x}(KT) - \bar{C}_d \, \bar{x}_o = y(KT) - Z_o \tag{230}$$

then,

$$\hat{v}(KT) = -L_d \left[y(KT) - Z_o \right] + \bar{K}_{2_d} \, \bar{W} \left[\hat{x}(K+1)T - \hat{x}(KT) \right]$$

$$= L_d \left[Z_o - y(KT) \right] + \bar{K}_{2_d} \, \bar{W} \left[\hat{x}(K+1)T - \hat{x}(KT) \right] \tag{231}$$

but,

$$\hat{x}(K+1)T - \hat{x}(KT) = \left[\bar{x}(K+1)T - \bar{x}_o \right] - \left[\bar{x}(KT) - \bar{x}_o \right]$$

$$= \bar{x}(K+1)T - \bar{x}(KT) \tag{232}$$

therefore,

$$\hat{v}(KT) = L_d \left[Z_o - y(KT) \right] + \bar{K}_{2_d} \, \bar{W} \left[\bar{x}(K+1)T - \bar{x}(KT) \right] \tag{233}$$

Using equation (194), this can be rewritten as:

$$u(K+1)T - u(KT) = L_d \left[Z_o - y(KT) \right] + \bar{K}_{2_d} \, \bar{W} \left[\bar{x}(K+1)T - \bar{x}(KT) \right] \tag{234}$$

Now letting $\overline{K}_{2_d} \cdot \overline{W} = \overline{N}_d$, this becomes:

$$u(K+1)T - u(KT) = L_d \left[Z_o - y(KT) \right] + \overline{N}_d \left[\overline{x}(K+1)T - \overline{x}(KT) \right] \tag{235}$$

where Z_o is the system input C^*_{com} , and y(KT) by equation (97) is $\overline{C}\ \overline{x}(KT)$. Since from equation (228):

$$\overline{W} = \overline{K}_{2_d}^{-1} \left(\overline{K}_{1_d} + L_d \overline{C}_d \right) \left(\overline{A}_d - \overline{I} \right)^{-1} \tag{236}$$

equation (220) can be expressed as:

$$\overline{I} = \left[\overline{K}_{2_d}^{-1} \left(\overline{K}_{1_d} + L_d \overline{C}_d \right) \left(\overline{A}_d - \overline{I} \right)^{-1} \right] \overline{B}_d \tag{237}$$

Using this information, L_d can be expressed as:

$$L_d = \left[\overline{K}_{2_d} - \overline{K}_{1_d} \left(\overline{A}_d - \overline{I} \right)^{-1} \overline{B}_d \right] \left[\overline{C}_d \left(\overline{A}_d - \overline{I} \right)^{-1} \overline{B}_d \right]^{-1} \tag{238}$$

while,

$$\overline{N}_d = \overline{K}_{2_d} \left[\overline{K}_{2_d}^{-1} \left(\overline{K}_{1_d} + L_d \overline{C}_d \right) \left(\overline{A}_d - \overline{I} \right)^{-1} \right] \tag{239}$$

or,

$$\overline{N}_d = \left(\overline{K}_{1_d} + L_d \overline{C}_d \right) \left(\overline{A}_d - \overline{I} \right)^{-1} \tag{240}$$

Equation (235) is the resulting recursive control expression which, when incorporated with equations (238) and (240), produces the sequence of optimal controls for the system of equations:

$$\overline{x}(K+1)T = \overline{A}_d\ \overline{x}(KT) + \overline{B}_d\ u(KT) \tag{96}$$

$$y(KT) = \overline{C}_d\ \overline{x}(KT) \tag{97}$$

Appendix E

Simulation Computer Program

The following program (SIM3) was developed and used for this investigation to solve the C^* discrete, optimal control problem discussed in the text. The reader is referred to Figures 22, 24, and 25 of the text for a detailed representation of the flow of logic in this algorithm. Explanatory comments are included in the program to clarify key areas/options. The program is easily adaptable to other aircraft or other flight conditions. As presented, the continuous aircraft plant (3 x 3) dynamics matrix ($\overline{A}$) and (3 x 1) control matrix ($\overline{B}$), as well as the (1 x 3) observer matrix ($\overline{CD}$) are for a YF-16 flying at Mach .8 at sea level. Additionally, the Q and R weightings are set to unity.

The program was run on the Intercom-Scope time sharing access system at AFIT. For execution, the program requires library access to the "AFITSUBROUTINES" package of computer programs and the Aeromedical Research Laboratory "CONTROL, CY=4" computer subroutine package both of which are available at AFIT.

```
C     ************************************************************
C     * THIS PROGRAM SOLVES THE DISCRETE C-STAR CONTROL          *
C     * PROBLEM IN AN OPTIMAL MANNER. BASED ON A SPECIFIED       *
C     * SAMPLE RATE (TDEL), A TRAJECTORY ERROR WEIGHTING         *
C     * (Q), AND A CONTROL PENALTY (R), THE OPTIMAL GAIN         *
C     * LD AND THE FEEDBACK GAIN MATRIX ND ARE DETERMINED.       *
C     *                                                          *
C     * ADDITIONALLY, A SIMULATION OF THE SYSTEM IS CON-         *
C     * DUCTED FOR EITHER A ZOH OR FOH APPROACH TO THE           *
C     * CONTROL PROBLEM.                            **************
C     *                                             *
C     * SET THE SAMPLE RATE BY SPECIFYING TDEL      *
C     *                                             *
C     * TO PRODUCE SIMULATION RESULTS SET FLAG      *
C     * TO 1 (ZERO ORDER HOLD) OR FLAG TO 2         *
C     * (FIRST ORDER HOLD) AND LONG TO THE          *
C     * DESIRED DURATION OF THE SIMULATION IN       *
C     * SECONDS (X.X)                               *
C     ***********************************************
C
C
      PROGRAM SIM3(INPUT,OUTPUT,TAPE6=OUTPUT,TAPE7,TAPE8,TAPE9)
      DIMENSION A(3,3),B(3,1),EA(3,3),EAINT(3,3),ROOTR(4),
     $CD(1,3),BD(3,1),XX(4,4),GAIN(1,4),FF(3,3),GG(3,3),
     $ND(1,3),K1(1,3),BDU(3,1),EX(3,1),ADX(3,1),RR(3,1),ROOTI(4)
      INTEGER NT,N,FLAG,COUNT
      REAL DEL,ND,LD,K2,K1,DELL,LONG
      COMMON/MAIN1/NDIM,NDIM1,COM1(4,4)
      NDIM=3
      NDIM1=4
C
C     ****************************************
C     * THE DISCRETIZATION TIME (TDEL)       *
C     * & SIMULATION FLAG FOLLOW             *
C     ****************************************
```

```
C
      TDEL=.01
      FLAG=1
      LONG=2.0
      MODI=IFIX(500.0*TDEL + .5)
      DI=MODI
      DEL=DI/500.
      WRITE(6,575)
575   FORMAT("1")
      PRINT*,"THE SAMPLE RATE SPECIFIED =",TDEL
      PRINT*,"TO SIMPLIFY THE CALCULATIONS,THE COMPUTER WILL USE ",DEL
      DO 7 I=1,3
      BD(I,1)=0.0
      DO 8 J=1,3
      EA(I,J)=0.0
      EAINT(I,J)=0.0
8     CONTINUE
7     CONTINUE
C
C     **************************************************
C     * THE CONTINUOUS PLANT A & B MATRICES ARE INPUT  *
C     * ALONG WITH THE OBSERVER MATRIX (CD) AND THE    *
C     * CONTROL LAW WEIGHTING VALUES Q & R             *
C     **************************************************
C
      A(1,1)=-2.603975
      A(1,2)=1.0
      A(1,3)=-.260965
      A(2,1)=15.058542
      A(2,2)=-2.682339
      A(2,3)=-47.676357
      A(3,1)=A(3,2)=0.0
      A(3,3)=-20.0
      B(1,1)=0.0
      B(2,1)=0.0
```

```
      B(3,1)=20.0
      CD(1,1)=77.7
      CD(1,2)=11.4
      CD(1,3)=-9.9
      DD=DEL
      R=1.0
      R=R/DEL
      N=3
      NT=10
C
C     ********************************************************
C     *  THE FOLLOWING SUBROUTINE TAKES THE CONTINUOUS PLANT  *
C     *  A & B MATRICES AND CALCULATES EXP(AT) CALLED THE     *
C     *  "CONTROL AD MATRIX" AND B TIMES THE INTEGRAL OF      *
C     *  EXP(AT) CALLED THE "CONTROL BD MATRIX". T IS THE     *
C     *  SAMPLE RATE. THIS IS DONE TO PROVIDE THE NECESSARY   *
C     *  DATA TO CONTINUE THE CALCULATIONS TOWARD THE LD AND  *
C     *  ND CONTROL GAINS.                                    *
C     ********************************************************
      CALL DSCRT(N,A,DEL,EA,FAINT,NT)
      PRINT 10,DEL
10    FORMAT(17H THE VALUE OF T= ,F12.9,3H SECONDS,/)
      PRINT*,"THIS IS THE RATE AT WHICH THE CONTROL IS UPDATED"
      PRINT*," "
      PRINT*,"THE CONTROL AD MATRIX IS :"
      DO 50 I=1,N
      WRITE(6,200)(EA(I,J),J=1,N)
200   FORMAT(3(3X,E20.10))
50    CONTINUE
      PRINT*,"  "
      CALL MMPY(FAINT,B,BD,3,3,1)
      PRINT*,"THE CONTROL BD MATRIX IS :"
      DO 60 I=1,3
      WRITE(6,300)(BD(I,1))
300   FORMAT(E20.10)
```

```
50    CONTINUE
      PRINT*," "
C
C     ************************************************
C     *  THE FOLLOWING SUBROUTINE CALCULATES THE (4X4) *
C     *  MATRIX VALUES OF THE RICATTI EQUATION          *
C     ************************************************
      CALL RIC(EA,BD,QD,P,CD,XX)
      PRINT*,"THE 'X (RICATTI)' MATRIX IS:"
      DO 55 I=1,4
      WRITE(6,400)(XX(I,J),J=1,4)
400   FORMAT(4(3X,E20.10))
55    CONTINUE
      PRINT*," "
C
C     ***********************************************
C     -  THE GAINK SUBROUTINE USES THE RICATTI (X)   *
C     *  MATRIX TO CALCULATE GAINS K1 (1X3) AND      *
C     *  K2 (SCALAR)                                 *
C     ***********************************************
      CALL GAINK(XX,R,EA,BD,GAIN)
      PRINT*,"THE GAIN VALUES FOLLOW"
      PRINT*,"THE K1 MATRIX IS:"
      PRINT*," "
      PRINT*," "
      WRITE(6,805)(GAIN(1,J),J=1,3)
805   FORMAT(3(3X,E20.10))
      PRINT*," "
      DO 44 J=1,3
      K1(1,J)=GAIN(1,J)
44    CONTINUE
      PRINT*,"THE K2 (1X1) GAIN IS"
      PRINT 17,GAIN(1,4)
17    FORMAT(E20.10)
      PRINT*," "
```

```
      K2=GAIN(1,4)
C
C     ************************************************
C     *  SUBROUTINE NDLD CALCULATES THE ND (1X3) AND *
C     *  LD (SCALAR) CONTROL LAW VALUES              *
C     ************************************************
      CALL NDLD(EA,BD,K1,K2,CD,ND,LD)
      PRINT 21,LD
21    FORMAT(18H THE VALUE OF LD =,E20.10)
      PRINT*,"  "
      PRINT*,"THE ND MATRIX IS :"
      WRITE(6,503) (ND(1,J),J=1,3)
503   FORMAT(3(3X,E20.10))
      PRINT*,"  "
      PRINT*,"  "
      DELL=.002
      FF(1,1)=.9948355471E+00
      FF(1,2)=.1989475242E-02
      FF(1,3)=-.6040579439E-03
      FF(2,1)=.2095859649E-01
      FF(2,2)=.9945796439E+00
      FF(2,3)=-.9322758715E-01
      FF(3,1)=FF(3,2)=0.0
      FF(3,3)=.9607894392E+00
      RR(1,1)=-.1153836563E-04
      RR(2,1)= -.1876620603E-02
      RR(3,1)=.3921056086E-01
      PRINT 31,DELL
31    FORMAT(31H PLANT WILL CHANGE STATE EVERY ,F5.3,8H SECONDS)
      PRINT*,"THIS IS THE PLANT DISCRETIZATION TIME"
      PRINT*,"THE AD MATRIX OF THE PLANT IS :"
      DO 59 I=1,3
      WRITE(6,200) (FF(I,J),J=1,3)
59    CONTINUE
      PRINT*,"  "
```

```
      PRINT*,"THE BD MATRIX OF THE PLANT IS :"
      DO 69 I=1,3
      WRITE(6,300)(RR(I,1))
69    CONTINUE
      PRINT*," "
C
C     ******************************************
C     *  AT THIS POINT, ALL THE INFORMATION IS  *
C     *  AVAILABLE FOR A CLOSED LOOP SIMULATION. *
C     *                                          *
C     *  FLAG=1 OR 2 WILL PRODUCE SIMULATION RE- *
C     *  SULTS IN LIST FORM  ALONG WITH TAPE8/TAPE9 *
C     *  FOR LATER PLOTTING                      *
C     ******************************************
      IF(FLAG.EQ.1) GO TO 99
      IF(FLAG.EQ.2) GO TO 43
      GO TO 13
C
C
C     ***************************
C     *  ZOH SIMULATION BEGINS  *
C     ***************************
C
C
99    COUNT=1.
      EX(1,1)=EX(2,1)=EX(3,1)=0.0
      MO=MODI+1
      U=0.0
      CS=0.0
      CSOLD=CS
      CSC=1.0
      KK=0
      TK=0.0
      T=TK/500.
      WRITE(6,576)
```

```
      PRINT*,"THE SIMULATION RESULTS FOLLOW :"
      PRINT*," "
      PRINT 100
100   FORMAT(1X,14HTIME (SECONDS),3X,5HALPHA,6X,9HTHETA DOT,
     $5X,7HDELTA H,5X,2HC*,5X,10HC* COMMAND,5X,1HU,//)
      PRINT 600,T,EX(1,1),EX(2,1),EX(3,1),CS,CSC,U
600   FORMAT(2X,E10.4,4X,E10.4,1X,E10.4,1X,E10.4,1X,E10.4,
     $1X,E10.4,1X,E10.4)
      WRITE(6,600) T,EX(1,1),EX(2,1),EX(3,1),CS,CSC,U
      KK=KK+1
      TK=TK+1.0
      T=TK/500.
      TSUM=0.0
      IPASS=1
C     ****************************************
C     *  ZOH CALCULATION OF THE STATES X(K)  *
C     ****************************************
36    IF(MOD(KK,MO))33,3,33
33    CALL MMPY(FF,EX,ADX,3,3,1)
      CALL MMPY(RR,U,BDU,3,1,1)
      DO 23 J=1,3
      EX(J,1)=ADX(J,1)+BDU(J,1)
23    CONTINUE
      CALL MMPY(CD,EX,CS,1,3,1)
2     PRINT 600,T,EX(1,1),EX(2,1),EX(3,1),CS,CSC,U
      WRITE(6,600) T,EX(1,1),EX(2,1),EX(3,1),CS,CSC,U
      COUNT=COUNT+1
      IF(T.GE.LONG) GO TO 73
      KK=KK+1
      TK=TK+1.0
      T= TK/500.
      GO TO 36
C     *****************************************
C     *  ZOH CALCULATION OF THE CONTROL U(K)  *
C     *                                       *
```

```
C     * THIS CONTROL UPDATE COMPUTATION IS      *
C     * ASSUMED TO TAKE << 1/500 SEC. TO        *
C     * ACCOMPLISH.                             *
C     * THIS ALLOWS US TO SAY THAT PRACTICAL-   *
C     * LY NO TIME HAS TRANSPIRED FROM THE      *
C     * TIME THE STATES WERE LAST CALCULATED    *
C     * TO THE BUILDING OF THIS NEW CONTROL     *
C     * I.E. THE STATES AT EX(KT+)=EX(KT)       *
C     *****************************************
3     SUM=1.0 - CSOLD
      SLD=LD*SUM
      TSUM=TSUM+SLD
      CALL MMPY(ND,EX,XND,1,3,1)
      U=TSUM+XND
      CALL MMPY(FF,EX,ADX,3,3,1)
      CALL MMPY(BR,U,BDU,3,1,1)
      DO 20 J=1,3
      EX(J,1)=ADX(J,1)+BDU(J,1)
20    CONTINUE
      CALL MMPY(CD,EX,CS,1,3,1)
      CSOLD=CS
      IF(IPASS.EQ.1) GO TO 53
      IF(IPASS.NE.2) GO TO 2
      MO=MODI
      KK=KK-2
      IPASS=IPASS+1
      GO TO 2
53    KK=KK+1
      IPASS=IPASS+1
      GO TO 2
73    WRITE(9,900) COUNT
900   FORMAT(1X,I4)
      PRINT*," "
      PRINT 66,COUNT
66    FORMAT(39H THE NUMBER OF LINES OF DATA ON TAPE8 =,I4)
```

```
      CALL RCOT(EA,BD,ND,LD,CD,ROOTR,ROOTI)
      PRINT*," "
      PRINT*," "
      PRINT*,"THE Z-PLANE ROOTS ARE (ZERO ORDER HOLD) :"
      DO 88 I=1,4
      WRITE(6,500) ROOTR(I),ROOTI(I)
500   FORMAT(2(3X,E20.10))
88    CONTINUE
      GO TO 13
C
C     ***************************
C     *  FOH SIMULATION REGINS  *
C     ***************************
C
43    COUNT=1
      EX(2,1)=EX(1,1)=EX(3,1)=0.0
      MO=MODI+1
      UN=0.0
      USAVE=UN
      UO=0.0
      SLOPE=(UN - UO)/DEL
      U=0.0
      CS=0.0
      CSOLD=CS
      CSC=1.0
      KK=0
      TK=0.0
      T=TK/500.
      WRITE(6,576)
      PRINT*,"THE SIMULATION RESULTS FOLLOW :"
      PRINT*," "
      PRINT 100
      PRINT 600,T,EX(1,1),EX(2,1),EX(3,1),CS,CSC,U
      WRITE(6,600) T,EX(1,1),EX(2,1),EX(3,1),CS,CSC,U
      KK=KK+1
```

```
      TK=TK+1.0
      T=TK/500.
      TSUM=0.0
      IPASS=1
C
C     *****************************************
C     *  FOH CALCULATION OF THE STATES X(K)   *
C     *****************************************
C
95    IF(MOD(KK,MO))96,97,95
96    U=SLOPE*DELL+UN
      CALL MMPY(FF,EX,ADX,3,3,1)
      CALL MMPY(RR,U,BOU,3,1,1)
      DO 98 J=1,3
      EX(J,1)=ADX(J,1)+BOU(J,1)
98    CONTINUE
      CALL MMPY(CO,EX,CS,1,3,1)
49    PRINT 600,T,EX(1,1),EX(2,1),EX(3,1),CS,CSC,U
      WRITE(6,600) T,EX(1,1),EX(2,1),EX(3,1),CS,CSC,U
      COUNT=COUNT+1
      IF(T.GE.LONG) GO TO 89
      KK=KK+1
      TK=TK+1.0
      T=TK/500.
      UN=U
      GO TO 95
C
C     *****************************************
C     *  FOH CALCULATION OF THE CONTROL J(K)  *
C     *****************************************
C
97    UO=USAVE
      SUM=1.0-CSOLD
      SLO=LO*SUM
      TSUM=TSUM+SLO
      CALL MMPY(NO,EX,XNO,1,3,1)
```

```
      U=TSUM+XND
      USAVE=U
      SLOPE=(U - UO)/DEL
      CALL MMPY(FF,EX,ADX,3,3,1)
      CALL MMPY(RR,U,BDU,3,1,1)
      DO 25 J=1,3
      EX(J,1)=ADX(J,1)+BDU(J,1)
25    CONTINUE
      CALL MMPY(CO,EX,CS,1,3,1)
      CSOLD=CS
      IF(IPASS.EQ.1) GO TO 46
      IF(IPASS.NE.2) GO TO 49
      MO=MODI
      KK=KK-2
      IPASS=IPASS+1
      GO TO 49
46    KK=KK+1
      IPASS=IPASS+1
      GO TO 49
49    WRITE(9,144) COUNT
144   FORMAT(1X,I4)
      PRINT*," "
      PRINT 77,COUNT
77    FORMAT(39H THE NUMBER OF LINES OF DATA ON TAPE8 =,I4)
13    STOP
      END
```

```
      SUBROUTINE RIC(EA,BD,QD,R,CD,XX)
      DIMENSION AA(4,4),HT(4,1),Q(4,4),X(4,4),XX(4,4),
     $QCD(1,3),CDT(3,1),QQ(3,3),CD(1,3),S(4,1),
     $Z(4,4),BD(3,1),EA(3,3)
      COMMON/MAIN1/NDIM,NDIM1,COM1(4,4)/INOU/KIN,KOUT
      NDIM=4
      NDIM1=5
      KIN=7
      KOUT=7
      AA(1,1)=EA(1,1)
      AA(1,2)=EA(2,1)
      AA(1,3)=EA(3,1)
      AA(1,4)=0.0
      AA(2,1)=EA(1,2)
      AA(2,2)=EA(2,2)
      AA(2,3)=EA(3,2)
      AA(2,4)=0.0
      AA(3,1)=EA(1,3)
      AA(3,2)=EA(2,3)
      AA(3,3)=EA(3,3)
      AA(3,4)=0.0


      AA(4,2)=BD(2,1)
      AA(4,1)=BD(1,1)
      AA(4,3)=BD(3,1)
      AA(4,4)=1.0
      HT(1,1)=HT(2,1)=HT(3,1)=0.0
      HT(4,1)=1.0
      CALL MMPY(QD,CD,QCD,1,1,3)
      CDT(1,1)=CD(1,1)
      CDT(2,1)=CD(1,2)
      CDT(3,1)=CD(1,3)
      CALL MMPY(CDT,QCD,QQ,3,1,3)
      Q(1,1)=QQ(1,1)
```

```
      Q(1,2)=QQ(1,2)
      Q(1,3)=QQ(1,3)
      Q(2,1)=QQ(2,1)
      Q(2,2)=QQ(2,2)
      Q(2,3)=QQ(2,3)
      Q(3,1)=QQ(3,1)
      Q(3,2)=QQ(3,2)
      Q(3,3)=QQ(3,3)
      Q(1,4)=Q(2,4)=Q(3,4)=Q(4,1)=Q(4,2)=Q(4,3)=Q(4,4)=0.0
      N=4
      M=1
      CALL KFLTR(N,M,AA,HT,Q,R,X,G,Z)
      DO 5 I=1,N
      DO 6 J=1,N
      XX(I,J)=X(I,J)
6     CONTINUE
5     CONTINUE
      RETURN
      END
```

```
      SUBROUTINE GAINK(XX,R,FA,BD,GAIN)
      DIMENSION H(1,4),HT(4,1),XX(4,4),AT(4,4),
     $FA(3,3),BD(3,1),S(1,4)
      REAL MSUM
      H(1,1)=H(1,2)=H(1,3)=0.0
      H(1,4)=1.0
      HT(1,1)=HT(2,1)=HT(3,1)=0.0
      HT(4,1)=1.0
      DO 14 I=1,3
      DO 15 J=1,3
      AT(I,J)=FA(I,J)
   15 CONTINUE
   14 CONTINUE
      AT(1,4)=BD(1,1)
      AT(2,4)=BD(2,1)
      AT(3,4)=BD(3,1)
      AT(4,1)=AT(4,2)=AT(4,3)=0.0
      AT(4,4)=1.0
      CALL MMPY(H,XX,S,1,4,4)
      CALL MMPY(S,HT,SHT,1,4,1)
      SUM=SHT+R
      CALL MINV(SUM,SUMI,1)
      CALL MMPY(S,AT,F,1,4,4)
      MSUM=-SUMI
      CALL MMPY(MSUM,F,GAIN,1,1,4)
      RETURN
      END
```

```
      SUBROUTINE NOLD(EA,BD,K1,K2,CD,ND,LD)
      DIMENSION EA(3,3),BD(3,1),K1(1,3),CD(1,3),ND(1,3),
     $I(3,3),D(3,3),DI(3,3),G(3,1),CL(1,3),AA(1,3)
      REAL I,K1,K2,ND,LD,M,N
      DO 3 L=1,3
      DO 4 J=1,3
      I(L,J)=0.0
      I(L,L)=1.0
    4 CONTINUE
    3 CONTINUE
      CALL MSUB(EA,I,D,3,3)
      CALL MINV(D,DI,3)
      CALL MMPY(DI,BD,G,3,3,1)
      CALL MMPY(K1,G,M,1,3,1)
      CALL MSUB(K2,M,N,1,1)
      CALL MMPY(CD,G,T,1,3,1)
      CALL MINV(T,TI,1)
      CALL MMPY(N,TI,LD,1,1,1)
      CALL MMPY(LD,CD,CL,1,1,3)
      DO 11 J=1,3
      AA(1,J)=K1(1,J)+CL(1,J)
   11 CONTINUE
      CALL MMPY(AA,DI,ND,1,3,3)
      RETURN
      END
```

```
      SUBROUTINE ROOT(EA,BD,ND,LD,CD,ROOTR,ROOTI)
      DIMENSION EA(3,3),BD(3,1),ND(1,3),CD(1,3),AA(4,4),
     $ROOTR(4),ROOTI(4),LCD(1,3),BND(3,3)
      REAL LD,ND,LCD
      COMMON/MAIN1/NDIM,NDIM1,COM1(4,4)/INOU/KIN,KOUT
      NDIM=4
      NDIM1=5
      KIN=7
      KOUT=7
      CALL MMPY(BD,ND,BND,3,1,3)
      DO 85 I=1,3
      DO 86 J=1,3
      AA(I,J)=EA(I,J)+BND(I,J)
86    CONTINUE
      AA(I,4)=BD(I,1)
85    CONTINUE
      AA(4,4)=1.0
      CALL MMPY(LD,CD,LCD,1,1,3)
      DO 87 I=1,3
      AA(4,I)=-LCD(1,I)
87    CONTINUE
      PRINT*," "
      PRINT*,"THE CLOSED LOOP SYSTEM MATRIX IS :"
      PRINT*," "
      DO 61 I=1,4
      WRITE(6,585) (AA(I,J),J=1,4)
585   FORMAT(4(1X,E11.5))
61    CONTINUE
      PRINT*," "
      PRINT*,"THE EIGENVALUES OF THIS MATRIX FOLLOW :"
      CALL EIGEN(4,AA,ROOTR,ROOTI,DUE,0)
      RETURN
      END
```

Appendix F

Zero Order Hold Simulation Output

The abbreviated computer product which follows is the output of the program found in Appendix E with the ZOH option selected (FLAG = 1). This particular run is for a specified sample rate of T = 1/40th second with R = 150.0 and Q = 1.0.

The first page of the output indicates that the sample rate has been adjusted, as per Table VI, from the specified value (.025) to the adjusted value (.026) used in the actual simulation. This is evident on page 170 where it is apparent that the first sample occurs after .026 seconds have elapsed. The control applied (u = -.1819E-02) is retained until the next sample occurs at .052 seconds at which time a new control is calculated and applied on the next iteration.

The three system states α , $\dot{\theta}$, and δ_e are listed for each time increment. Additionally, the system output (C^*) is listed along with the pilot commanded C^* response. By comparing the actual C^* response to the C^* commanded value, the tracking capability of the particular system configuration can be determined. Successful system "lock-on" to the commanded 1-G climb is evident on page 171. At an elapsed time of 1.606 seconds from the time the climb command (C^* command) is initiated, zero error is achieved and maintained by the system.

The abbreviated example of the simulation output is concluded on page 172 where the Z-plane system roots are listed.

```
THE SAMPLE RATE SPECIFIED =.025
TO SIMPLIFY THE CALCULATIONS,THE COMPUTER WILL USE .025
THE VALUE OF T=    .025000000 SECONDS

THIS IS THE RATE AT WHICH THE CONTROL IS UPDATED

THE CONTROL AD MATRIX IS :
        .9392950682E+00        .2431444476E-01        -.1813729285E-01
        .7661401025E+00        .9373896379E+00        -.3736817214E+00
       0.                     0.                       .5945205476E+00

THE CONTROL BD MATRIX IS :
    -.3842103305E-02
    -.2650346526E+00
     .4057734524E+00

THE "X (RICATTI)" MATRIX IS:
        .1503006879E+04        .3240803568E+03        -.6387116465E+03        -.1225534406E+04
        .7240803568E+03        .5712633799E+02        -.1358091187E+03        -.2812284622E+03
       -.6387116465E+03       -.1358091187E+03         .2829209183E+03         .6185859251E+03
       -.1225534406E+04       -.2812284622E+03         .6185859251E+03         .2088172812E+04

THE GAIN VALUES FOLLOW
THE K1 MATRIX IS:


        .1595083776E+00        .3734297514E-01        -.8305132697E-01

THE K2 (1X1) GAIN IS
    -.3078338691E+00

THE VALUE OF LD =     -.1819060501E-02

THE NO MATRIX IS :
        .1415935815E+01        .2846496135E+00        -.5583780610E+00


PLANT WILL CHANGE STATE EVERY   .002 SECONDS
THIS IS THE PLANT DISCRETIZATION TIME
THE AD MATRIX OF THE PLANT IS :
        .9948355471E+00        .1989475742E-02        -.6940579499E-03
        .2995859649E-01        .9946796539E+00        -.3322758715E-01
       0.                     0.                       .9607894392E+00

THE BD MATRIX OF THE PLANT IS :
    -.1157835563E-04
    -.1877520603E-02
     .3921056085E-01
```

THE SIMULATION RESULTS FOLLOW :

TIME (SECONDS)	ALPHA	THETA'DOT	DELTA H	C*	C* COMMAND	U
0.	0.	0.	0.	0.	.1000E+01	0.
.2000E-02	0.	0.	0.	0.	.1000E+01	0.
.4000E-02	0.	0.	0.	0.	.1000E+01	0.
.6000E-02	0.	0.	0.	0.	.1000E+01	0.
.8000E-02	0.	0.	0.	0.	.1000E+01	0.
.1000E-01	0.	0.	0.	0.	.1000E+01	0.
.1200E-01	0.	0.	0.	0.	.1000E+01	0.
.1400E-01	0.	0.	0.	0.	.1000E+01	0.
.1600E-01	0.	0.	0.	0.	.1000E+01	0.
.1800E-01	0.	0.	0.	0.	.1000E+01	0.
.2000E-01	0.	0.	0.	0.	.1000E+01	0.
.2200E-01	0.	0.	0.	0.	.1000E+01	0.
.2400E-01	0.	0.	0.	0.	.1000E+01	0.
.2600E-01	0.	0.	0.	0.	.1000E+01	0.
.2800E-01	.2099E-07	.3417E-05	-.7133E-04	.7467E-03	.1000E+01	-.1819E-02
.3000E-01	.9175E-07	.1347E-04	-.1309E-03	.1545E-02	.1000E+01	-.1819E-02
.3200E-01	.2275E-06	.2983E-04	-.2037E-03	.2394E-02	.1000E+01	-.1819E-02
.3400E-01	.4270E-06	.5230E-04	-.2690E-03	.3292E-02	.1000E+01	-.1819E-02
.3600E-01	.7123E-06	.8052E-04	-.3237E-03	.4238E-02	.1000E+01	-.1819E-02
.3800E-01	.1069E-05	.1143E-03	-.3831E-03	.5230E-02	.1000E+01	-.1819E-02
.4000E-01	.1555E-05	.1533E-03	-.4442E-03	.6267E-02	.1000E+01	-.1819E-02
.4200E-01	.2132E-05	.1974E-03	-.4932E-03	.7349E-02	.1000E+01	-.1819E-02
.4400E-01	.2856E-05	.2463E-03	-.5439E-03	.8477E-02	.1000E+01	-.1819E-02
.4600E-01	.3384E-05	.2997E-03	-.5917E-03	.9640E-02	.1000E+01	-.1819E-02
.4800E-01	.4645E-05	.3577E-03	-.6475E-03	.1085E-01	.1000E+01	-.1819E-02
.5000E-01	.5744E-05	.4196E-03	-.6935E-03	.1209E-01	.1000E+01	-.1819E-02
.5200E-01	.6939E-05	.4955E-03	-.7376E-03	.1338E-01	.1000E+01	-.1819E-02
.5400E-01	.8400E-05	.5777E-03	-.8203E-03	.1522E-01	.1000E+01	-.3077E-02
.5600E-01	.1000E-04	.6781E-03	-.9174E-03	.1717E-01	.1000E+01	-.3077E-02
.5800E-01	.1161E-04	.7267E-03	-.1002E-02	.1912E-01	.1000E+01	-.3077E-02
.6000E-01	.1384E-04	.8220E-03	-.1083E-02	.2117E-01	.1000E+01	-.3077E-02
.6200E-01	.1603E-04	.9243E-03	-.1152E-02	.2329E-01	.1000E+01	-.3077E-02
.6400E-01	.1863E-04	.1034E-02	-.1237E-02	.2548E-01	.1000E+01	-.3077E-02
.6600E-01	.2133E-04	.1151E-02	-.1309E-02	.2773E-01	.1000E+01	-.3077E-02
.6800E-01	.2433E-04	.1273E-02	-.1373E-02	.3005E-01	.1000E+01	-.3077E-02
.7000E-01	.2751E-04	.1401E-02	-.1445E-02	.3242E-01	.1000E+01	-.3077E-02
.7200E-01	.3116E-04	.1535E-02	-.1509E-02	.3486E-01	.1000E+01	-.3077E-02
.7400E-01	.3500E-04	.1674E-02	-.1570E-02	.3735E-01	.1000E+01	-.3077E-02

Time (Seconds)	Alpha	Theta Dot	Delta H	C^*	C^*_{Com}	U
.1564E+01	.9402E-02	.2497E-01	.1553E-02	.9997E+00	.1000E+01	.1568E-02
.1566E+01	.9402E-02	.2497E-01	.1553E-02	.9997E+00	.1000E+01	.1568E-02
.1568E+01	.9402E-02	.2497E-01	.1553E-02	.9997E+00	.1000E+01	.1568E-02
.1570E+01	.9402E-02	.2497E-01	.1553E-02	.9998E+00	.1000E+01	.1568E-02
.1572E+01	.9402E-02	.2497E-01	.1553E-02	.9998E+00	.1000E+01	.1568E-02
.1574E+01	.9403E-02	.2497E-01	.1553E-02	.9998E+00	.1000E+01	.1568E-02
.1576E+01	.9403E-02	.2497E-01	.1554E-02	.9998E+00	.1000E+01	.1568E-02
.1578E+01	.9403E-02	.2497E-01	.1554E-02	.9998E+00	.1000E+01	.1568E-02
.1580E+01	.9403E-02	.2497E-01	.1554E-02	.9998E+00	.1000E+01	.1568E-02
.1582E+01	.9403E-02	.2497E-01	.1554E-02	.9998E+00	.1000E+01	.1568E-02
.1584E+01	.9403E-02	.2497E-01	.1554E-02	.9998E+00	.1000E+01	.1568E-02
.1586E+01	.9404E-02	.2497E-01	.1554E-02	.9999E+00	.1000E+01	.1568E-02
.1588E+01	.9404E-02	.2497E-01	.1555E-02	.9999E+00	.1000E+01	.1569E-02
.1590E+01	.9404E-02	.2497E-01	.1555E-02	.9999E+00	.1000E+01	.1569E-02
.1592E+01	.9404E-02	.2497E-01	.1555E-02	.9999E+00	.1000E+01	.1569E-02
.1594E+01	.9404E-02	.2497E-01	.1555E-02	.9999E+00	.1000E+01	.1569E-02
.1596E+01	.9404E-02	.2497E-01	.1555E-02	.9999E+00	.1000E+01	.1569E-02
.1598E+01	.9404E-02	.2497E-01	.1555E-02	.9999E+00	.1000E+01	.1569E-02
.1600E+01	.9405E-02	.2497E-01	.1556E-02	.9999E+00	.1000E+01	.1569E-02
.1602E+01	.9405E-02	.2497E-01	.1556E-02	.9999E+00	.1000E+01	.1569E-02
.1604E+01	.9405E-02	.2497E-01	.1556E-02	.9999E+00	.1000E+01	.1569E-02
.1606E+01	.9405E-02	.2497E-01	.1556E-02	.1000E+01	.1000E+01	.1569E-02
.1608E+01	.9405E-02	.2497E-01	.1556E-02	.1000E+01	.1000E+01	.1569E-02
.1610E+01	.9406E-02	.2497E-01	.1556E-02	.1000E+01	.1000E+01	.1569E-02
.1612E+01	.9406E-02	.2497E-01	.1556E-02	.1000E+01	.1000E+01	.1569E-02
.1614E+01	.9406E-02	.2497E-01	.1557E-02	.1000E+01	.1000E+01	.1571E-02
.1616E+01	.9406E-02	.2497E-01	.1557E-02	.1000E+01	.1000E+01	.1571E-02
.1618E+01	.9406E-02	.2497E-01	.1557E-02	.1000E+01	.1000E+01	.1571E-02
.1620E+01	.9406E-02	.2497E-01	.1557E-02	.1000E+01	.1000E+01	.1571E-02
.1622E+01	.9406E-02	.2497E-01	.1557E-02	.1000E+01	.1000E+01	.1571E-02
.1624E+01	.9406E-02	.2497E-01	.1557E-02	.1000E+01	.1000E+01	.1571E-02
.1626E+01	.9406E-02	.2497E-01	.1558E-02	.1000E+01	.1000E+01	.1571E-02
.1628E+01	.9407E-02	.2497E-01	.1558E-02	.1000E+01	.1000E+01	.1571E-02
.1630E+01	.9407E-02	.2497E-01	.1558E-02	.1000E+01	.1000E+01	.1571E-02
.1632E+01	.9407E-02	.2497E-01	.1558E-02	.1000E+01	.1000E+01	.1571E-02
.1634E+01	.9407E-02	.2497E-01	.1558E-02	.1000E+01	.1000E+01	.1571E-02
.1636E+01	.9407E-02	.2497E-01	.1558E-02	.1000E+01	.1000E+01	.1571E-02
.1638E+01	.9407E-02	.2497E-01	.1558E-02	.1000E+01	.1000E+01	.1571E-02
.1640E+01	.9407E-02	.2497E-01	.1558E-02	.1000E+01	.1000E+01	.1572E-02
.1642E+01	.9408E-02	.2497E-01	.1559E-02	.1000E+01	.1000E+01	.1572E-02
.1644E+01	.9408E-02	.2497E-01	.1559E-02	.1000E+01	.1000E+01	.1572E-02
.1646E+01	.9408E-02	.2497E-01	.1559E-02	.1000E+01	.1000E+01	.1572E-02
.1648E+01	.9408E-02	.2497E-01	.1559E-02	.1000E+01	.1000E+01	.1572E-02

Time (Seconds)	Alpha	Theta Dot	Delta H	C^*	C^*_{Com}	U
.1960E+01	.9415E-02	.2493E-01	.1573E-02	.1000E+01	.1000E+01	.1573E-02
.1962E+01	.9415E-02	.2493E-01	.1573E-02	.1000E+01	.1000E+01	.1573E-02
.1964E+01	.9415E-02	.2493E-01	.1573E-02	.1000E+01	.1000E+01	.1573E-02
.1966E+01	.9415E-02	.2492E-01	.1573E-02	.1000E+01	.1000E+01	.1573E-02
.1968E+01	.9415E-02	.2492E-01	.1573E-02	.1000E+01	.1000E+01	.1573E-02
.1970E+01	.9415E-02	.2492E-01	.1573E-02	.1000E+01	.1000E+01	.1573E-02
.1972E+01	.9415E-02	.2492E-01	.1573E-02	.1000E+01	.1000E+01	.1573E-02
.1974E+01	.9415E-02	.2492E-01	.1573E-02	.1000E+01	.1000E+01	.1573E-02
.1976E+01	.9415E-02	.2492E-01	.1573E-02	.1000E+01	.1000E+01	.1573E-02
.1978E+01	.9415E-02	.2492E-01	.1573E-02	.1000E+01	.1000E+01	.1572E-02
.1980E+01	.9415E-02	.2492E-01	.1573E-02	.1000E+01	.1000E+01	.1572E-02
.1982E+01	.9415E-02	.2492E-01	.1573E-02	.1000E+01	.1000E+01	.1572E-02
.1984E+01	.9415E-02	.2492E-01	.1573E-02	.1000E+01	.1000E+01	.1572E-02
.1986E+01	.9415E-02	.2492E-01	.1573E-02	.1000E+01	.1000E+01	.1572E-02
.1988E+01	.9415E-02	.2492E-01	.1573E-02	.1000E+01	.1000E+01	.1572E-02
.1990E+01	.9415E-02	.2492E-01	.1573E-02	.1000E+01	.1000E+01	.1572E-02
.1992E+01	.9415E-02	.2492E-01	.1573E-02	.1000E+01	.1000E+01	.1572E-02
.1994E+01	.9415E-02	.2492E-01	.1573E-02	.1000E+01	.1000E+01	.1572E-02
.1996E+01	.9415E-02	.2492E-01	.1573E-02	.1000E+01	.1000E+01	.1572E-02
.1998E+01	.9415E-02	.2492E-01	.1573E-02	.1000E+01	.1000E+01	.1572E-02
.2000E+01	.9415E-02	.2492E-01	.1573E-02	.1000E+01	.1000E+01	.1572E-02

THE NUMBER OF LINES OF DATA ON TAPE3 =.001

THE CLOSED LOOP SYSTEM MATRIX IS :

```
 .933865E+00  .232215E-01 -.159325E-01 -.784215E-02
-.118325E-01  .361415E+00 -.764435E+00 -.266035E+00
 .574175E+00  .115425E+00  .366115E+00  .[illegible]E+00
 .141345E+00  .207375E-01 -.186095E-01  .100000E+01
```

THE EIGENVALUES OF THIS MATRIX FOLLOW :

THE Z-PLANE ROOTS ARE (ZERO ORDER HOLD :

```
.9933072952E+00      0.
.9773057096E+00      .1296497131E+00
.9773057096E+00     -.1296497131E+00
.9144527172E+00      0.
```

*********** M0150J1 //// END OF LIST ////

Appendix G

Plotting Algorithm

The following program (GRAPH) was developed and used to produce the plotted information found in this investigation. All plotted information was produced on a ZETA Research Inc. 230 series Zeta plotter using ZETA PLOT subroutines (Ref. 19). The information is supplied by the main program found in Appendix E. The main program, in addition to listing the information, places all the generated data onto magnetic tapes. Tape8 is used to store the values of the three states, C^*_{Act} , C^*_{Com} , and the particular control, for each 1/500th second time increment of the simulation. Tape9 is used to store an integer which equals the total number of lines of information to be found on Tape8. For example, for a one second simulation run, Tape8 would contain 501 lines of output information (includes zero-time initial condition values) and Tape9 would store the number 501. As presented, the routine is limited to a maximum of 1,001 lines of data corresponding to a maximum simulation run time of 2.0 seconds. This limit is a result of array and field length restrictions on the Intercom-Scope time sharing access system on which the program was run.

The program uses the subroutines ZTPLOT and CCAUX, both available at AFIT, which must be attached before the program can be executed. On the intercom system, these subroutines are attached as follows:

```
ATTACH, CCAUX, ID = X654321, SN = AFIT
ATTACH, ZTPLOT, ID = AFIT.
LIBRARY, ZTPLOT, CCAUX
```

Additionally, the program includes a flag which determines which plots are produced. This is accomplished by setting the IFLAG variable in the program to 1, 2, or 3. These options have the following effects:

Option	Plots Produced
IFLAG = 3	States vs Time Output vs Time Control vs Time
IFLAG = 2	Output vs Time Control vs Time
IFLAG = 1	Control vs Time

Numerous explanatory comments are included throughout the complete listing of the program which follows:

```
C     ***********************************************************
C     *                                                         *
C     *                                                         *
C     * THIS IS AN AUXILIARY PROGRAM WHICH PRODUCES THREE PLOTS *
C     * FROM THE DATA FURNISHED BY THE SIMULATION PROGRAM .     *
C     *                                                         *
C     *                                                         *
C     ***********************************************************
C
      PROGRAM GRAPH(INPUT,OUTPUT,TAPE8,TAPE9,PLOT)
      COMMON TT(1004),D1(1004),D2(1004),D3(1004)
      INTEGER CT
C     ****************************************************************
C     * IFLAG DETERMINES WHICH PLOTS ARE PRODUCED                    *
C     *             IFLAG=3          PLOT OF CONTROL VS TIME         *
C     *                                                              *
C     *             IFLAG=2          PLOT OF OUTPUT VS TIME          *
C     *                              PLOT OF CONTROL VS TIME         *
C     *                                                              *
C     *             IFLAG=1          PLOT OF STATES VS TIME          *
C     *                              PLOT OF OUTPUT VS TIME          *
C     *                              PLOT OF CONTROL VS TIME         *
C     ****************************************************************
      IFLAG=1
      REWIND 8
      REWIND 9
900   FORMAT(1X,I4)
C
C     * READ FROM TAPE9 THE NUMBER OF LINES OF DATA = CT (COUNT)     *
C
      READ(9,900) CT
      PRINT 66,CT
66    FORMAT(21H THE VALUE OF COUNT =,I4)
500   FORMAT(2X,E10.4,4X,E10.4,1X,E10.4,1X,E10.4,1X,E10.4,
     $1X,E10.4,1X,E10.4)
```

AD-A053 441 AIR FORCE INST OF TECH WRIGHT-PATTERSON AFB OHIO SCH--ETC F/G 1/3
INVESTIGATION OF A DISCRETE C-STAR TRANSIENT RESPONSE CONTROLLE--ETC(U)
DEC 77 P D MONICO

UNCLASSIFIED AFIT/GGC/EE/77-8 NL

3 OF 3
ADA
053441

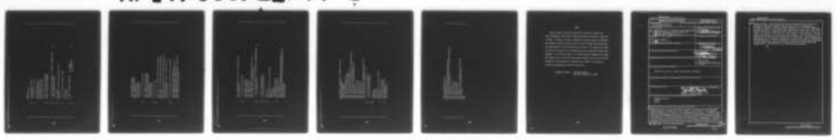

END
DATE
FILMED
6 -78
DDC

```
      KCY=1
      CALL PLOTS(30)
C
C     ************************
C      POSITION PEN
C     ************************
C
      CALL PLOT(0.0,-11.0,-3)
      CALL PLOT(0.8,2.5,-3)
      IF(IFLAG.EQ.1) GO TO 17
      IF(IFLAG.EQ.2) GO TO 18
      IF(IFLAG.EQ.3) GO TO 19
C
C     ******************************
C      PLOT OF T VS STATE VARIABLES
C     ******************************
C
C
C     * READ IN DATA FOR PLOTTING. THE NUMBER OF LINES OF DATA        *
C     * EQUALS THE VALUE OF COUNT.                                    *
C     * DATA IS TAKEN FROM TAPE8.                                     *
C
17    DO 5 K=1,CT
      READ(8,600) TT(K),D1(K),D2(K),D3(K),A,B,C
5     CONTINUE
C
C     * THE TIME AXIS IS MANUALLY SCALED                              *
C
      TT(CT+1)=0.0
      TT(CT+2)=.2
C
C     * SCALE THE STATE VARIABLES:      D1 =ALPHA                     *
C     *                                 D2 = THETA DOT                *
C     *                                 D3 = DELTA H                  *
C
```

```
      CALL SCALE(D1,6.,CT,KCY)
      CALL SCALE(D2,6.,CT,KCY)
      CALL SCALE(D3,6.,CT,KCY)
      CALL FACTOR(.7)
      D1(CT+2)=-D1(CT+2)
      D2(CT+2)=-D2(CT+2)
      D3(CT+2)=-D3(CT+2)
C
C     * PLOT THE THREE SETS OF DATA                          *
C
      CALL LINE(D1,TT,CT,KCY,100,1)
      CALL LINE(D2,TT,CT,KCY,100,4)
      CALL LINE(D3,TT,CT,KCY,100,5)
      D1(CT+2)=-D1(CT+2)
      D2(CT+2)=-D2(CT+2)
      D3(CT+2)=-D3(CT+2)
C
C     * DRAW AND LABEL AXES                                  *
C
      CALL AXIS(0.0,0.0,10HTIME (SEC),-10,10.,90.0,0.0,
     $.2)
      CALL AXIS(0.,0.,11HALPHA (RAD),11,5.,180.,D1(CT+1),
     $D1(CT+2))
      CALL AXIS(0.,-.60,19HTHETA DOT (RAD/SEC),19,5.,180.,
     $D2(CT+1),D2(CT+2))
      CALL AXIS(0.0,-1.2,13HDELTA H (RAD),13,6.,180.,
     $D3(CT+1),D3(CT+2))
C
C     * LABEL THE PLOTS BY DEFINING THE SYMBOLS USED         *
C
      CALL SYMBOL(-7.0,4.5,0.14,1,90.0,-1)
      CALL SYMBOL(999.,999.,0.14,8H - ALPHA,90.0,8)
      CALL SYMBOL(-6.75,4.5,0.14,4,90.0,-1)
      CALL SYMBOL(999.,999.,0.14,12H - THETA DOT,90.0,12)
      CALL SYMBOL(-6.5,4.5,0.14,5,90.0,-1)
```

```
      CALL SYMBCL(999.,999.,0.14,10H - DELTA H,90.0,10)
      CALL FACTOR(1.0)
C
C     * BOX IN AND LABEL THE PLOT                                 *
C
      CALL PLOT(+.7,-1.5,-3)
      CALL PLOT(0.,9.3,+2)
      CALL PLOT(-6.,9.3,+2)
      CALL PLOT(-6.,0.,+2)
      CALL PLOT(0.,0.,+2)
      CALL SYMBOL(+.3,2.5,.2,14HSTATES VS TIME,90.,14)
      CALL SYMBOL(.3,0.9,.14,5HFIG -,90.,5)
C
C     * THE REMAINING TWO PLOTS ARE GENERATED IN A MANNER SIMILAR *
C     * TO THE PROCESS ABOVE.                                     *
C
C
C
C     ***************************
C     *  PLOT OF TIME VS CSTAR  *
C     ***************************
C
18    REWIND 8
      DO 7 K=1,CT
      READ(8,600) TT(K),A,B,C,D1(K),D2(K),F
7     CONTINUE
      TT(CT+1)=0.0
      TT(CT+2)=.2
      IF(IFLAG.EQ.2) GO TO 28
      CALL PLOT(7.7,1.5,-3)
28    CALL SCALE(D1,6.,CT,KCY)
      CALL FACTOR(.7)
      CALL AXIS(0.0,0.0,10HTIME (SEC),-10,10.,90.,0.0,.2)
      CALL AXIS(0.,0.,10HC-STAR (G),10,6.,180.,D1(CT+1),D1(CT+2))
      D2(CT+1)=D1(CT+1)
      D2(CT+2)=D1(CT+2)
```

```
      CALL AXIS(0.,-.55,20HC-STAR COMMANDED (G),20,6.,
     $180.,D2(CT+1),D2(CT+2))
      D1(CT+2)=-D1(CT+2)
      D2(CT+2)=-D2(CT+2)
      CALL LINE(D1,TT,CT,KCY,0,2)
      CALL LINE(D2,TT,CT,KCY,100,11)
      CALL GRID(0.0,0.0,-.5,.5,13,21)
      CALL SYMBOL(-7.,4.5,0.14,11,90.,-1)
      CALL SYMBOL(999.,999.,0.14,18H = CSTAR COMMANDED,90.,18)
      CALL SYMBOL(-6.75,4.5,.14,24,90.,-1)
      CALL SYMBOL(999.,999.,.14,8H = CSTAR,90.,8)
      CALL FACTOR(1.0)
      CALL PLOT(+.7,-1.5,-3)
      CALL PLOT(5.,9.3,+2)
      CALL PLOT(-6.,9.3,+2)
      CALL PLOT(-6.,0.,+2)
      CALL PLOT(0.,0.,+2)
      CALL SYMBOL(+.3,2.5,.2,14HOUTPUT VS TIME,90.,14)
      CALL SYMBOL(+.3,0.9,.14,5HFIG -,90.,5)
C
C     *****************************
C     *  PLOT OF TIME VS CONTROL  *
C     *****************************
C
19    REWIND 8
      TT(CT+1)=0.0
      TT(CT+2)=.2
      DO 8 K=1,CT
      READ(8,600) TT(K),A,B,C,D,E,D1(K)
8     CONTINUE
      IF(IFLAG.EQ.3) GO TO 21
      CALL PLOT(7.7,1.5,-3)
21    CALL SCALE(D1,6.,CT,KCY)
      CALL FACTOR(.7)
      D1(CT+2)=-D1(CT+2)
```

```
CALL LINE(D1,IT,CT,KCY,0,2)
D1(CT+2)=-D1(CT+2)
CALL AXIS(0.,0.,10HTIME (SEC),-10,10.,90.,0.,.2)
CALL AXIS(0.,0.,13HCONTROL (RAD),13,6.,180.,D1(CT+1),D1(CT+2))
CALL GRID(0.,0.,-.5,.5,13,21)
CALL FACTOR(1.0)
CALL PLOT(+.7,-1.5,-3)
CALL PLOT(0.,9.3,+2)
CALL PLOT(-6.,9.3,+2)
CALL PLOT(-6.,0.,+2)
CALL PLOT(0.,0.,+2)
CALL SYMBOL(+.3,2.5,.2,15HCONTROL VS TIME,90.,15)
CALL SYMBOL(+.3,0.9,.14,5HFIG -,90.,5)
CALL PLOTE(N)
STOP
END
```

VITA

Paul D. Monico was born 31 May 1946 in Bristol, Connecticut. He was graduated from Bristol Central High School, Bristol, Connecticut in 1965. In 1969 he received a Bachelor of Science degree in Engineering Sciences from the United States Air Force Academy and concurrently was commissioned in the United States Air Force. He earned pilot wings in 1970 after completion of Undergraduate Pilot Training at Vance AFB, Oklahoma. He performed duties as a B-52G Aircraft Commander at Loring AFB, Maine prior to June 1976 when Captain Monico entered the Air Force Institute of Technology as a candidate for a Master of Science in Electrical Engineering, Guidance and Control.

Permanent address: 20 George Street
Bristol, Connecticut 06010

UNCLASSIFIED

SECURITY CLASSIFICATION OF THIS PAGE (When Data Entered)

REPORT DOCUMENTATION PAGE

READ INSTRUCTIONS BEFORE COMPLETING FORM

1. REPORT NUMBER
14 AFIT/GGC/EE/77-8

2. GOVT ACCESSION NO.

3. RECIPIENT'S CATALOG NUMBER

4. TITLE (and Subtitle)
6 INVESTIGATION OF A DISCRETE C-STAR TRANSIENT RESPONSE CONTROLLER FOR THE YF-16 AT A SELECTED FLIGHT CONDITION

5. TYPE OF REPORT & PERIOD COVERED
9 ~~MS Thesis~~ Master's Thesis

6. PERFORMING ORG. REPORT NUMBER

7. AUTHOR(s)
10 Paul D. Monico
[redacted]

8. CONTRACT OR GRANT NUMBER(s)

9. PERFORMING ORGANIZATION NAME AND ADDRESS

10. PROGRAM ELEMENT, PROJECT, TASK AREA & WORK UNIT NUMBERS
16 Project 7073-50-12
17 001

11. CONTROLLING OFFICE NAME AND ADDRESS

12. REPORT DATE
11 Dec [redacted] 77

13. NUMBER OF PAGES
12 [redacted] 200 p.

14. MONITORING AGENCY NAME & ADDRESS (if different from Controlling Office)

15. SECURITY CLASS. (of this report)
Unclassified

15a. DECLASSIFICATION/DOWNGRADING SCHEDULE

16. DISTRIBUTION STATEMENT (of this Report)

Approved for public release; distribution unlimited

17. DISTRIBUTION STATEMENT (of the abstract entered in Block 20, if different from Report)

18. SUPPLEMENTARY NOTES

Approved for public release; IAW AFR 190-17

JERRAL F. GUESS, Captain, USAF
Director of Information

19. KEY WORDS (Continue on reverse side if necessary and identify by block number)

Discrete Control
C-Star
YF-16

20. ABSTRACT (Continue on reverse side if necessary and identify by block number)

The feasibility of a discrete digital flight controller for the YF-16 Lightweight Fighter Prototype aircraft at Mach .8 at sea level is investigated. The investigation is limited to the longitudinal pitch axis. A reduced state, short period mathematical model of the YF-16 is developed from available data. The open loop stability and response characteristics of the model are shown to be unacceptable, necessitating the use of closed loop compensation. The minimization of a discrete cost function is used to develop a recursive discrete

next page

DD FORM 1473, 1 JAN 73 EDITION OF 1 NOV 65 IS OBSOLETE

UNCLASSIFIED

SECURITY CLASSIFICATION OF THIS PAGE (When Data Entered)

012225

hc

cont.

control formula. The thesis discusses and incorporates the concept of a proposed C-Star handling qualities criterion in the determination of acceptable response. Digital computer simulation on a CDC 6600 computer for various sample rates using a zero order hold or first order hold control scheme, results in a stabilized system model whose output falls within the bounds of a defined C-Star envelope, and capable of performing the tracking task of following a 1-G climb pilot input command. Typical results in the form of plotted time history information are discussed. Also discussed are the effects on the system of variations in sample rate, and cost functional penalty parameters. Control weighting is shown to be inversely proportional to the natural frequency while the trajectory weighting determines the damping ratio. Also discussed are servo saturation effects.